



Anthrax toxins regulate pain signaling and can deliver molecular cargoes into ANTXR2⁺ DRG sensory neurons

Nicole J. Yang¹, Jörg Isensee², Dylan V. Neel¹, Andreza U. Quadros³, Han-Xiong Bear Zhang⁴, Justas Lauzadis⁵, Sai Man Liu⁶, Stephanie Shiers⁷, Andreea Belu², Shilpa Palan⁶, Sandra Marlin⁶, Jacquie Maignel⁸, Angela Kennedy-Curran¹, Victoria S. Tong¹, Mahtab Moayeri⁹, Pascal Röderer^{10,11}, Anja Nitzsche^{10,11}, Mike Lu¹², Bradley L. Pentelute^{12,13,14,15}, Oliver Brüstle¹⁰, Vineeta Tripathi⁶, Keith A. Foster⁶, Theodore J. Price¹³, R. John Collier¹⁶, Stephen H. Leppla⁹, Michelino Puopolo⁵, Bruce P. Bean⁴, Thiago M. Cunha³, Tim Hucho² and Isaac M. Chiu¹ ✉

Bacterial products can act on neurons to alter signaling and function. In the present study, we found that dorsal root ganglion (DRG) sensory neurons are enriched for ANTXR2, the high-affinity receptor for anthrax toxins. Anthrax toxins are composed of protective antigen (PA), which binds to ANTXR2, and the protein cargoes edema factor (EF) and lethal factor (LF). Intrathecal administration of edema toxin (ET (PA + EF)) targeted DRG neurons and induced analgesia in mice. ET inhibited mechanical and thermal sensation, and pain caused by formalin, carrageenan or nerve injury. Analgesia depended on ANTXR2 expressed by Na_v1.8⁺ or Advillin⁺ neurons. ET modulated protein kinase A signaling in mouse sensory and human induced pluripotent stem cell-derived sensory neurons, and attenuated spinal cord neurotransmission. We further engineered anthrax toxins to introduce exogenous protein cargoes, including botulinum toxin, into DRG neurons to silence pain. Our study highlights interactions between a bacterial toxin and nociceptors, which may lead to the development of new pain therapeutics.

Pain is an unpleasant sensation initiated by nociceptive somatosensory neurons in response to harmful thermal, mechanical and chemical stimuli¹. The identification of new strategies to selectively target and silence nociceptive neurons may contribute to the development of improved pain therapeutics. Naturally occurring toxins are a rich source of evolutionarily selected molecular agents that target neuronal function. We and others have recently found that bacterial products can act on sensory neurons to modulate pain or cough during pathogenic infection². In the present study, we aimed to identify receptors for bacterial products expressed on DRG sensory neurons and determine whether the corresponding products regulate pain. By mining transcriptional data^{3–5}, we identified ANTXR2, the high-affinity receptor for anthrax toxin, being expressed by Na_v1.8⁺ DRG neurons.

The bacterium *Bacillus anthracis* is the etiological agent of anthrax. Anthrax toxin is a major virulence factor of *B. anthracis*, composed of three proteins: PA, LF and EF, which form two bipartite toxins: lethal toxin (LT) (PA + LF) and ET (PA + EF). During intoxication, PA binds to anthrax toxin receptors and forms pores in endocytic vesicles⁶. LF and EF bind to the PA pore through their

N-terminal domains and are translocated into the cytoplasm. LF is a zinc metalloprotease that cleaves mitogen-activated protein (MAP) kinase kinases⁷, the inflammasome sensor Nlrp1 (ref. ⁸) and regulatory subunits of phosphoinositide-3 kinase, p85 α and p85 β ⁹. EF is a calcium- and calmodulin-dependent adenyl cyclase that converts ATP into cAMP¹⁰.

There are two validated receptors for PA, which are structurally homologous: ANTXR1 (also known as TEM8) and ANTXR2 (also known as CMG2)^{11,12}. PA binds to ANTXR2 with substantially higher affinity than ANTXR1 (ref. ¹³), and ANTXR2-deficient mice are resistant to challenge by anthrax toxins and *B. anthracis* infection¹⁴. These observations indicate that ANTXR2 is the major, physiologically relevant receptor for anthrax toxin in vivo.

Beyond their roles in bacterial pathogenesis, anthrax toxins have been utilized as a delivery system for transporting functional molecular cargo into the cytoplasm of cells of interest, such as cancer cells¹⁵. Linking the N-terminal domain of LF (LF_N) with exogenous molecules enables their delivery through the PA pore. Cargoes that have been delivered via this methodology include protein binders¹⁶, noncanonical polypeptides¹⁷ and nucleic acids¹⁸. The breadth

¹Department of Immunology, Harvard Medical School, Boston, MA, USA. ²Translational Pain Research, Department of Anesthesiology and Intensive Care Medicine, Faculty of Medicine and University Hospital Cologne, University of Cologne, Cologne, Germany. ³Center for Research in Inflammatory Diseases, Department of Pharmacology, Ribeirão Preto Medical School, University of São Paulo, Ribeirão Preto, Brazil. ⁴Department of Neurobiology, Harvard Medical School, Boston, MA, USA. ⁵Department of Anesthesiology, Stony Brook Medicine, Stony Brook, NY, USA. ⁶Ipsen Bioinnovation Ltd, Abingdon, UK. ⁷Department of Neuroscience, Center for Advanced Pain Studies, University of Texas at Dallas, Richardson, TX, USA. ⁸Ipsen Innovation, Les Ulis, France. ⁹Laboratory of Parasitic Diseases, National Institute of Allergy and Infectious Diseases, National Institutes of Health, Bethesda, MD, USA. ¹⁰Institute of Reconstructive Neurobiology, University of Bonn Medical Faculty and University Hospital Bonn, Bonn, Germany. ¹¹Cellomics Unit, LIFE & BRAIN GmbH, Bonn, Germany. ¹²Department of Chemistry, Massachusetts Institute of Technology, Cambridge, MA, USA. ¹³The Koch Institute for Integrative Cancer Research, Massachusetts Institute of Technology, Cambridge, MA, USA. ¹⁴Broad Institute of MIT and Harvard, Cambridge, MA, USA. ¹⁵Center for Environmental Health Sciences, Massachusetts Institute of Technology, Cambridge, MA, USA. ¹⁶Department of Microbiology, Harvard Medical School, Boston, MA, USA. ✉e-mail: Isaac_Chiu@hms.harvard.edu

of these applications support utility of the anthrax toxin system as a tool for targeting neurons.

In the present study, we describe a striking pattern of ANTXR2 expression in the nervous system, where it is mostly absent in central nervous system (CNS) neurons but enriched in $\text{Na}_v1.8^+$ DRG neurons. We found that intrathecally administered ET targets DRG neurons in vivo and silences thermal and mechanical pain modalities across multiple mouse models. This analgesia was dependent on the expression of ANTXR2 on $\text{Na}_v1.8^+$ or Advillin⁺ neurons, but not other non-neuronal cells. ET attenuated neurotransmission to the spinal cord dorsal horn. The anthrax toxin system delivered multiple types of non-native proteins into sensory neurons, demonstrating potential as a protein delivery platform for blocking pain. In summary, we identify ANTXR2 as a marker enriched in nociceptive sensory neurons and propose new strategies for modulating sensory function based on anthrax toxin-mediated targeting of DRG neurons.

Results

ANTXR2 is expressed in $\text{Na}_v1.8^+$ DRG neurons. To determine new bacterial mechanisms that may modulate pain-related signaling, we mined our mouse transcriptional dataset of FACS-sorted DRG neuron populations³, and found that *Antxr2* was enriched fivefold in $\text{Na}_v1.8$ lineage (*Scn10a*^{Rosa26-TdTomato+}) neurons compared with parvalbumin-lineage (*Pvalb-cre*^{Rosa26-TdTomato+}) proprioceptive neurons (Fig. 1a). In a single-cell RNA-sequencing (scRNA-seq) dataset of mouse DRG neurons⁴, expression of *Antxr2* was highest in those expressing nociceptor-associated transcripts including *Scn10a* ($\text{Na}_v1.8$), *Trpv1*, *Calca* (CGRP), *P2rx3* and *Ntrk1* (TrkA) (Fig. 1b). In a separate dataset⁵, *Antxr2* was highly expressed in C-fiber subsets including calcitonin gene-related peptide-positive (CGRP⁺) neurons, nonpeptidergic nociceptors and somatostatin-positive (SST⁺) neurons (Extended Data Fig. 1a). The low-affinity anthrax toxin receptor *Antxr1* was largely absent in DRG neurons (Extended Data Fig. 1b).

We next performed RNAscope analysis, which validated the presence of *Antxr2* transcripts in the mouse DRGs. The highest levels of expression were observed in small- and medium-diameter neurons (Fig. 1c). Our transcriptional dataset of FACS-sorted DRG neuron populations³ showed that *Antxr2* was evenly enriched in Isolectin B4⁺ and Isolectin B4⁻ $\text{Na}_v1.8$ -lineage neurons compared with parvalbumin-lineage proprioceptors (Fig. 1d). RNAscope analysis also showed that most *Scn10a*⁺ cells express *Antxr2*, compared with only a small subset of *Pvalb*⁺ cells (Fig. 1e,f).

Mining whole-tissue expression databases of the nervous system, we found that *Antxr2* is highly expressed in the DRGs but absent in CNS tissues, including the spinal cord and brain regions (Fig. 1g). Public in situ hybridization (ISH) data also showed that the *Antxr2*

probe signal is detected in the DRG, but mostly absent throughout the brain and spinal cord (Fig. 1h). Quantitative (q)PCR analysis for *Antxr2* expression in different mouse nervous tissues confirmed that *Antxr2* expression is higher in the DRGs compared with various regions of the CNS (Fig. 1i). We note that the RNA-seq dataset of the mouse nervous system⁴ showed that *Antxr2* is also expressed in enteric and sympathetic neurons in the peripheral nervous system, although largely absent from most CNS neurons (Extended Data Fig. 1c).

RNAscope analysis of human DRG neurons revealed that ANTXR2 is widely expressed in human somatosensory neurons, including *CALCA*⁺, *P2RX3*⁺ and *CALCA*⁺/*P2RX3*⁺ neurons, which mediate nociception (Fig. 1j,k). We also found that ANTXR2 is primarily expressed in small- and medium-diameter DRG neurons by size (Fig. 1l). In addition, human ANTXR2 was expressed at higher levels in DRG RNA compared with brain RNA (Fig. 1m). Collectively, our results demonstrated that *Antxr2* is expressed in both human and mouse somatosensory neurons, including nociceptors.

LT and ET induce signaling in DRG cells. Given the expression of ANTXR2 in sensory neurons, we next investigated whether the anthrax toxins LT and ET affect intracellular signaling in DRG culture (Fig. 2a). We observed significant cleavage of MEK3 (Extended Data Fig. 2a) and reduced phosphorylation of p38 (Extended Data Fig. 2b), specifically with LT treatment. LF alone had no effect on either measure, indicating that PA was required for delivery of LF into cells. We also observed increases in cAMP only with ET treatment (Extended Data Fig. 2c). Combined with a fixed concentration of PA (10 nM), EF induced cAMP with a half-maximal effective concentration (EC_{50}) of 46 pM (Extended Data Fig. 2d). Our results show that anthrax toxins can act on DRG cultures to perturb intracellular signaling in a PA-dependent manner.

Intrathecal ET administration blocks pain behaviors. Having determined that anthrax toxins act on DRG cultures in vitro, we next examined whether the toxins affect sensory or pain-like behaviors in mice. Given the selectivity of ANTXR2 in DRG neurons compared with CNS tissues, we reasoned that intrathecal injection of the toxins into the spinal subarachnoid space would efficiently target them to the DRGs while minimizing exposure to non-neuronal cells in the periphery. We used dosages of 2 μg of PA, alone or in combination with 2 μg of LF or 2 μg of EF. In an injection volume of 5 μl , these amounts correlated to molar concentrations of 4.8 μM PA, 4.4 μM LF and 4.5 μM EF. Intrathecal administration of ET significantly increased mechanical sensitivity thresholds (Fig. 2b) and thermal latency (Fig. 2c) for several hours. The effects of ET were repeatable, where a second intrathecal injection of ET 2 d after

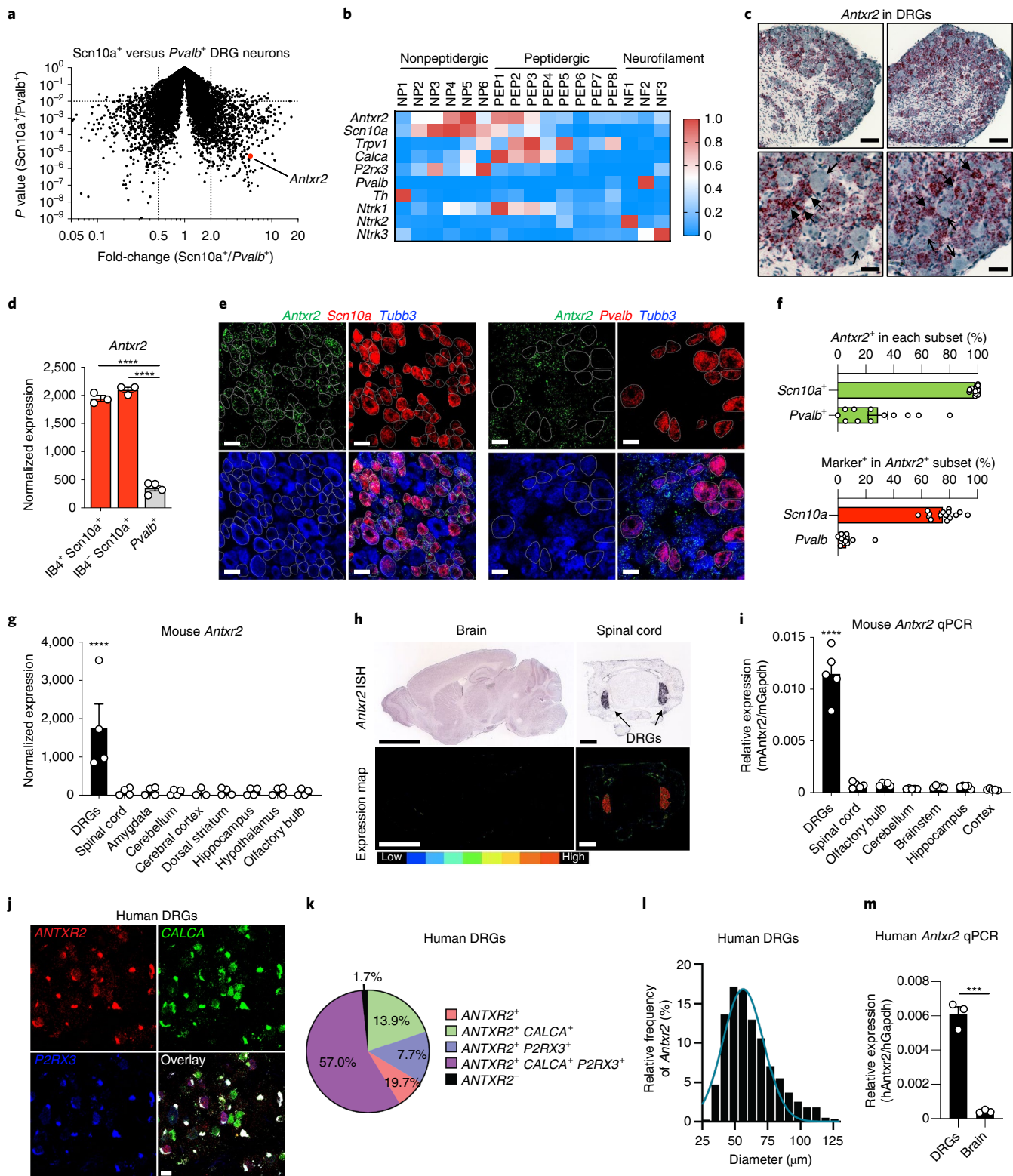
Fig. 1 | $\text{Na}_v1.8^+$ mouse DRG neurons and human DRG neurons express *Antxr2*. **a**, Gene expression comparison of FACS-purified DRG neuron subsets³. *Antxr2* is enriched in $\text{Na}_v1.8$ lineage neurons by 5.7-fold ($P = 5.48 \times 10^{-6}$). **b**, Expression of *Antxr2* and subgroup markers across sensory neuron subsets from published RNA-seq data⁴. **c**, Representative images of ISH analysis of *Antxr2* in mouse DRGs. Solid and open arrowheads point to neurons with high and low levels of *Antxr2* transcripts, respectively. Scale bar, 100 μm (top row) or 35 μm (bottom row). **d**, Microarray analysis of *Antxr2* expression in sorted DRG neuron subsets³ ($n = 3$ mice for $\text{IB4}^+\text{Na}_v1.8^+$ and $\text{IB4}^-\text{Na}_v1.8^+$; $n = 4$ mice for *Pvalb*⁺). **e**, Representative ISH images of *Antxr2*, *Scn10a* and *Tubb3* (left) or *Antxr2*, *Pvalb* and *Tubb3* (right) in mouse DRGs. Scale bar, 40 μm . **f**, Expression of *Antxr2*, *Scn10a* and *Pvalb* scored in all *Tubb3*⁺ neurons ($n = 15$ fields for *Scn10a* analysis and 12 fields for *Pvalb* analysis, both collected across 3 mice). **g**, *Antxr2* expression in mouse DRGs and brain regions from public microarray data⁵²⁻⁵⁴ ($n = 4$ samples). **h**, *Antxr2* expression in adult (P56) brain and juvenile (P4) spinal cord from public ISH data⁵⁵. Bottom: color map of expression levels. Scale bar, 3,000 μm (brain) or 400 μm (spinal cord). **i**, The qPCR analysis of *Antxr2* expression in mouse DRGs and brain regions ($n = 5$ mice). **j**, Representative ISH images of human DRGs labeled for *CALCA*, *P2RX3*, ANTXR2 and DAPI. Lipofuscin that autofluoresces in all three channels and appears white in the overlay image is background signal present in all human nervous tissue. **k**, Distribution of ANTXR2 across neuronal subpopulations in human DRGs ($n = 603$ neurons from 3 donors). **l**, Size profile of all ANTXR2⁺ neurons in human DRGs ($n = 594$ neurons from 3 donors). Scale bar, 50 μm . **m**, The qPCR analysis of ANTXR2 expression from human DRG RNA (pooled from 4 individuals) and total brain RNA (pooled from 21 individuals) ($n = 3$ technical replicates). Statistical significance was assessed using two-tailed Student's *t*-test with unequal variances (**a**), one-way ANOVA with post-hoc comparisons (**d**, **g** and **i**) or two-tailed, unpaired Student's *t*-test (**m**). *** $P < 0.001$, **** $P < 0.0001$. Data represent mean \pm s.e.m. For detailed statistical information, see Supplementary Table 2.

the first also elevated mechanical sensitivity thresholds (Fig. 2d). The analgesic effects were stronger after the second administration, which may be due to the ET-induced upregulation of ANTXR2 reported to occur in other cell types¹⁹.

We next examined whether intrathecal ET induces signaling in specific regions of the nervous system or the periphery. ET increased cAMP levels in the DRGs at 2 h post-injection (h.p.i.), which returned to baseline by 24 h (Fig. 2e). In the spinal cord,

we observed a small but significant increase at 2 h.p.i., potentially reflecting elevated cAMP in the central terminals of nociceptors, which comprise a fraction of the total spinal cord tissue (Fig. 2e). No changes were observed in the footpad (Supplementary Fig. 1a).

Intrathecal administration of ET also attenuated responses to noxious thermal and mechanical stimuli at 2 h.p.i., including hot plate (Fig. 2f), cold plate (Fig. 2g) and pinprick (Fig. 2h). Responses to the Randall–Selitto test were attenuated at 2 h.p.i. (Fig. 2i) but



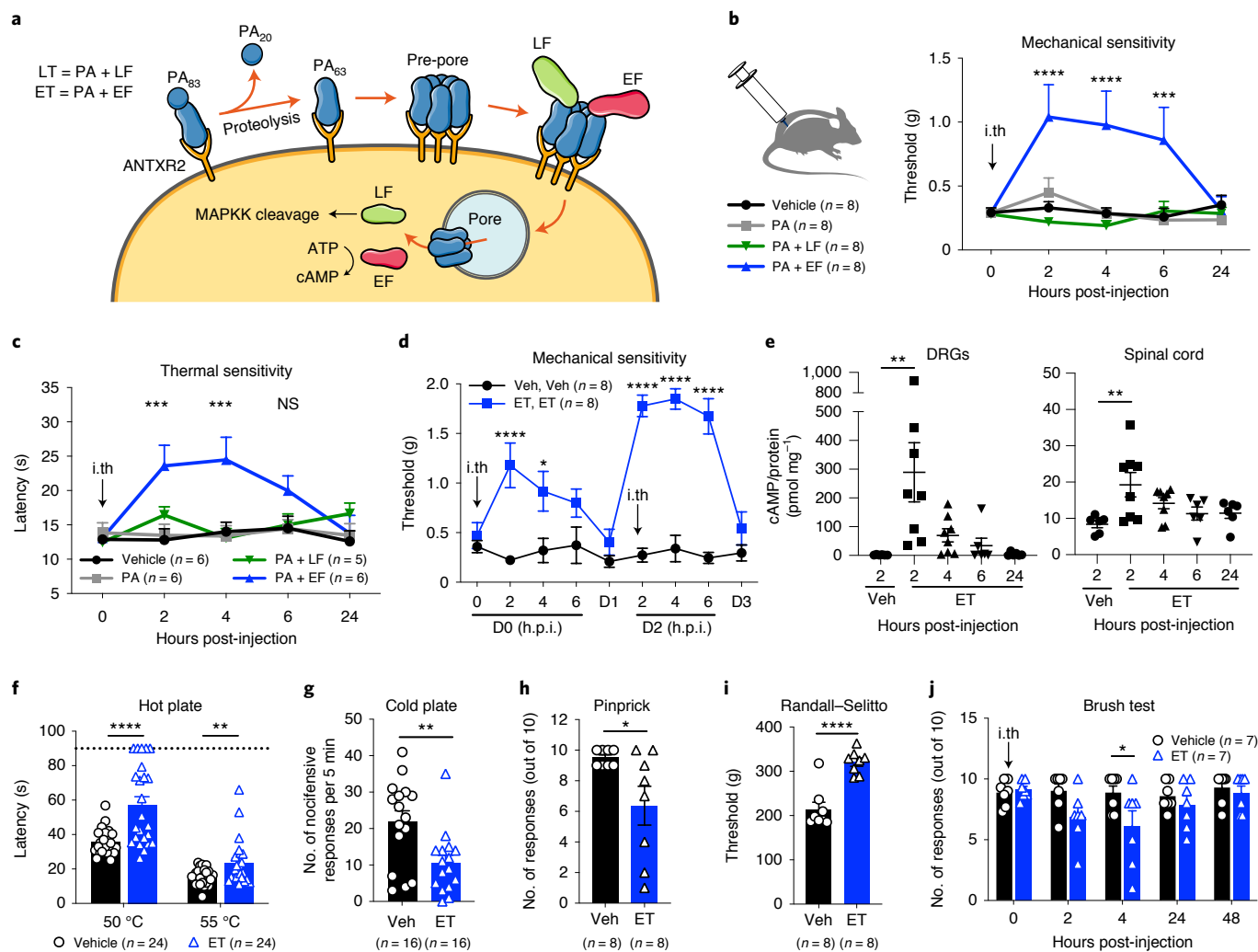


Fig. 2 | ET intrathecal administration silences mechanical and thermal sensation in mice. **a**, Schematic depicting the intoxication mechanism of anthrax LT and ET. **b**, Mechanical sensitivity thresholds after intrathecal administration of vehicle (Veh, PBS), PA (2 μg), LT (2 μg of PA + 2 μg of LF) or ET (2 μg of PA + 2 μg of EF) (n = 8 mice per group). **c**, Thermal sensitivity thresholds after intrathecal administration of vehicle (PBS; n = 6 mice), PA (2 μg; n = 6 mice), LT (2 μg of PA + 2 μg of LF; n = 5 mice) or ET (2 μg of PA + 2 μg of EF; n = 6 mice). **d**, Mice treated with intrathecal vehicle (PBS) or ET (2 μg of PA + 2 μg of EF) at 0 and 48 h. Mechanical sensitivity thresholds were monitored the day of and 24 h after each injection (n = 8 mice per group). **e**, The cAMP levels in lumbar DRGs or spinal cord after intrathecal administration of vehicle (PBS; n = 6 mice) or ET (2 μg of PA + 2 μg of EF; n = 8 mice for 2 and 4 h.p.i., n = 6 mice for 6 and 24 h.p.i.). **f–j**, Mice received intrathecal administration of vehicle (PBS) or ET (2 μg of PA + 2 μg of EF). Responses were measured at 2 h post-injection to the hot plate test (50 °C, 55 °C; n = 24 mice) (**f**), cold plate test (0 °C; n = 16 mice) (**g**), pinprick test (n = 8 mice) (**h**), Randall-Selitto test (n = 8 mice) (**i**) or light touch (n = 7 mice) (**j**). Statistical significance was assessed by two-way repeated-measures (RM) ANOVA (**b**, **c**, **d** and **j**) with post-hoc comparisons, one-way ANOVA with Dunnett's post-hoc test (**e**) or two-tailed, unpaired Student's *t*-test (**f–i**). **P* < 0.05, ***P* < 0.01, ****P* < 0.001, *****P* < 0.0001, NS, not significant. Data represent mean ± s.e.m. For detailed statistical information, see Supplementary Table 2.

not at 5 h.p.i. (Supplementary Fig. 1b). We also observed a partial impairment in light touch (Fig. 2j), potentially reflecting expression of ANTXR2 in some Aβ- and Aδ-low-threshold mechanosensory neurons. The effects of intrathecal ET injection on thermal and mechanical sensory modalities were mostly independent of sex (Extended Data Fig. 3a–f). Overall, we found that intrathecal ET elevates mechanical and thermal sensitivity thresholds to both low-threshold and noxious stimuli.

Beyond sensory function, gross motor function and coordination measured by the rotarod test were not significantly affected by ET administration (Supplementary Fig. 1c). ET also did not affect sympathetic readouts such as heart rate or body temperature (Supplementary Fig. 2a,b), suggesting that it does not produce major off-target effects on motor or sympathetic function.

ANTXR2 in sensory neurons mediates ET-induced analgesia. Given the broad expression of ANTXR2 in peripheral tissues outside the nervous system²⁰, we next investigated whether the effects of ET on sensory function are mediated through ANTXR2 expressed on DRG neurons. We first generated *Antxr2* conditional knockout (CKO) mice lacking expression in Na_v1.8⁺ nociceptive neurons (*Scn10a^{cre/+}/Antxr2^{fl/fl}*) (Fig. 3a) and confirmed reduced expression of the full-length *Antxr2* transcript in the DRGs (Extended Data Fig. 4a). ET-induced analgesia was significantly attenuated in *Scn10a^{cre/+}/Antxr2^{fl/fl}* mice compared with littermate controls (Fig. 3b). The cAMP induction was also reduced in DRG cells harvested from *Scn10a^{cre/+}/Antxr2^{fl/fl}* mice and treated with ET (Extended Data Fig. 4b).

The endogenous function of ANTXR2 is not fully understood, with reported roles in binding to extracellular matrix proteins and

mediating their internalization and degradation²¹. We found that the absence of ANTXR2 in $Na_v1.8^+$ neurons does not affect most pain modalities at baseline (Extended Data Fig. 4c), and produces a slight decrease in the second phase of formalin-induced pain (Extended Data Fig. 4d), with no defects in carrageenan-induced mechanical allodynia (Extended Data Fig. 4e). Overall our results indicated that ANTXR2 does not play a major role in nociceptor function at baseline, but is critical for ET-induced analgesia.

To further determine the role of sensory neuron-expressed ANTXR2, we generated *Advillin*-creERT2-driven *Antxr2* KO mice (*Avil^{creERT2}/Antxr2^{fl/fl}*) (Fig. 3c) to ablate ANTXR2 expression from all peripheral somatosensory neurons in adult mice²². ET-induced analgesia was nearly abolished in *Advillin*-specific *Antxr2* KO mice (Fig. 3d). A stronger attenuation was observed in *Avil^{creERT2}/Antxr2^{fl/fl}* mice than in *Scn10a^{cre/+}/Antxr2^{fl/fl}* mice, potentially reflecting a contribution from a small population of ANTXR2⁺, $Na_v1.8^-$ neurons.

We next examined whether non-neuronal cells such as endothelial cells or immune cells, which may be exposed to intrathecally injected ET, play a role in the analgesic mechanism. To this end, we used endothelial cell-specific *Cdh5^{cre/+}/Antxr2^{fl/fl}* (Fig. 3e) and myeloid immune cell-specific *Lyz2^{cre}/Antxr2^{fl/fl}* CKO mice (Fig. 3g)²⁰. In both strains, ET-induced analgesia was not significantly affected in the *Antxr2* CKO mice (Fig. 3f,h). Together, our results showed that neuronal ANTXR2 is critical to the anti-nociceptive effects of ET in vivo, whereas endothelial cells and myeloid immune cells play a minimal role.

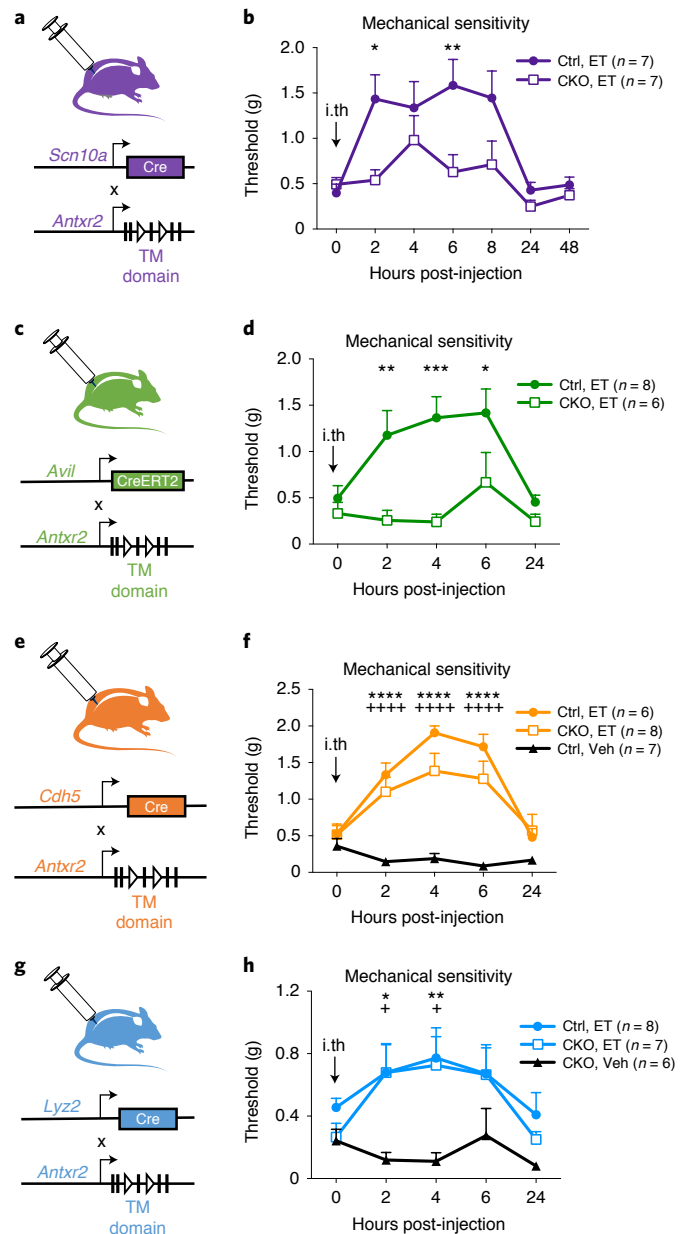
Intraplantar ET induces mechanical allodynia. In contrast to intrathecally administered ET, ET injected subcutaneously into the footpad induced mechanical allodynia lasting for 8 h (Extended Data Fig. 5a) and swelling of the footpad (Extended Data Fig. 5b)²⁰. Intraplantar ET elevated cAMP levels in the footpad but not the DRGs or spinal cord (Extended Data Fig. 5c), indicating that activity

of the toxin is locally confined. *Scn10a^{cre/+}/Antxr2^{fl/fl}* mice developed mechanical allodynia in an identical manner to *Scn10a^{+/+}/Antxr2^{fl/fl}* littermates (Extended Data Fig. 5d), suggesting that ET sensitizes nociceptors through an indirect mechanism in the periphery.

ET induces PKA signaling in mouse and human iPSC neurons. ET is known to signal in target cells via cAMP and protein kinase A (PKA), which are key modulators of nociceptor signaling and pain²³. We thus quantified PKA activation in DRG neurons. The type II isoforms of PKA (PKA-II) contain the regulatory subunit RII α or RII β (collectively referred to as RII), of which RII β is highly expressed in nociceptors²⁴. In immunological staining of fixed neurons, the phosphorylated inhibitory site of RII (pRII) becomes accessible to antibodies after cAMP triggers dissociation of the catalytic subunits²⁵. We identified sensory neurons by ubiquitin C-terminal hydrolase L1 (UCHL1), nociceptors by RII β and PKA-II activation by pRII. Positive control forskolin (Fsk) induced a long-lasting and dose-dependent increase in PKA-II activity in almost all DRG neurons (Fig. 4a). ET steadily increased PKA-II activity in a subgroup of DRG neurons to saturate by 2 h with a

Fig. 3 | ANTXR2 expressed by Nav1.8⁺ or Advillin⁺ neurons mediates

ET-induced analgesia. **a**, *Scn10a*-cre mice were bred with a conditionally targeted allele of *Antxr2* in the transmembrane region (*Antxr2^{fl/fl}*) to generate animals lacking ANTXR2 function in $Na_v1.8$ lineage nociceptors. **b**, Mechanical sensitivity thresholds in *Scn10a^{cre/+}/Antxr2^{fl/fl}* mice (CKO; $n=7$ mice) or *Scn10a^{+/+}/Antxr2^{fl/fl}* littermates (Ctrl; $n=7$ mice) which were injected intrathecally with ET. **c**, *Advillin*-creERT2 (*Avil^{creERT2/+}*) mice were bred with *Antxr2^{fl/fl}* mice to generate animals lacking ANTXR2 function in all somatosensory neurons. **d**, Mechanical sensitivity thresholds in *Avil^{creERT2/+}/Antxr2^{fl/fl}* mice (CKO; $n=6$ mice) or *Avil^{+/+}/Antxr2^{fl/fl}* littermates (Ctrl; $n=8$ mice) injected intrathecally with ET. Ablation of ANTXR2 was induced in adult mice by tamoxifen injection 2 weeks before the experiment. **e**, *Cdh5*-cre mice were bred with *Antxr2^{fl/fl}* mice to generate animals lacking ANTXR2 function in endothelial cells. **f**, Mechanical sensitivity thresholds in *Cdh5^{cre/+}/Antxr2^{fl/fl}* mice (CKO) injected intrathecally with ET ($n=8$ mice), or their *Cdh5^{+/+}/Antxr2^{fl/fl}* littermates (Ctrl) injected intrathecally with vehicle (PBS; $n=7$ mice) or ET ($n=6$ mice). *comparison of Ctrl, Veh versus Ctrl, ET groups; *comparison of Ctrl, Veh versus CKO, ET groups. **g**, *Lyz2*-cre (also known as *LysM*-cre) mice were bred with *Antxr2^{fl/fl}* mice to generate animals lacking ANTXR2 function in myeloid cells. **h**, Mechanical sensitivity thresholds in CKO mice (*Lyz2^{cre/+}/Antxr2^{fl/fl}* or *Lyz2^{cre/cre}/Antxr2^{fl/fl}*) injected intrathecally with vehicle (PBS; $n=6$ mice) or ET ($n=8$ mice), or in control littermates (Ctrl; *Lyz2^{cre/cre}/Antxr2^{fl/fl}* or *Lyz2^{cre/+}/Antxr2^{fl/fl}* or *Lyz2^{cre/+}/Antxr2^{+/+}* or *Lyz2^{cre/+}/Antxr2^{fl/fl}*) injected intrathecally with ET ($n=8$ mice). *comparison of CKO, Veh versus Ctrl, ET groups; *comparison of CKO, Veh versus CKO, ET groups. The dose of ET was 2 μ g of PA + 2 μ g of EF in all experiments. Statistical significance was assessed using two-way RM ANOVA with post-hoc comparisons (**b**, **d**, **f**, and **h**). * $P < 0.05$, ** $P < 0.01$, *** $P < 0.001$, **** $P < 0.0001$, + $P < 0.05$, +++++ $P < 0.0001$. Data represent mean \pm s.e.m. For detailed statistical information, see Supplementary Table 2.



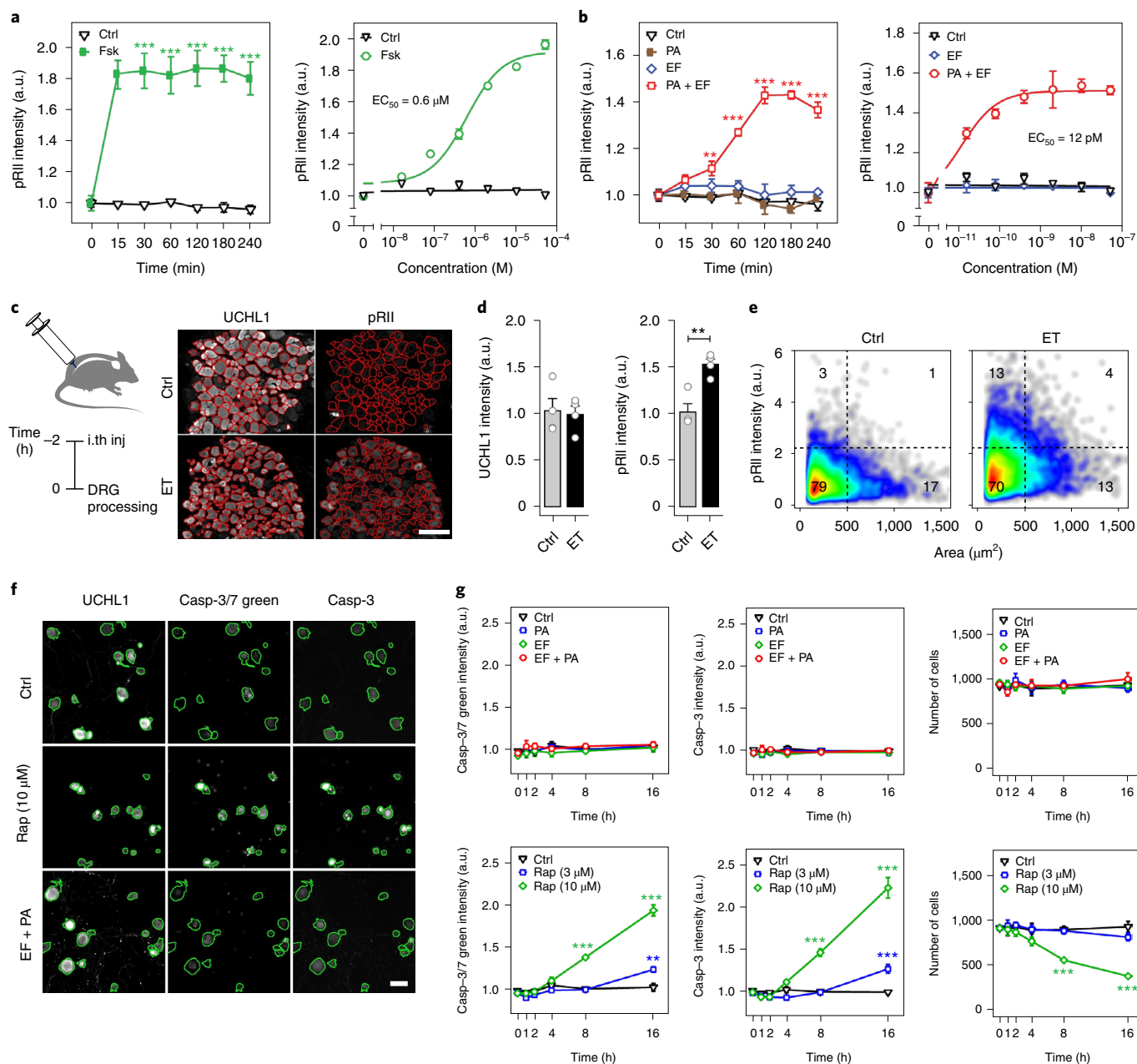


Fig. 4 | ET induces PKA signaling in DRG neurons but does not affect neuronal viability. **a**, Time-course (left) and dose-response (right) of pRII intensity in DRG neurons stimulated with Fsk ($10\ \mu\text{M}$ or 2 h) ($n = 3$ experiments, $>2,500$ neurons per condition). **b**, Left: time-course of pRII intensity in DRG neurons stimulated with Ctrl (0.1% BSA), PA (10 nM), EF (10 nM) or a combination of both factors. Right: dose-response curve of pRII intensity in DRG neurons stimulated with EF (0–50 nM, 2 h) in the presence of a constant concentration of PA (10 nM) ($n = 3$ experiments, $>2,500$ neurons per condition). **c**, Representative images of frozen L3–L6 DRG sections obtained from mice 2 h post-intrathecal injection of vehicle (PBS) or ET (2 μg of PA + 2 μg of EF). The red lines indicate the mask used to quantify signal intensities in DRG neurons. Scale bar, 100 μm . **d**, Mean UCHL1 and pRII intensities quantified in DRG sections of the respective mice ($n = 4$ mice per group, 15–20 images of 4 nonconsecutive sections per animal, $1,951 \pm 279$ neurons per animal). **e**, Single-cell data of the quantified DRG neurons. **f**, Representative images of mouse DRG neurons stimulated with solvent control (Ctrl), rapitinal (Rap; 3 or 10 μM) or ET (10 nM of PA + 10 nM of EF) for 16 h. Cultures were stained for UCHL1, caspase-3/7 green detection reagent and cleaved caspase-3. The cells were fixed about 1 h after adding the caspase-3/7 dye, stained with a standard immunocytochemistry protocol and analyzed by HCS microscopy. Green encircled neurons indicate automatically selected objects (see Methods). Scale bar, 50 μm . **g**, Time-course of caspase-3/7 green detection reagent, cleaved caspase-3 intensity and corresponding cell numbers per analyzed well ($n = 4$ experiments). Statistical significance was assessed using two-way ANOVA with Bonferroni's post-hoc test (**a**, **b**, and **g**) or two-tailed, unpaired Student's *t*-test (**d**). $^{**}P < 0.01$, $^{***}P < 0.001$. Data represent mean \pm s.e.m. For detailed statistical information, see Supplementary Table 2. a.u., arbitrary units.

picomolar EC_{50} value, whereas EF or PA alone had no effect (Fig. 4b). PA, LF alone or LT did not affect PKA-II activity (Extended Data Fig. 6a,b). We next characterized the subset of DRG neurons responding to ET. We detected PKA activation within all nociceptive

and non-nociceptive subgroups but to varying degrees (Extended Data Fig. 6c). Responses to ET positively correlated with CaMKII α and Na $_v$ 1.8 expression, but inversely so with NF200 (Extended Data Fig. 6d). ET did not increase pRII levels in non-neuronal cells, in

contrast to Fsk (Extended Data Fig. 6e,f). Overall, our analyses showed that ET dose dependently activates PKA within hours of application in sensory neurons and nociceptive subsets.

We next examined whether intrathecal administration of ET activates PKA in DRG neurons in vivo (Fig. 4c). Quantification of $\approx 2,000$ neurons per animal in DRG sections revealed that ET induces substantial PKA-II activity in DRG neurons in vivo (Fig. 4d,e).

As we previously found that *Antxr2* is expressed in human DRG neurons, we next investigated whether ET activates PKA signaling in human iPSC (iPSC)-derived sensory neurons. We differentiated human iPSCs into sensory neurons of a nociceptor phenotype following a previously established small molecule-based differentiation protocol²⁶. Stimulation with ET elevated pRII levels (Extended Data Fig. 7a,b) with a picomolar EC₅₀ value (Extended Data Fig. 7c), suggesting that human sensory neurons may be targeted by anthrax toxin.

ET treatment does not affect the viability of DRG neurons. Systemic injection of ET has been shown to cause extensive tissue damage and necrosis in other peripheral organs²⁷. However, treatment of DRG cultures with ET for 16 h did not induce any quantifiable caspase-3/7 activity, which was in contrast with the mitochondrial poison rapamycin (Fig. 4f,g). We also failed to detect activated caspase-3 in the DRGs of ET-injected mice (Supplementary Fig. 3). Altogether, our results indicated that ET is not acutely toxic to neurons and the analgesic effects of ET are unlikely to stem from cell death.

ET modulation of neural activity and analgesia induction. Previous work has shown that cAMP and PKA activation can modify multiple conductances in nociceptors^{28–30}, resulting in hyperexcitability and hyperalgesia²³. This raised the question of how ET is affecting neuronal excitability. ET-treated DRG neurons showed enhanced excitability when tested by injection of small or moderate currents (Extended Data Fig. 8a–c), which occurred without detectable differences in the resting membrane potential or input resistance of the neurons (Extended Data Fig. 8d,e).

Voltage-dependent calcium channels in nociceptive DRG neurons are regulated by many second-messenger pathways that can mediate powerful presynaptic inhibition. However, voltage-activated calcium currents recorded in ET-treated neurons did not significantly differ from the control (Supplementary Fig. 4). ET treatment also did not affect KCl-induced release of CGRP in DRG culture (Supplementary Fig. 5).

We next investigated whether ET may activate nociceptive neurons to produce stress-induced analgesia mediated by endogenous opioid or cannabinoid signaling^{31,32}. The opioid receptor antagonists naltrexone and naloxone or the CB1 antagonist/inverse agonist rimonabant did not significantly affect the anti-nociceptive effects of ET (Supplementary Fig. 6a,b). In addition, mice that underwent chemical sympathectomy still showed significant analgesia (Supplementary Fig. 7). We alternatively hypothesized that cAMP could be secreted extracellularly and become converted to adenosine³³, which then acts on adenosine receptors on nociceptors to block pain³⁴. However, systemic administration of the pan-adenosine receptor antagonist CGS15943 did not prevent the ET-induced increase in thermal sensitivity thresholds (Supplementary Fig. 6c).

Intrathecal ET induces DRG transcriptional changes. Given that cAMP and PKA signaling are known to induce phosphorylation of CREB (cAMP response element-binding protein) and other transcription factors, we hypothesized that ET may induce transcriptional changes that affect neuronal responsiveness to stimuli. Transcriptional profiling analysis of the DRG 2 h after intrathecal administration of ET identified major transcriptional changes, including upregulation of *Dusp1*, *Fosb* and *Btg2* (Extended Data

Fig. 9a), and alteration of several pathways, including negative regulation of phosphorylation (Extended Data Fig. 9b). DUSP1 is a phosphatase that blocks MAPK signaling pathways involved in pain³⁵. Pharmacological inhibition of DUSP1 using the DUSP1/DUSP6 antagonist BCI did not affect ET-induced analgesia (Extended Data Fig. 9c). Although we did not find a specific role for DUSP1, our results showed that ET induces intrinsic transcriptional changes in the DRGs in vivo within hours of injection.

ET attenuates neurotransmission at DRG central terminals. Intrinsic changes in DRG neurons could lead to modulation of regulatory pathways localized to presynaptic DRG nerve terminals in the spinal cord in vivo, affecting central neurotransmission to second-order neurons. We thus investigated the effect of ET on neurotransmission using intrathecal capsaicin injection as a stimulus for primary afferent central branches and phosphorylated extracellular signal-regulated kinase (pERK) as a readout for activation in dorsal horn neurons³⁶. Intrathecal injection of vehicle followed by capsaicin increased the number of pERK-positive cells in the dorsal horn (Fig. 5a,b). Pre-injection of ET before capsaicin significantly reduced pERK induction (Fig. 5a,b).

We next examined the effect of ET application on excitatory post-synaptic currents (EPSCs) in lamina I neurons evoked by stimulation of dorsal roots (Fig. 5c). Application of ET slowly reduced the C-fiber-mediated EPSCs (Fig. 5d) with a reduction of $37\% \pm 4\%$ (Fig. 5e, $n = 13$). There was no significant change in the paired-pulse ratio (Fig. 5f, $n = 13$). We also recorded miniature EPSCs (mEPSCs) in the absence and presence of $1 \mu\text{M}$ tetrodotoxin. In both conditions, changes in median frequency and median amplitude of mEPSCs measured in each cell before and after ET application showed no meaningful differences (Supplementary Fig. 8). As most mEPSCs appear to originate from spinal cord interneurons with very little contribution of vesicle release from primary afferents³⁷, the small effects on mEPSCs relative to the larger reduction of EPSCs are consistent with our earlier evidence that ET acts via ANTXR2 on primary afferent neurons. Overall, our results suggested that ET inhibits synaptic transmission from C-fibers to lamina I neurons and diminishes activation of the latter in the dorsal horn.

Intrathecal ET silences neuropathic and inflammatory pain. We next investigated whether ET could have therapeutic efficacy in animal models of pain. ET blocked mechanical allodynia in the spared nerve injury (SNI) model of neuropathic pain, whereas PA alone, EF alone or LT had no effect (Fig. 6a,b). ET raised the mechanical sensitivity threshold in both ipsilateral and contralateral paws of mice (Supplementary Fig. 9) and elevated cAMP levels in ipsilateral and contralateral DRGs (Fig. 6c). ET also attenuated the first and second phases of formalin-induced pain (Fig. 6d). In the carrageenan model of inflammatory pain, ET blocked mechanical allodynia (Fig. 6e), dependent on ANTXR2 expression on Na_v1.8⁺ neurons (Fig. 6f). There were no differences in ET efficacy in males and females for the formalin and carrageenan models (Extended Data Fig. 10).

Engineered anthrax toxins deliver cargoes into DRG neurons. We next tested whether the PA + LF_N anthrax toxin system could deliver exogenous proteins into the cytoplasm of sensory neurons (Fig. 7a). First, we utilized the reagent LF_N-DTA³⁸ (Fig. 7b) in which the A chain of diphtheria toxin (DTA) inhibits protein translation in mammalian cells. PA + LF_N-DTA blocked translation with a sub-picomolar EC₅₀ in DRG cultures (Fig. 7b) and produced cell death (Supplementary Fig. 10a). LF_N-DTA alone had no effect on both measures, indicating that LF_N-DTA was specifically internalized via PA.

Next, we generated a chimera of LF and EF where LF_N is linked to the C-terminal catalytic domain of EF (EF_C), herein referred to as LF_N-EF_C (Supplementary Fig. 10b). PA + LF_N-EF_C robustly induced cAMP in DRG cultures (Supplementary Fig. 10b).

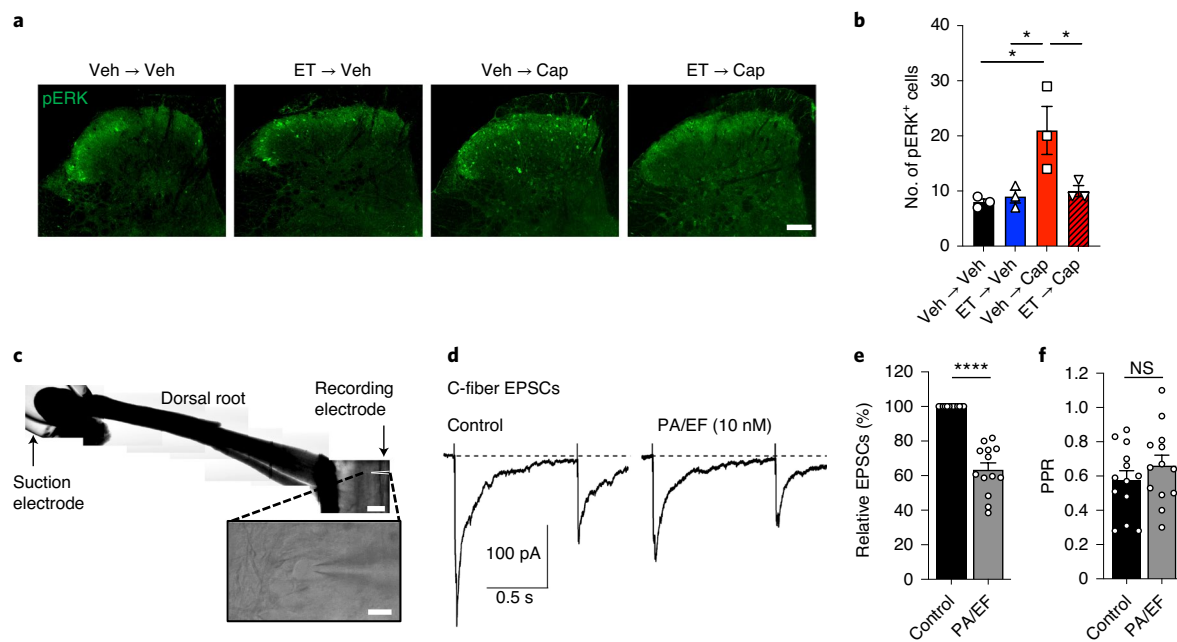


Fig. 5 | ET attenuates neurotransmission at nociceptor central terminals. a, b, Mice received intrathecal injection of vehicle or ET (2 μ g of PA + 2 μ g of EF), followed by intrathecal injection of vehicle or capsaicin (Cap) (1 μ g) after 2 h. Spinal cords were harvested after 20 min and stained for pERK. **a,** Representative images of pERK staining in the dorsal horn. Scale bar, 100 μ m. **b,** Quantification of the number of pERK-positive cells in the superficial laminae of the dorsal horn; 8–12 sections were quantified and averaged per animal ($n=3$ mice). **c,** Representative horizontal spinal cord slice preparation with the attached L4 dorsal root and a lamina I neuron (inset). Scale bar, 500 μ m and 20 μ m (inset). **d,** C-fiber EPSCs elicited in a lamina I neuron by stimulation of the L4 dorsal root (paired 400- μ A stimuli at a 1-s interval). The measured conduction velocity was 0.7 $m s^{-1}$, consistent with C-fiber activation. **e, f,** Collected results ($n=13$ cells). **e,** Application of ET (10 nM PA + 10 nM EF) reduced the first EPSC by 37% \pm 4%. **f,** No significant changes observed in the paired-pulse ratio (PPR). Statistical significance was assessed using one-way ANOVA with Tukey's post-hoc test (**b**) or a two-tailed, paired Student's *t*-test (**e** and **f**). NS, not significant, * $P < 0.05$, **** $P < 0.0001$. Data represent mean \pm s.e.m. For detailed statistical information, see Supplementary Table 2.

Finally, we designed a novel LF_N-based construct based on botulinum neurotoxin (BoNT). The enzymatic light chain (LC) of BoNT cleaves components of the SNARE complex to prevent neurotransmitter release from synaptic vesicles. We fused the LC of BoNT serotype A1 (LC/A), which targets SNAP-25, to the C terminus of LF_N. In addition, a free cysteine toward the C terminus of LC/A was mutated to a serine (Cys699Ser) (Fig. 7c). LF_N-LC/A^{C699S} retained enzymatic activity with an EC₅₀ of 89.5 pM in a cell-free assay. PA + LF_N-LC/A^{C699S}, but not LC/A^{C699S} alone, produced dose-dependent cleavage of SNAP-25 (Fig. 7d,e) and inhibited CGRP release (Fig. 7f) in DRG cultures.

Anthrax toxin delivery of BoNT/A LC blocks pain. We next wished to determine whether delivery of botulinum toxin LC by the PA + LF_N system can silence pain in vivo. Three daily intrathecal administrations of PA + LF_N-LC/A^{C699S} produced significant blockade of pain in the SNI model (Fig. 7g) without affecting body weight (Supplementary Fig. 10c) or motor function (Fig. 7h,i). We further investigated potential off-target effects of PA + LF_N-LC/A^{C699S} on motor neurons using the ex vivo mouse phrenic nerve-hemidiaphragm (mPNHD) assay. Whereas BoNT/A produced a concentration-dependent decrease in muscle contractility, both PA + LF_N-LC/A^{C699S} and LF_N-LC/A^{C699S} alone did not affect contractility at equivalent concentrations (Fig. 7j). Overall, our results demonstrate proof of concept for specifically targeting sensory function and pain in vivo using the PA + LF_N anthrax toxin system.

Discussion

Bacterial products targeting the nervous system may be used to modulate function and behavior. In the present study, we

described ANTXR2 as a receptor enriched in nociceptive sensory neurons and identified *B. anthracis* ET as a modulator of neuronal signaling and pain. ET induced cAMP/PKA signaling in DRG neurons, blockade of neurotransmission and analgesic effects in mice, dependent on neuronal ANTXR2. This contrasted with the traditional paradigm of cAMP/PKA signaling in pain, where previous work has shown that inflammatory mediators promote nociceptor sensitization by activating adenylyl cyclases and PKA²³. Injection of membrane-permeable cAMP³⁹ or Fsk⁴⁰ produces mechanical hyperalgesia. A key difference between these molecules and ET is their targeting specificity and potency. ET preferentially acts on small-diameter nociceptive sensory neurons and is orders of magnitude more potent than mammalian adenylyl cyclases⁴¹, creating waves of cAMP emanating from the perinuclear region⁴². The nature of downstream signaling pathways induced by large quantities of unregulated cAMP in the DRG remains to be examined.

ET partially inhibited synaptic transmission from C-fibers in isolated spinal cord preparations and inhibited capsaicin-induced activation of pERK in the spinal cord dorsal horn. One possible mechanism linking inhibition of synaptic transmission to the ability of ET to increase cAMP could be a cAMP-mediated enhancement of γ -aminobutyric acid (GABA)_A-receptor chloride channels in the nerve terminals of C-fibers. In mice, presynaptic GABA_A-receptors on the axons or terminals of primary nociceptors mediate spinal pain control⁴³, probably through a mechanism of presynaptic inhibition mediated by depolarization of the primary afferents, resulting from the depolarized chloride equilibrium potential in DRGs of about -30 mV⁴⁴. GABA_A-receptor activation on nerve terminals can produce powerful presynaptic inhibition by preventing

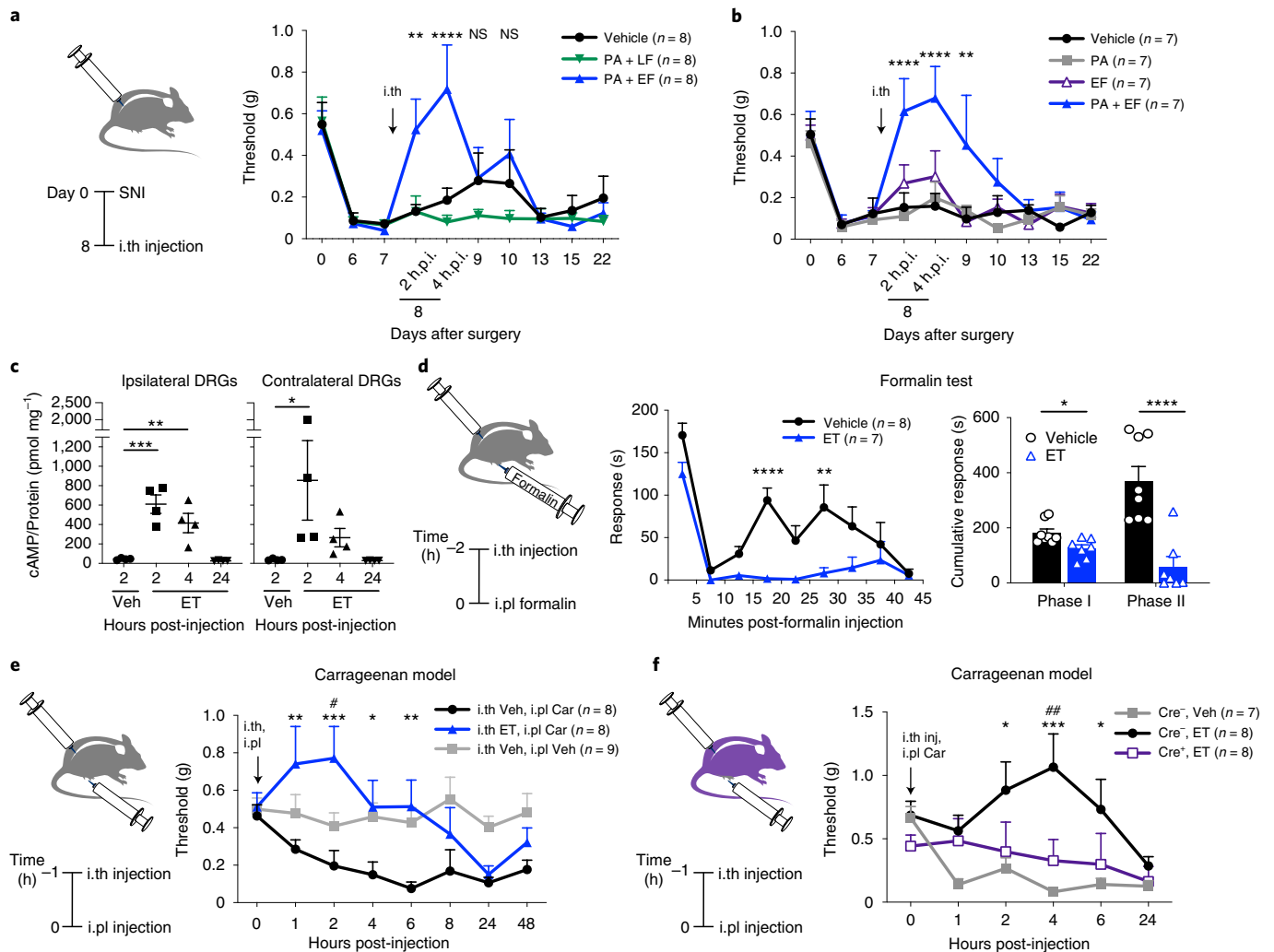


Fig. 6 | Anthrax ET silences pain in mouse models of neuropathic and inflammatory pain. **a**, Mechanical sensitivities in SNI mice injected intrathecally with vehicle, LT (2 μ g of PA + 2 μ g of LF) or ET (2 μ g of PA + 2 μ g of EF) ($n = 8$ mice per group). *Comparison of vehicle and ET groups. **b**, Mechanical sensitivities in SNI mice injected intrathecally with vehicle, PA (2 μ g), EF (2 μ g) or ET (2 μ g of PA + 2 μ g of EF) ($n = 7$ mice per group). *Comparison of vehicle and ET groups. **c**, The cAMP levels in the ipsilateral or contralateral DRGs (L3–L5) of SNI mice injected intrathecally with vehicle or ET ($n = 4$ mice per group). **d**, Left, mice were given an intrathecal injection of vehicle ($n = 8$ mice) or ET ($n = 7$ mice) 2 h before intraplantar injection of 5% formalin. Center, acute pain-like behaviors measured at 5-min intervals. Right, cumulative responses during phase I (0–5 min) or phase II (15–35 min). **e**, Mechanical sensitivities in mice that received intrathecal (i.th) injection of vehicle or ET 1 h before intraplantar (i.pl) injection of vehicle (0.9% saline) or 2% carrageenan (Car) ($n = 8$ mice for i.th Veh, i.pl Car and i.th ET, i.pl Car groups; $n = 9$ mice for i.th Veh and i.pl Veh groups). *Comparison of i.th Veh, i.pl Car versus i.th ET, i.pl Car groups. #Comparison of i.th Veh, i.pl Veh versus i.th ET, i.pl Car groups. **f**, Mechanical sensitivities in *Scn10a^{Cre/+}/Antxr2^{fl/fl}* (Cre⁺) mice or *Scn10a^{+/+}/Antxr2^{fl/fl}* (Cre⁻) littermates injected intrathecally with vehicle or ET 1 h before intraplantar injection of 2% Car ($n = 7$ mice for Cre⁻, Veh; $n = 8$ mice for Cre⁻, ET and Cre⁺, ET groups). *Comparison of Cre⁻, Veh versus Cre⁻, ET groups. #Comparison of Cre⁻, ET versus Cre⁺, ET groups. The dose of ET was 2 μ g of PA + 2 μ g of EF and the vehicle was PBS in all experiments. Statistical significance was assessed using two-way RM ANOVA with post-hoc comparisons (**a**, **b**, **d**, left, **e** and **f**), one-way ANOVA with Dunnett's post-hoc test (**c**) or two-tailed, unpaired Student's *t*-test (**d**, right). NS, not significant, * $P < 0.05$, ** $P < 0.01$, *** $P < 0.001$, **** $P < 0.0001$, # $P < 0.05$, ## $P < 0.01$. Data represent mean \pm s.e.m. For detailed statistical information, see Supplementary Table 2.

propagation of action potentials into the terminals, as a result of depolarizing the nerve terminals and adjacent axon to inactivate sodium channels, and providing a shunting conductance in the terminal⁴⁴. Currents through GABA_A-receptor channels can be enhanced by cAMP-mediated activation of PKA⁴⁵.

Another well-described effect of cAMP in DRG neurons is to shift the voltage dependence of activation of tetrodotoxin-resistant sodium channels to more hyperpolarized voltages⁴⁶. This effect contributes to an enhancement of excitability in DRG cell bodies by cAMP⁴⁷, as we saw for ET exposure. However, in nerve terminals, the activation of a steady-state sodium current at small depolarizations could enhance the steady depolarization from

GABA_A channel-mediated depolarization to inactivate the transient sodium current mediating action potentials, and thereby promote presynaptic inhibition. Such a mechanism might produce all-or-none loss of action potential propagation in individual branches of primary afferents, and therefore would not affect the paired-pulse ratio from branches that remain functional. Although the exact mechanism by which intrathecal ET produces analgesia remains to be determined, collectively our data show that ET targets ANTXR2 on primary nociceptive neurons to induce intrinsic changes at the transcriptional and signaling levels, leading to inhibition of synaptic transmission to second-order neurons in the spinal cord.

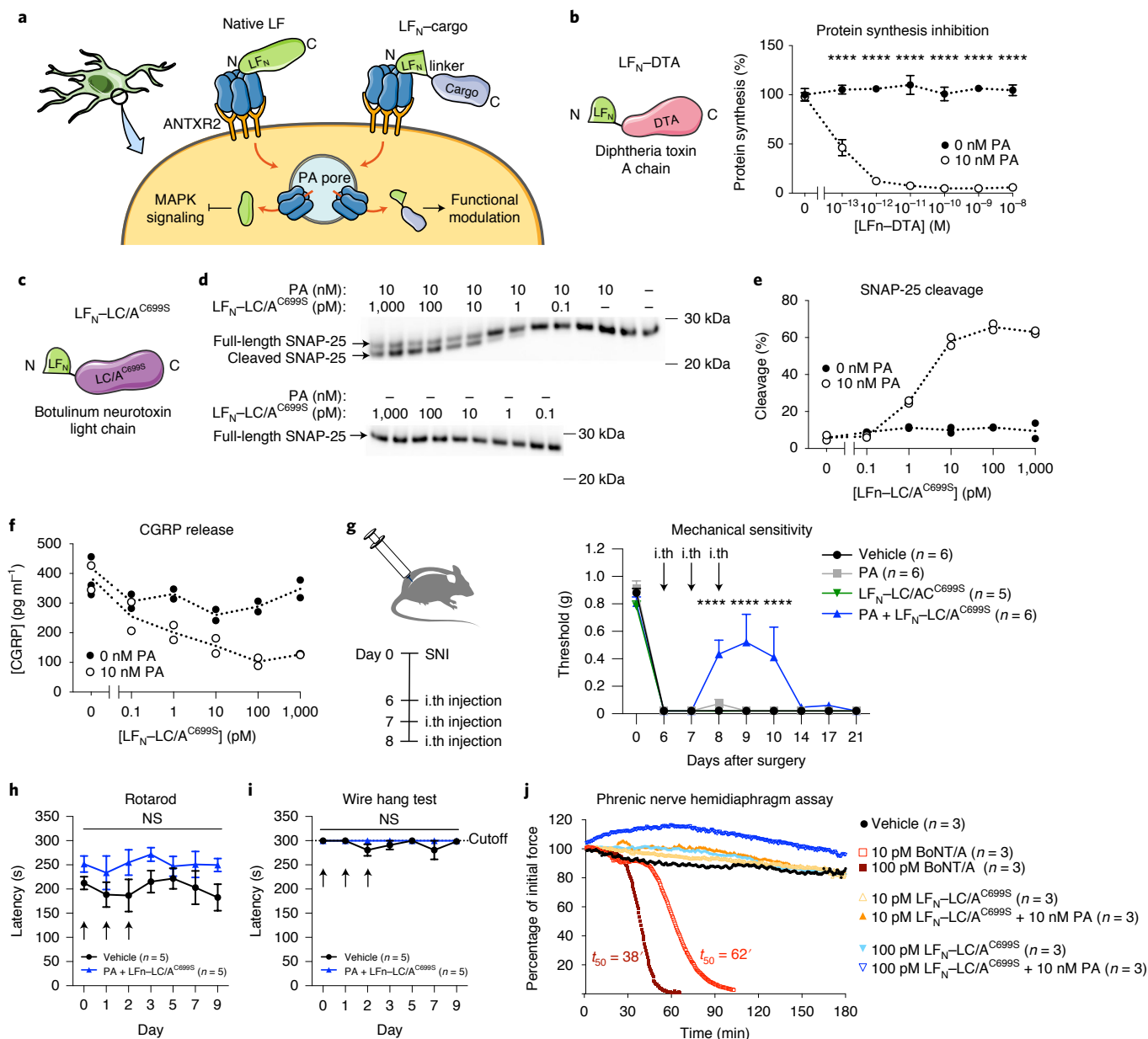


Fig. 7 | Engineered anthrax toxins deliver molecular cargo into DRG sensory neurons and block pain in vivo. **a**, Schematic of exogenous cargo delivery into neurons by the PA + LF_N system. **b**, Left, design of LF_N-DTA. Right, protein synthesis levels in DRG cultures after 6 h of treatment with the indicated concentrations of LF_N-DTA ± PA (10 nM) (*n* = 3 experiments). Data represent the mean ± s.e.m. **c**, Design of LF_N-LC/A^{C699S} linking LF_N to a mutated LC of type A botulinum neurotoxin (LC/A^{C699S}). **d-f**, DRG cultures were treated with the indicated concentrations of LF_N-LC/A^{C699S} ± PA (10 nM) for 24 h and stimulated with 80 mM KCl for 10 min (*n* = 2 wells per condition). The dotted lines connect the means. **d**, SNAP-25 cleavage in cell lysates measured by western blotting. Estimated molecular mass markers are shown. **e**, The percentage cleavage was calculated using band intensities with the following formula: cleaved/(intact + cleaved). **f**, CGRP release in the supernatant. **g**, Mechanical sensitivity thresholds in SNI mice that received three daily intrathecal injection of vehicle (PBS; *n* = 6 mice), PA only (500 ng; *n* = 6 mice), LF_N-LC/A^{C699S} only (200 ng; *n* = 5 mice) or PA + LF_N-LC/A^{C699S} (500 ng + 200 ng; *n* = 6 mice). Data represent the mean ± s.e.m. **h,i**, Mice received three daily intrathecal injection of vehicle (PBS) or PA + LF_N-LC/A^{C699S} (500 ng + 200 ng), starting on day 0 (*n* = 5 mice per group), and were monitored by the rotarod test (**h**) or wire hang test (**i**). Data represent the mean ± s.e.m. **j**, The effects of BoNT/A, LF_N-LC/A^{C699S} alone and PA + LF_N-LC/A^{C699S} tested on an ex vivo mPNHD preparation (*n* = 3 experiments). Data represent the mean. Statistical significance was assessed using two-way ANOVA with Sidak's post-hoc test (**b**) or two-way RM ANOVA with post-hoc comparisons (**g**, **h** and **i**). NS, not significant, *****P* < 0.0001. For detailed statistical information, see Supplementary Table 2.

Potential therapeutic and research applications. The enriched expression of ANTXR2 in DRG nociceptive neurons compared with CNS neurons offers an opportunity for selective targeting. It is important to note that the intrathecal route of injection probably restricts ET within the spinal cord and DRGs, preventing potential

toxicity in peripheral organs, which has been observed with systemic injection of larger doses of ET²⁷. As a cautionary note, ET has also been implicated in disrupting the integrity of the blood-brain barrier during infection⁴⁸ and further study will be required to characterize any potential effects of intrathecal ET injection on

the brain. Nevertheless, intrathecal administration of ET may provide an avenue to treat pain with higher specificity compared with existing analgesics. For example, ziconotide, the synthetic version of ω -conotoxin, inhibits N-type calcium channels and is administered via intrathecal infusion devices to treat severe chronic pain. However, possibly due to channel expression in the brain, ziconotide can also cause psychiatric symptoms and neurological impairment⁴⁹. Alternatively, opioids can induce addiction and dependence through acting on opioid receptors in the brain.

Beyond native anthrax toxins, the PA + LF_N system delivered three separate enzymatic entities into DRG sensory neurons, demonstrating flexibility and modularity as a delivery platform. Anthrax toxin-mediated delivery of botulinum toxin LC also demonstrated proof of concept as a therapeutic strategy to block pain, joining an emerging field of engineered bacterial toxins that silence pain⁵⁰. Potentially, multiple LF_N-linked cargoes could be delivered together for synergistic effects. A reported limitation of the PA + LF_N system involves protein payloads that are very stable, which do not unfold efficiently enough to be translocated through the PA pore, but could be successfully delivered with the introduction of destabilizing mutations⁵¹. The delivery capacity of the system, including the rate and efficiency of delivery, remains to be fully characterized in sensory neurons and optimized for in vivo applications.

As a protein-based delivery platform, the PA + LF_N system may provide several advantages over genetic or viral approaches for targeting sensory neurons in vitro or in vivo, such as quicker introduction of working cargo and tighter temporal control. In addition, compared with adeno-associated virus-based methods that can be limited by packaging capacity, there are no known size limitations for transportation across the PA pore. Anthrax toxin-mediated delivery of cytosolic inhibitors, effectors or sensors could complement the existing arsenal of research tools for studying somatosensory function. Altogether, we propose that anthrax toxins provide unique opportunities for targeting sensory neurons and merit further development as a platform for modulating their intracellular biology.

Online content

Any methods, additional references, Nature Research reporting summaries, source data, extended data, supplementary information, acknowledgements, peer review information; details of author contributions and competing interests; and statements of data and code availability are available at <https://doi.org/10.1038/s41593-021-00973-8>.

Received: 20 June 2020; Accepted: 1 November 2021;

Published online: 20 December 2021

References

- Basbaum, A. I., Bautista, D. M., Scherrer, G. & Julius, D. Cellular and molecular mechanisms of pain. *Cell* **139**, 267–284 (2009).
- Deng, L. & Chiu, I. M. Microbes and pain. *PLoS Pathog.* **17**, e1009398 (2021).
- Chiu, I. M. et al. Transcriptional profiling at whole population and single cell levels reveals somatosensory neuron molecular diversity. *eLife* **3**, e04660 (2014).
- Zeisel, A. et al. Molecular architecture of the mouse nervous system. *Cell* **174**, 999–1014.e22 (2018).
- Sharma, N. et al. The emergence of transcriptional identity in somatosensory neurons. *Nature* **577**, 392–398 (2020).
- Young, J. A. T. & Collier, R. J. Anthrax toxin: receptor binding, internalization, pore formation, and translocation. *Annu. Rev. Biochem.* **76**, 243–265 (2007).
- Duesbery, N. S. et al. Proteolytic inactivation of MAP-kinase-kinase by anthrax lethal factor. *Science* **280**, 734–737 (1998).
- Hellmich, K. A. et al. Anthrax lethal factor cleaves mouse Nlrp1b in both toxin-sensitive and toxin-resistant macrophages. *PLoS ONE* **7**, e49741 (2012).
- Mendenhall, M. A. et al. Anthrax lethal factor cleaves regulatory subunits of phosphoinositide-3 kinase to contribute to toxin lethality. *Nat. Microbiol.* **5**, 1464–1471 (2020).
- Leppala, S. H. Anthrax toxin edema factor: a bacterial adenylate cyclase that increases cyclic AMP concentrations of eukaryotic cells. *Proc. Natl Acad. Sci. USA* **79**, 3162–3166 (1982).
- Bradley, K. A., Mogridge, J., Mourez, M., Collier, R. J. & Young, J. A. T. Identification of the cellular receptor for anthrax toxin. *Nature* **414**, 225–229 (2001).
- Scobie, H. M., Rainey, G. J. A., Bradley, K. A. & Young, J. A. T. Human capillary morphogenesis protein 2 functions as an anthrax toxin receptor. *Proc. Natl Acad. Sci. USA* **100**, 5170–5174 (2003).
- Wigelsworth, D. J. et al. Binding stoichiometry and kinetics of the interaction of a human anthrax toxin receptor, CMG2, with protective antigen. *J. Biol. Chem.* **279**, 23349–23356 (2004).
- Liu, S. et al. Capillary morphogenesis protein-2 is the major receptor mediating lethality of anthrax toxin in vivo. *Proc. Natl Acad. Sci. USA* **106**, 12424–12429 (2009).
- Bachran, C. & Leppla, S. H. Tumor targeting and drug delivery by anthrax toxin. *Toxins* **8**, 197 (2016).
- Liao, X., Rabideau, A. E. & Pentelute, B. L. Delivery of antibody mimics into mammalian cells via anthrax toxin protective antigen. *ChemBioChem* **15**, 2458–2466 (2014).
- Rabideau, A. E., Liao, X., Akçay, G. & Pentelute, B. L. Translocation of non-canonical polypeptides into cells using protective antigen. *Sci. Rep.* **5**, 11944 (2015).
- Dyer, P. D. R. et al. Disarmed anthrax toxin delivers antisense oligonucleotides and siRNA with high efficiency and low toxicity. *J. Controlled Release* **220**, 316–328 (2015).
- Maldonado-Arocho, F. J., Fulcher, J. A., Lee, B. & Bradley, K. A. Anthrax oedema toxin induces anthrax toxin receptor expression in monocyte-derived cells. *Mol. Microbiol.* **61**, 324–337 (2006).
- Liu, S. et al. Key tissue targets responsible for anthrax-toxin-induced lethality. *Nature* **501**, 63–68 (2013).
- Bürgi, J. et al. CMG2/ANTXR2 regulates extracellular collagen VI which accumulates in hyaline fibromatosis syndrome. *Nat. Commun.* **8**, 15861 (2017).
- Lau, J. et al. Temporal control of gene deletion in sensory ganglia using a tamoxifen-inducible Advillin-Cre-ERT2 recombinase mouse. *Mol. Pain* **7**, 100 (2011).
- Aley, K. O. & Levine, J. D. Role of protein kinase A in the maintenance of inflammatory pain. *J. Neurosci.* **19**, 2181–2186 (1999).
- Isensee, J. et al. Pain modulators regulate the dynamics of PKA-RII phosphorylation in subgroups of sensory neurons. *J. Cell Sci.* **127**, 216–229 (2014).
- Isensee, J. et al. PKA-RII subunit phosphorylation precedes activation by cAMP and regulates activity termination. *J. Cell Biol.* **217**, 2167–2184 (2018).
- Chambers, S. M. et al. Combined small-molecule inhibition accelerates developmental timing and converts human pluripotent stem cells into nociceptors. *Nat. Biotechnol.* **30**, 715–720 (2012).
- Firoved, A. M. et al. *Bacillus anthracis* edema toxin causes extensive tissue lesions and rapid lethality in mice. *Am. J. Pathol.* **167**, 1309–1320 (2005).
- Fitzgerald, E. M., Okuse, K., Wood, J. N., Dolphin, A. C. & Moss, S. J. cAMP-dependent phosphorylation of the tetrodotoxin-resistant voltage-dependent sodium channel SNS. *J. Physiol.* **516**, 433–446 (1999).
- Emery, E. C., Young, G. T., Berrocoso, E. M., Chen, L. & McNaughton, P. A. HCN2 ion channels play a central role in inflammatory and neuropathic pain. *Science* **333**, 1462–1466 (2011).
- Nuwer, M. O., Picchione, K. E. & Bhattacharjee, A. PKA-induced internalization of slack KNa channels produces dorsal root ganglion neuron hyperexcitability. *J. Neurosci.* **30**, 14165–14172 (2010).
- Lewis, J. W., Cannon, J. T. & Liebeskind, J. C. Opioid and nonopioid mechanisms of stress analgesia. *Science* **208**, 623–625 (1980).
- Hohmann, A. G. et al. An endocannabinoid mechanism for stress-induced analgesia. *Nature* **435**, 1108–1112 (2005).
- Brundege, J. M., Diao, L., Proctor, W. R. & Dunwiddie, T. V. The role of cyclic AMP as a precursor of extracellular adenosine in the rat hippocampus. *Neuropharmacology* **36**, 1201–1210 (1997).
- Post, C. Antinociceptive effects in mice after intrathecal injection of 5'-N-ethylcarboxamide adenosine. *Neurosci. Lett.* **51**, 325–330 (1984).
- Ndong, C., Landry, R. P., DeLeo, J. A. & Romero-Sandoval, E. A. Mitogen activated protein kinase phosphatase-1 prevents the development of tactile sensitivity in a rodent model of neuropathic pain. *Mol. Pain* **8**, 34 (2012).
- Ji, R.-R., Baba, H., Brenner, G. J. & Woolf, C. J. Nociceptive-specific activation of ERK in spinal neurons contributes to pain hypersensitivity. *Nat. Neurosci.* **2**, 1114–1119 (1999).
- Yang, K. & Li, Y.-Q. Origins of spontaneous and noxious stimuli-evoked miniature EPSCs in substantia gelatinosa. *NeuroReport* **12**, 39–42 (2001).
- Arora, N. & Leppla, S. H. Fusions of anthrax toxin lethal factor with shiga toxin and diphtheria toxin enzymatic domains are toxic to mammalian cells. *Infect. Immun.* **62**, 4955–4961 (1994).

39. Sluka, K. A. Stimulation of deep somatic tissue with capsaicin produces long-lasting mechanical allodynia and heat hypoalgesia that depends on early activation of the cAMP pathway. *J. Neurosci.* **22**, 5687–5693 (2002).
40. Yang, H.-B. et al. cAMP-dependent protein kinase activated Fyn in spinal dorsal horn to regulate NMDA receptor function during inflammatory pain. *J. Neurochem* **116**, 93–104 (2011).
41. Shen, Y., Zhukovskaya, N. L., Guo, Q., Florián, J. & Tang, W.-J. Calcium-independent calmodulin binding and two-metal-ion catalytic mechanism of anthrax edema factor. *EMBO J.* **24**, 929–941 (2005).
42. Dal Molin, F. et al. Cell entry and cAMP imaging of anthrax edema toxin. *EMBO J.* **25**, 5405–5413 (2006).
43. Witschi, R. et al. Presynaptic alpha2-GABAA receptors in primary afferent depolarization and spinal pain control. *J. Neurosci.* **31**, 8134–8142 (2011).
44. Willis, W. D. Dorsal root potentials and dorsal root reflexes: a double-edged sword. *Exp. Brain Res.* **124**, 395–421 (1999).
45. Celotto, L., Eroli, F., Nistri, A. & Vilotti, S. Long-term application of cannabinoids leads to dissociation between changes in cAMP and modulation of GABAA receptors of mouse trigeminal sensory neurons. *Neurochem. Int.* **126**, 74–85 (2019).
46. England, S., Bevan, S. & Docherty, R. J. PGE2 modulates the tetrodotoxin-resistant sodium current in neonatal rat dorsal root ganglion neurones via the cyclic AMP–protein kinase A cascade. *J. Physiol.* **495**, 429–440 (1996).
47. Gold, M. S., Levine, J. D. & Correa, A. M. Modulation of TTX-R INa by PKC and PKA and their role in PGE2-induced sensitization of rat sensory neurons in vitro. *J. Neurosci.* **18**, 10345–10355 (1998).
48. Ebrahimi, C. M., Sheen, T. R., Renken, C. W., Gottlieb, R. A. & Doran, K. S. Contribution of lethal toxin and edema toxin to the pathogenesis of anthrax meningitis. *Infect. Immun.* **79**, 2510–2518 (2011).
49. Schmidtke, A., Lötsch, J., Freynhagen, R. & Geisslinger, G. Ziconotide for treatment of severe chronic pain. *Lancet* **375**, 1569–1577 (2010).
50. Maiarù, M. et al. Selective neuronal silencing using synthetic botulinum molecules alleviates chronic pain in mice. *Sci. Transl. Med.* **10**, eaar7384 (2018).
51. Verdurmen, W. P. R., Luginbühl, M., Honegger, A. & Plückthun, A. Efficient cell-specific uptake of binding proteins into the cytoplasm through engineered modular transport systems. *J. Control. Release* **200**, 13–22 (2015).
52. Wu, C., Macleod, I. & Su, A. I. BioGPS and MyGene.info: organizing online, gene-centric information. *Nucleic Acids Res.* **41**, D561–D565 (2013).
53. Su, A. I. et al. A gene atlas of the mouse and human protein-encoding transcriptomes. *Proc. Natl Acad. Sci. USA* **101**, 6062–6067 (2004).
54. Lattin, J. E. et al. Expression analysis of G protein-coupled receptors in mouse macrophages. *Immunome Res.* **4**, 5 (2008).
55. Lein, E. S. et al. Genome-wide atlas of gene expression in the adult mouse brain. *Nature* **445**, 168–176 (2007).

Publisher's note Springer Nature remains neutral with regard to jurisdictional claims in published maps and institutional affiliations.

© The Author(s), under exclusive licence to Springer Nature America, Inc. 2022

Methods

Animals. C57BL/6J mice were purchased from Jackson Laboratory and bred at Harvard Medical School. For high-content screening (HCS) microscopy experiments, male C57BL/6N mice were obtained from Charles River Laboratories. For the mPNHD assay, male CD1 mice were purchased from Janvier Labs. For histological analysis of pERK and biotelemetry experiments, C57BL/6 mice were obtained from the Central Animal Care Facility of Ribeirao Preto Medical School, University of Sao Paulo. For spinal cord electrophysiology experiments, Sprague Dawley rats were purchased from Envigo. *Scn10a*-Cre mice were originally provided by J. Wood (University College London)⁵⁶ on the C57BL/6 background. *Antxr2*^{fl/fl} mice in which the sequence encoding the transmembrane domain of *Antxr2* is flanked by loxP sites were obtained from Jackson Laboratory (catalog no. 0277703) on the C57BL/6 background. Mice lacking functional ANTXR2 in Na_v1.8-lineage neurons were generated at Harvard Medical School by crossing *Scn10a*-Cre mice with *Antxr2*^{fl/fl} mice to obtain *Scn10a*^{cre/+}/*Antxr2*^{fl/fl} mice and control *Scn10a*^{+/+}/*Antxr2*^{fl/fl} littermates. Genotyping of this strain was performed as previously described⁵⁰. *Avil*-CreERT2 mice on a mixed C57BL/6J and CD1 background were provided by D. Ginty (Harvard Medical School). Mice lacking functional ANTXR2 in somatosensory neurons were generated at Harvard Medical School by crossing *Avil*-CreERT2 mice with *Antxr2*^{fl/fl} mice to obtain *Avil*^{creERT2/+}/*Antxr2*^{fl/fl} mice and control *Avil*^{+/+}/*Antxr2*^{fl/fl} littermates. Endothelial cell-specific *Cdh5*^{cre/+}/*Antxr2*^{fl/fl} CKO mice and their *Cdh5*^{+/+}/*Antxr2*^{fl/fl} control littermates, and myeloid cell-specific *Ly2z*^{cre/+}/*Antxr2*^{fl/fl} or *Ly2z*^{cre/cre}/*Antxr2*^{fl/fl} CKO mice and their control littermates (*Ly2z*^{cre/cre}/*Antxr2*^{+/+}, *Ly2z*^{cre/+}/*Antxr2*^{+/+} or *Ly2z*^{cre/+}/*Antxr2*^{fl/fl}) were generated and bred by S. Leppla (National Institutes of Health (NIH)) and transported to Harvard Medical School for testing. Both endothelial- and myeloid-specific *Antxr2* CKO mouse strains were on the C57BL/6 background.

Expression analyses of murine *Antxr2* (Fig. 1c,e–f,i and Extended Data Fig. 4a), analyses involving primary mouse cells or tissue (Figs. 6c, 7b,d–f, Extended Data Figs. 2a–d, 4b, 5c and 9c, and Supplementary Figs. 1a, 5 and 10a,b), transcriptional profiling analysis of the mouse DRGs (Extended Data Fig. 9c), and all behavior experiments were performed with age-matched mice aged between 6 and 14 weeks. Male and female mice were used at equivalent ratios for behavior experiments, except for the following, which were performed with male mice only: Figs. 2j and 6a,b. For HCS microscopy experiments, male C57BL/6N mice were used at ages between 8 and 10 weeks and >24 g in weight. For the mPNHD assay, male CD1 mice were used that were between 18 and 28 g in weight at the time of the experiment. For histological analysis of pERK and biotelemetry experiments, male C57BL/6 mice were used at ages between 6 and 10 weeks. For spinal cord electrophysiology experiments, Sprague Dawley rats were used at ages between postnatal day (P)18 and P27 at equivalent ratios of males and females.

Animal care and ethics. Animal experiments were approved by the Harvard Medical School Institutional Animal Care and Use Committee, Stony Brook University Institutional Animal Care and Use Committee, the Committee for Ethics in Animal Research of the Ribeirao Preto Medical School (process no. 16/2021), or the State Office for Nature, Environment and Consumer Protection North Rhine-Westphalia (LANUV) in Germany, in compliance with German animal welfare law. The mPNHD assay was performed in accordance with Council Directive no. 2010/63/UE of 22 September 2010, on the protection of animals used for scientific purposes in France. Animals were housed in temperature (22 ± 2 °C) and humidity (55 ± 5%) controlled care facilities at the respective institutions on a 12 h light:dark cycle, and provided with freely available food and water.

Reagents. Fsk (10 mM in dimethylsulfoxide (DMSO)) was purchased from Tocris. LF was purchased from List Biological Laboratories (catalog no. 169, recombinant from *B. anthracis*). PA was obtained through BEI Resources, National Institute of Allergy and Infectious Diseases (NIAID), NIH (catalog no. NR-140, recombinant from *B. anthracis*).

Antibodies. The following antibodies were used in the present study: rabbit polyclonal anti-MEK-3 (1:500, Santa Cruz Biotechnology, catalog no. sc-961), rabbit polyclonal anti-p38 (1:1,000, Cell Signaling Technology, catalog no. 9212), rabbit monoclonal anti-phospho-p38 (Thr180/Tyr182; clone D3F9, Cell Signaling Technology, catalog no. 4511, 1:1,000), rabbit polyclonal anti-SNAP-25 (1:1,000, MilliporeSigma, catalog no. S9684), rabbit polyclonal anti-GAPDH (1:30,000, MilliporeSigma, catalog no. G9545), goat anti-rabbit immunoglobulin G (IgG) (1:1,000, Cell Signaling Technology, catalog no. 7074), chicken polyclonal anti-UCHL1 (1:2,000, Novus, catalog no. NB110-58872), rabbit monoclonal anti-R11α (phospho-Ser96; 1:1,000, clone 151, Abcam, catalog no. ab32390), mouse monoclonal anti-R11β (1:2,000, BD Transduction Laboratories, catalog no. 610625), mouse monoclonal anti-NF200 (clone N52, Sigma-Aldrich, catalog no. N0142, 1:1,000), mouse monoclonal anti-CaMKII alpha-subunit (clone 6G9, Thermo Fisher Scientific, catalog no. MA1-048, 1:1,000), mouse monoclonal anti-Na_v1.8 (clone N134/12, Neuromab Facility, catalog no. 75-166, 1:500), mouse monoclonal anti-CGRP (clone 4901, biorbyt, catalog no. orb319478, 1:500), goat polyclonal anti-TrkA (R&D Systems, catalog no. AF1056, 1:500), goat polyclonal anti-TRPV1 (R&D Systems, catalog no. AF3066, 1:500), rabbit monoclonal anti-cleaved caspase-3 (Asp175, clone 5A1E, Cell Signaling Technology, catalog

no. 9664, 1:500), rabbit anti-pERK (Thr202/Tyr204; D13.14.4E, Cell Signaling Technology, catalog no. 4370S, 1:200), highly crossadsorbed Alexa-647-, -555- and -488-conjugated secondary antibodies (Thermo Fisher Scientific).

Recombinant protein expression and purification. Sequences for all recombinant proteins are reported in Supplementary Fig. 11. The EF clone employed in the present study contains an extra alanine at the N terminus compared with the native sequence, which has been shown to have a stabilizing effect on activity⁵⁷. EF and LF_N-DTA were expressed using the Champion pET SUMO expression system (Thermo Fisher Scientific) in BL21 (DE3) *Escherichia coli* and purified using a HisTrap FF Ni-nitrilotriacetic acid column (GE Healthcare Life Sciences). The small ubiquitin-like modifier (SUMO) tag was cleaved by incubation with SUMO protease (Thermo Fisher Scientific) for 1 h at room temperature (RT) and removed by size-exclusion chromatography. EF underwent additional endotoxin removal by anion exchange chromatography (AEC) using a HiTrap Q HP anion exchange column (GE Healthcare Life Sciences). Endotoxin levels in the final product were measured using the Pierce LAL Chromogenic Endotoxin Quantitation Kit (Thermo Fisher Scientific) to be 0.29 endotoxin units (EU) mg⁻¹.

LF_N-EF_C linking the N-terminal domain of LF (residues 1–255 of native LF) and the C-terminal catalytic domain of EF (residues 258–766 of native EF) was cloned into the expression vector pSJ115 using standard molecular techniques. LF_N-EF_C and EF were expressed and purified from the avirulent *B. anthracis* strain BH460 as previously described^{58,59}.

For the LF_N-LC/A^{C699S} construct, the N-terminal domain of LF (residues 1–262 of native LF) and the catalytic domain of BoNT/A1 (residues 1–448 of native BoNT/A1) separated by a (GGS)₂ linker was codon optimized and cloned into the pK8 expression vector with a cleavable C-terminal His-tag. This was expressed in *E. coli* strain NiCo21 (DE3) using conditions previously described⁶⁰ and purified by immobilized metal affinity chromatography (IMAC) using NiHP (GE Healthcare Life Sciences) and AEC using Q HP (GE Healthcare Life Sciences) columns. The His-tag was removed by overnight incubation with tobacco etch virus protease (MilliporeSigma) at 4 °C followed by negative IMAC, and the final product was desalted into phosphate-buffered saline (PBS), pH 7.2, and stored at –80 °C.

Analysis of published microarray, scRNA-seq, tissue expression and ISH data.

Microarray data of sorted mouse DRG neuron populations were obtained from Chiu et al.³. The dataset is deposited at the National Center for Biotechnology Information (NCBI) Gene Expression Omnibus (GEO) database under accession no. GSE55114. Affymetrix CEL files were normalized using the robust multi-array average algorithm with quantile normalization, background correction and median scaling. Microsoft Excel was used to calculate *P* values using two-tailed, unequal variance Student's *t*-tests.

scRNA-seq data of mouse DRG neurons were obtained from Zeisel et al.⁴ and Sharma et al.⁵, respectively available from the Sequence Read Archive (SRA) database (accession no. SRP135960) or GEO database (accession no. GSE139088). Average transcript levels of *Antxr2*, *Scn10a*, *Trpv1*, *Calca*, *Ntrk1*, *Ntrk2* and *Ntrk3* across DRG neuron clusters were obtained from mousebrain.org⁴ and plotted as a relative heatmap using GraphPad Prism. The clusters were originally designated as PSPEP1-8, PSNF1-3 and PSNP1-6 by Zeisel et al.⁴. Expression of *Antxr2* and *Antxr1* in DRG neurons across development³ were plotted as a force-directed layout through https://kleintools.hms.harvard.edu/tools/springViewer_1_6_dev.html?datasets/Sharma2019/all and filtered for adult neurons only.

Microarray data of *Antxr2* expression in the DRGs and brain regions were obtained from BioGPS.org⁵² (<http://biogps.org/#goto=genereport&id=71914>) for the datasets GeneAtlas GNF1M⁵³ and MOE430 (ref. 54). ISH data of *Antxr2* in the adult brain (P56) and juvenile spinal cord (P4) were obtained from the 2004 Allen Mouse Brain Atlas⁵⁵ (<http://mouse.brain-map.org/experiment/show/69526659>) and the 2008 Allen Spinal Cord Atlas (<http://mousespinal.brain-map.org/imageseries/detail/100019979.html>) from the Allen Institute.

Quantitative PCR. For analysis of mouse tissue, animals were anesthetized with Avertin solution (500 mg kg⁻¹, MilliporeSigma) and perfused with 10 ml of cold PBS before harvest. RNA was isolated using the RNeasy mini kit (QIAGEN). For analysis of human tissue, total brain or DRG RNA was obtained from Clontech (catalog nos. 636530 and 636150). Brain RNA was pooled from four Asian men, aged 21–29 years, with an unknown cause of death. DRG RNA was pooled from 21 white males and females, aged 16–65 years, who died suddenly. Per the supplier, RNA was isolated by a modified guanidium thiocyanate method, and integrity and purity were confirmed using an Agilent 2100 Bioanalyzer. Reverse transcription was performed using the iScript cDNA Synthesis Kit (Bio-Rad). Real-time qPCR (RT-qPCR) was performed using the Power SYBR Green PCR Master Mix (Thermo Fisher Scientific) on a StepOnePlus RT PCR system (Applied Biosystems) or a LightCycler 96 (Roche). Expression relative to *Gapdh* was calculated using the comparative C_T method:

mAntxr1 F: CTCGCCATCAAGGGAAACT

mAntxr1 R: TACTGGCTGGCTGACTGTTT

mAntxr2 F: CAGTGAGCATTTCAGCCAAGTTT

mAntxr2 R: CTGCAATCCATTGGTACATTCTG

Primers to measure *Antxr2* expression in Na_v1.8/*Antxr2* mice were designed to span the deleted region:

mAntxr2 F (for CKO): ATTGCAGCCATCGTAGCTATTT
mAntxr2 R (for CKO): GCCAAAACCACCACATCAAG
mGapdh F: GGGTGTGAACCACGAGAATATG
mGapdh R: TGTGAGGGAGATGCTCAGTGTG
hAntxr2 F: TGTGTGGGGAGGAATTCAG
hAntxr2 R: AGGATAGGTGCAGGACAAAGC
hGapdh F: TGGCATTGCCCTCAACGA
hGapdh R: TGTGAGGAGGGGAGATTCACT

ISH of mouse DRG neurons. For chromogenic detection of *Antxr2*, freshly dissected lumbar DRGs were post-fixed in 10% neutral buffered formalin (NBF, Thermo Fisher Scientific) for 2 h at 4°C, dehydrated in 30% sucrose in PBS overnight at 4°C, embedded in OCT medium (Tissue-Tek) and frozen in a dry ice/isopentane bath. For fluorescent detection of *Antxr2*, *Scn10a*, *Pvalb* and *Tubb3*, DRGs were embedded and frozen immediately after dissection. DRGs were cryo-sectioned to 12 µm and mounted on to Superfrost Plus slides (Thermo Fisher Scientific). ISH was performed using the RNAscope system (Advanced Cell Diagnostics) following the manufacturer's protocol. For chromogenic detection, sections were digested with Protease Plus for 5 min at RT and processed with the RNAscope 2.5HD RED detection kit using the probe Mm-Antxr2-C1 (catalog no. 46851). The manufacturer's positive control probe against mouse *Pipb* (catalog no. 313911) and negative control probe against the bacterial *DapB* gene (catalog no. 310043) were used as controls. For fluorescent detection, sections were digested with protease IV for 30 min at RT and processed with the RNAscope Multiplex Fluorescent detection kit v.2, using the following probe combinations: (1) Mm-Antxr2-C1 (catalog no. 46851), Mm-Scn10a-C2 (catalog no. 426011-C2) and Mm-Tubb3-C3 (catalog no. 423391-C3) or (2) Mm-Antxr2-C1 (catalog no. 46851), Mm-Tubb3-C2 (catalog no. 423391-C2) and Mm-Pvalb-C3 (catalog no. 421931-C3). The manufacturer's 3-plex negative control probe against *DapB* (catalog no. 320871) was used as a negative control. Widefield images were acquired at ×20 magnification on an Eclipse TE2000-E Inverted Fluorescence Microscope (Nikon) using NIS-Elements software (Nikon). The raw image files were brightened and contrasted using ImageJ software. Aside from adjusting brightness and contrast, we did not perform digital image processing to subtract background. For quantification, cell boundaries were drawn manually in ImageJ based on the *Tubb3* signal. Each cell was scored manually by a blinded observer as positive or negative for *Antxr2*, *Scn10a* or *Pvalb* expression. Results from 12–15 fields (4–5 fields from 3 mice) were combined for analysis.

ISH of human DRG neurons. *Tissue preparation.* All human tissue procurement procedures were approved by the institutional review boards at the University of Texas at Dallas. Samples from medically cleared donors were provided by the Southwest Transplant Alliance with written familial consent. All samples were de-identified before use in the present study. The sex, age and cause of death of the donors are provided in Supplementary Table 1. Human DRGs (L5) were collected, frozen on dry ice and stored in a –80°C freezer. The human DRGs were gradually embedded with OCT in a cryomold by adding small volumes of OCT over dry ice to avoid thawing. All tissues were cryostat sectioned at 20 µm on to SuperFrost Plus charged slides. Sections were only briefly thawed to adhere to the slide, but were immediately returned to the –20°C cryostat chamber until completion of sectioning. The slides were then immediately utilized for histology.

RNAscope ISH. RNAscope ISH multiplex v.1 was performed as instructed by Advanced Cell Diagnostics (ACD). Slides were removed from the cryostat and immediately transferred to cold (4°C) 10% formalin for 15 min. The tissues were then dehydrated in 50% ethanol (5 min), 70% ethanol (5 min) and 100% ethanol (10 min) at RT. The slides were air dried briefly and then boundaries were drawn around each section using a hydrophobic pen (ImmEdge PAP pen; Vector Labs). When hydrophobic boundaries had dried, protease IV reagent was added to each section until fully covered and incubated for 2–5 min at RT. The protease IV incubation period was optimized for the specific lot of protease IV reagent and for each DRG as recommended by ACD. Slides were washed briefly in 1× PBS, pH 7.4 at RT. Each slide was then placed in a prewarmed humidity control tray (ACD) containing dampened filter paper and a 50:1:1 dilution (as directed by ACD due to stock concentrations) of *ANTXR2* (ACD, catalog no. 855501; Channel 1), *CALCA* (ACD, catalog no. 605551; Channel 2), *P2RX3* (ACD, catalog no. 406301; Channel 3) was pipetted on to each section until fully submerged. This was performed one slide at a time to avoid liquid evaporation and section drying. The humidity control tray was placed in a HybEZ oven (ACD) for 2 h at 40°C. After probe incubation, the slides were washed twice in 1× RNAscope wash buffer and returned to the oven for 30 min after submersion in AMP-1 reagent. Washes and amplification were repeated using AMP-2, AMP-3 and AMP-4 reagents with a 15-min, 30-min and 15-min incubation period, respectively. AMP-4 ALT C (Channel 1 = Atto 550, Channel 2 = Atto 647, Channel 3 = Alexa-488) was used for all experiments. Slides were washed twice in 0.1 M phosphate buffer (PB, pH 7.4) and then incubated in DAPI (1:5,000) in 0.1 M PB for 1 min, before being washed, air dried and cover-slipped with Prolong Gold Antifade mounting medium.

Tissue quality check. All human DRGs were checked for RNA quality by using a positive control probe cocktail (ACD), which contains probes for high-, medium- and low-expressing messenger RNAs that are present in all cells (ubiquitin C > peptidyl-prolyl *cis-trans* isomerase B > DNA-directed RNA polymerase II subunit RPB1). DRGs that showed signal for all three positive control probes were used to generate experimental data. A negative control probe against the bacterial *DapB* gene (ACD) was used to check for nonspecific/background label.

Image analysis. DRG sections were imaged on an Olympus FV3000 confocal microscope at ×20 magnification. Three ×20 images were acquired for each human DRG section, and three to four sections were imaged per human donor. The acquisition parameters were set based on guidelines for the FV3000 provided by Olympus. In particular, the gain was kept at the default setting 1, HV ≤ 600, offset = 4 and laser power ≤ 15%. The raw image files were brightened and contrasted in Olympus CellSens software (v.1.18), and then analyzed manually one cell at a time for expression of each gene target. Cell diameters were measured using the Polyline Tool. Total neuron counts for human samples were acquired by counting all the probe-labeled neurons and all neurons that were clearly outlined by DAPI (satellite cell) signal and contained lipofuscin in the overlay image.

Large globular structures and/or signal that autofluoresced in all three channels (488, 550 and 647 nm; appears white on the overlay images) was considered to be background lipofuscin and was not analyzed. Aside from adjusting brightness/contrast, we performed no digital image processing to subtract background. We attempted to optimize automated imaging analysis tools for our purposes, but these tools were designed to work with fresh, low-background rodent tissues, not human samples taken from older organ donors. As such, we chose to implement a manual approach in our imaging analysis, in which we used our own judgment of the negative/positive controls and target images to assess the mRNA label. Images were not analyzed in a blinded fashion.

Data analysis and statistics. Graphs were generated using GraphPad Prism v.8.2.0–8.4.3 (GraphPad Software, Inc.). All pie charts were generated by averaging the population distributions from each human DRG ($n = 3$). The total number of neurons assessed between all subjects is indicated on the pie chart; however, the pie charts were generated based on population averages as noted above. Relative frequency distribution histograms with a Gaussian distribution curve were generated using the diameters of all target-positive neurons.

DRG neuron dissection and culture. DRG cultures were prepared as previously described⁶¹ with minor modifications. In brief, adult mice aged 6–12 weeks were euthanized using CO₂ asphyxiation and DRGs were harvested from all segments of the spinal cord. After enzymatic dissociation in collagenase A and dispase II for 40 min at 37°C, DRGs were triturated with decreasing diameters of syringe needles (18G, 22G, 25G) and purified through a layer of 15% bovine serum albumin (BSA) in neurobasal medium (NBM). The resulting pellet was filtered through a 70-µm strainer and resuspended in NBM supplemented with B27 (Thermo Fisher Scientific) and L-glutamine (Thermo Fisher Scientific). Cells were then seeded in laminin-coated tissue culture plates and cultured in the presence of 50 ng µl⁻¹ of nerve growth factor (NGF; Thermo Fisher Scientific) unless otherwise noted.

Detection of cAMP from DRG cultures. DRG neurons were prepared as described in DRG neuron dissection and culture and seeded at 4,000 cells per well in 96-well plates. After overnight culture, cells were treated with the indicated toxin components in NBM containing 50 ng µl⁻¹ of NBM for 2 h at 37°C, lysed by manual scraping in 0.1 M HCl containing 0.5% Triton X-100 and clarified by centrifugation. The cAMP levels in clarified lysates were measured using the Direct cAMP ELISA kit from Enzo Life Sciences (catalog no. ADI-900-066) following the manufacturer's protocol. Absorbance was measured on a Synergy Mx multi-mode microplate reader (BioTek) and fitted using GraphPad Prism.

Detection of cAMP from tissue. Mice were administered intrathecal or intraplantar PBS or ET (2 µg of PA + 2 µg of EF). At the indicated timepoint, animals were euthanized by CO₂ asphyxiation and blood was drained by cardiac puncture. Lumbar DRGs, lumbar spinal cord or the glabrous skin of the footpad was harvested and homogenized in 0.1 M HCl + 0.5% Triton X-100 using glass beads and a TissueLyser II (QIAGEN). Lysate was centrifuged at 18,000g and 4°C for 40–60 min to pellet cell debris. The cAMP levels in clarified lysates were measured using the Direct cAMP ELISA kit from Enzo Life Sciences (catalog no. ADI-900-066) following the manufacturer's protocol. The protein concentration in clarified lysates were measured using the Pierce BCA Protein Assay kit (Thermo Fisher Scientific) following the manufacturer's protocol. Absorbances were measured on a Synergy Mx multi-mode microplate reader (BioTek) and fitted using GraphPad Prism. The concentration of cAMP in each sample was normalized by the corresponding protein concentration.

Western blot analysis. DRG neurons were prepared as described in DRG neuron dissection and culture and seeded at 15,000 cells per well in 96-well plates. After overnight culture, cells were treated with combinations of 10 nM PA, 10 nM LF and 10 nM EF in NBM containing 50 ng µl⁻¹ for 24 h at 37°C. Cells were then lysed by

manual scrapping in cold NP-40 lysis buffer (Thermo Fisher Scientific) containing Halt protease and phosphatase inhibitors (Thermo Fisher Scientific). Samples were separated by sodium dodecylsulfate–polyacrylamide gel electrophoresis (SDS–PAGE) and transferred to a poly(vinylidene fluoride) (PVDF) membrane, which was blocked in Tris-buffered saline and Tween-20 (TBST) + 5% nonfat milk (NFM) for 1 h at RT and washed with TBST. The membrane was incubated with the following primary antibodies in TBST + 5% BSA at 4°C overnight: rabbit polyclonal anti-MEK-3 (1:500, Santa Cruz Biotechnology, catalog no. sc-961), rabbit polyclonal anti-p38 (1:1,000, Cell Signaling Technology, catalog no. 9212) or rabbit monoclonal anti-phospho-p38 (Thr180/Tyr182; clone D3F9, Cell Signaling Technology, catalog no. 4511, 1:1,000). Incubation with horseradish peroxidase (HRP)-linked goat anti-rabbit IgG (1:2,000, Cell Signaling Technology, catalog no. 7074) in TBST + 2.5% BSA was performed for 1 h at RT. The signal was developed using the SuperSignal West Pico chemiluminescent substrate (Thermo Fisher Scientific) and imaged on an Amersham Imager 600 (GE Healthcare Life Sciences). The membrane was then stripped with Restore western blot stripping buffer (Thermo Fisher Scientific) for 15 min at 37°C, and re-probed with rabbit polyclonal anti-glyceraldehyde-3-phosphate dehydrogenase (GAPDH; 1:30,000, MilliporeSigma, catalog no. G9545) in TBST + 5% BSA. Band intensities were quantified using ImageJ and each target was normalized to its respective loading control.

Protein synthesis assay. DRG neurons were prepared as described in DRG neuron dissection and culture and seeded at 15,000 cells per well in 96-well plates. After overnight culture, cells were treated with 0.1 pM to 10 nM LF_{α} -DTA, with or without 10 nM PA, in NBM containing 50 ng μ l⁻¹ of NGF for 6 h at 37°C. Cells were then washed with leucine-free F12K medium and incubated with 20 μ Ci ml⁻¹ of [³H]leucine in the same medium for 1 h at 37°C. Cells were washed 3× with PBS and lysed in MicroScint-20 (PerkinElmer). Scintillation counting was performed on a MicroBeta TriLux (PerkinElmer).

Botulinum toxin LC activity assay. Activity of botulinum toxin LCs was measured using the BoTest A/E BoNT detection kit (BioSentinel) following the manufacturer's instructions. Fluorescence was measured on a Synergy Mx multi-mode microplate reader (BioTek).

CGRP release and SNAP-25 cleavage assays. DRG neurons were prepared as described in DRG neuron dissection and culture and seeded at 7,500 cells per well in 96-well plates. Cells were cultured for a week in NBM + 50 ng μ l⁻¹ of NGF and pulsed with an additional 10 nM cytosine arabinoside for 3 d during days 3–5 of culture. Cells were then incubated with 0.1 pM to 1 nM LF_{α} -LC/A⁶⁹⁹⁵, with or without 10 nM PA, for 24 h at 37°C. Cells were stimulated with Krebs–Ringer buffer containing 80 mM KCl for 10 min at 37°C. The concentration of CGRP in the supernatant was determined using a CGRP ELISA kit (Cayman Chemical) following the manufacturer's protocol. The remaining cells were lysed in Bolt LDS sample buffer (Thermo Fisher Scientific) containing 0.1 M DTT (Thermo Fisher Scientific) and 0.125 units μ l⁻¹ of benzonase (MilliporeSigma). Samples were then separated by SDS–PAGE and transferred to a PVDF membrane, which was blocked with TBST + 5% NFM for 1 h at RT. The membrane was blotted with rabbit polyclonal anti-SNAP-25 (1:1,000, MilliporeSigma, catalog no. S9684) in TBST + 5% NFM and HRP-linked goat anti-rabbit IgG (1:1,000, Cell Signaling Technology, catalog no. 7074) in TBST + 5% NFM. The signal was developed using the SuperSignal West Pico chemiluminescent substrate (Thermo Fisher Scientific) and imaged on an Amersham Imager 600 (GE Healthcare Life Sciences). Band intensities were quantified using ImageJ and percentage cleavage was calculated using the following formula: cleaved SNAP-25/(uncleaved SNAP-25 + cleaved SNAP-25).

Mouse DRG recordings. *Cell preparation.* DRG neurons were prepared as described in DRG neuron dissection and culture and cultured overnight in NBM containing 50 ng μ l⁻¹ of NGF and 2 ng μ l⁻¹ of glial cell-derived neurotrophic factor (GDNF). Cells were plated on laminin-coated glass coverslips and incubated at 37°C (95% O₂, 5% CO₂) overnight. Cells were treated with 10 nM PA + 10 nM EF in NBM + 50 ng μ l⁻¹ of NGF + 2 ng μ l⁻¹ of GDNF or vehicle for 2–10 h at 37°C. Recordings were made within 1 h of removal from treatment.

Whole-cell current clamp and calcium current recordings. Small DRG neurons (membrane capacitance: 6.6 ± 0.5 pF) were recorded at RT. Whole-cell recordings were made using an Axon Instruments Multiclamp 700B Amplifier (Molecular Devices) and a Digidata 1322-A data acquisition interface using pClamp 9.2 software (Molecular Devices). Membrane voltage and current signals were filtered at 10 kHz and digitized at 100 kHz. Analysis was performed with Igor Pro (Wavemetrics) using DataAccess (Bruxon Software) to import pClamp data. Recordings were made using electrodes with resistances of 5–9 M Ω (current clamp) or 2–7 M Ω (voltage clamp) with tips wrapped by strips of Parafilm to reduce pipette capacitance. Current clamp recordings were made using an internal solution containing 140 mM potassium aspartate, 13.5 mM NaCl, 1.6 mM MgCl₂, 0.09 mM (ethylenebis(oxonitrilo)tetra-acetate (EGTA), 9 mM HEPES, 14 mM creatine phosphate (Tris salt), 4 mM MgATP, 0.3 mM Tris-GTP, pH 7.2, adjusted

with KOH and an external Tyrode's solution containing 155 mM NaCl, 3.5 mM KCl, 1.5 mM CaCl₂, 1 mM MgCl₂, 10 mM HEPES and 10 mM glucose, pH 7.4 adjusted with NaOH. Reported membrane potentials were corrected for a liquid junction potential of –10 mV between the internal and extracellular solutions⁶². After breaking into the cells, pipette capacitance was compensated (50–60%) and bridge balance was set to compensate for series resistance. Action potential firing was recorded with injection of a series of 1-s depolarizing current pulses ranging from 1 pA to 150 pA. Cell input resistance was measured using a 30-pA hyperpolarizing current injection. Voltage clamp recordings of currents through voltage-dependent calcium channels were made using an internal solution containing 140 mM CsCl, 13.5 mM NaCl, 1.8 mM MgCl₂, 0.09 mM EGTA, 9 mM HEPES, 14 mM creatine phosphate (Tris salt), 4 mM MgATP and 0.3 mM Tris-GTP, pH 7.2 adjusted with CsOH, and an external solution containing 5 mM BaCl₂, 160 mM tetraethylammonium chloride, 10 mM HEPES and 10 mM glucose, pH 7.4, adjusted with tetraethylammonium hydroxide, and 5 μ M tetrodotoxin. Calcium channel currents were evoked using a series of 100-ms voltage steps from –60 mV to +70 mV, delivered from a holding voltage of –70 mV. Collected data are presented as mean ± s.e.m.

Spinal cord slice recordings. *Horizontal spinal cord slices.* Horizontal spinal cord slices were made from P18–P27 Sprague Dawley rats. Rats were deeply anesthetized with isoflurane before decapitation. After decapitation, the ventral aspect of the vertebral column was exposed and immersed in ice-cold dissecting solution (in mM): 87 NaCl, 2.5 KCl, 1.25 NaH₂PO₄·H₂O, 26 NaHCO₃, 6 MgCl₂, 0.5 CaCl₂, 20 glucose, 77 sucrose and 1 kynurenic acid, and oxygenated with 95%:5% O₂:CO₂. Using a bilateral ventral laminectomy, the lumbar part of the spinal cord was exposed and carefully removed with L4 and L5 dorsal roots attached. Horizontal slices were made manually. First, the spinal cord was cut in half with micro-ophthalmic scissors through the parasagittal plane to produce a hemisected spinal cord. With a second cut, ~30–45° angle with respect to the parasagittal plane, the ventral part of the hemisected cord was removed such that the result was a horizontal slice (400- to 500- μ m thick) with the L4–L5 dorsal roots (7- to 10-mm length) attached⁶³. Spinal cord slices were then immersed in oxygenated recovery solution (same as the dissecting solution, but without kynurenic acid) at 35°C and allowed to recover for 1 h. After 1 h the slices were transferred to a storage solution (same as recovery solution, at RT) and kept for the next 4–5 h. In horizontal slices, lamina I neurons were visualized through the white matter by using an infrared light-emitting diode (LED) illumination^{64–66}, a CCD video camera (Oly 150, Olympus), and a ×40 water immersion objective mounted on an upright microscope (BX51WI, Olympus). To restrict the analysis mainly to lamina I projection neurons, large neurons with soma cross-sectional area >250 μ m² and cell capacitance >75 pF, located in the outer portion of lamina I, just below the white matter, were selected for recording^{63,67,68}. Neurons had a cross-sectional area of 313 ± 90 μ m² and capacitance of 98 ± 31 pF (n = 13).

Patch clamp electrophysiology. After recovery, slices were transferred to a submersion recording chamber and mounted on the stage of an upright microscope (BX51WI, Olympus). Slices were then perfused with artificial cerebrospinal fluid (aCSF) (in mM: 125 NaCl, 2.5 KCl, 26 NaHCO₃, 1.25 NaH₂PO₄ and 20 glucose), oxygenated with 95%:5% O₂:CO₂. Whole-cell voltage clamp recordings were made using a Multiclamp 700B amplifier (Molecular Devices). Patch pipettes were pulled from borosilicate glass (WPI) using a Sutter P97 puller (Sutter Instrument). The resistance of the patch pipette was 1.3–1.8 M Ω when filled with the standard internal cesium methanesulfonate-based solution. The shank of the patch pipette was wrapped with Parafilm to reduce pipette capacitance. In whole-cell mode, the capacity current was reduced by using the amplifier circuitry. To reduce voltage errors, 40–50% of series resistance compensation was applied. For recording EPSCs in voltage clamp, the external solution was the oxygenated aCSF; the internal solution was (in mM): 125 cesium methanesulfonate, 10 NaCl, 2 MgCl₂, 14 phosphocreatine, 4 MgATP, 0.3 Na-GTP, 10 EGTA, 10 HEPES and 5 QX-314, pH 7.2 with CsOH. EPSCs in voltage clamp were recorded at –70 mV. Drugs were dissolved in the aCSF and applied to the spinal cord slice through the perfusion system at a speed of 2 ml min⁻¹. Recordings were made at 35 ± 1°C by heating the solutions with a temperature controller (Warner TC-344B, Warner Instruments).

Dorsal root stimulation. EPSCs were evoked by stimulating the dorsal root with a suction electrode connected to an isolated current stimulator (ISO-Flex Stimulus Isolator; A.M.P.I.). The dorsal root was stimulated at 0.016 Hz (duration 0.1 ms). The stimulus intensity was gradually increased to recruit fibers with increasing threshold. Stimulation of the dorsal root started with 25 μ A of current to test for synaptic inputs from A α / β -fibers^{69–71}. The stimulus intensity was then gradually increased to 80, 200, 300, 400 and 500 μ A of current to recruit A δ - and C-fibers and until the maximum EPSC was elicited. Once the maximum EPSC had been elicited, then the stimulus intensity was set at 30% higher (usually between 400 and 500 μ A). Only monosynaptic responses were included in the analysis. Monosynaptic responses elicited by stimulation of A δ - and C-fibers were identified based on the absence of synaptic failures and low variability (<15%) in synaptic delay during 15 consecutive stimuli: 80 μ A, 2 Hz (for A δ -fibers) and 500 μ A, 1 Hz

(for C-fibers)^{63,69,71–73}. Isolation of A δ - and C-fiber components was confirmed with the measured conduction velocity: A δ -fibers (0.5–2 m s⁻¹) and C-fibers (<0.5 m s⁻¹)^{71,74}.

Data acquisition and analysis. Currents and voltages were controlled and sampled using a Digidata 1440A interface and pCLAMP 10.3 software (Molecular Devices). In voltage clamp, currents were filtered at 2 kHz (3 dB, 4-pole Bessel) and digitized at 50 kHz. Analysis was performed using Clampfit 10.3 and IGOR Pro (v.6.2; WaveMetrics) using DataAccess (Bruyton) to import pCLAMP files into IGOR. Analyses of evoked synaptic currents and paired-pulse ratio were carried out by measuring the peak current of three averaged consecutive traces in each condition. For analysis of mEPSCs, the threshold was set at twice the average noise. The frequency and peak of mEPSCs were determined during a 2-min period in each condition. Reported voltages were corrected for -8 mV junction potential (pipette relative to bath, for the methanesulfonate-based internal solution), which was measured using a flowing 3 M KCl reference electrode⁶².

DRG neurons for HCS microscopy. Mice were euthanized between 9 am and 12 midday by CO₂ intoxication, and cervical, lumbar and thoracic DRGs were removed within 30 min per animal. DRGs were incubated in Neurobasal-A/B27 Medium (Invitrogen) containing collagenase P (Roche) (0.2 U ml⁻¹, 1 h, 37 °C, 5% CO₂). DRGs were dissociated by trituration with fire-polished Pasteur pipettes. Axon stumps and disrupted cells were removed by BSA gradient centrifugation (15% BSA, 120 g, 8 min). Viable cells were resuspended in Neurobasal-A/B27 Medium, plated in 0.1 mg ml⁻¹ of poly(L-ornithine)/5 μ g ml⁻¹ on laminin-precoated 96-well imaging plates (Greiner) and incubated overnight (37 °C, 5% CO₂). Neuron density was 1,500 neurons cm⁻². DRG neurons were stimulated 24 h after isolation in 96-well imaging plates.

Generation of iPSC-derived sensory neurons. The present study employed the iPSC line UKBi013-A (<https://hpscereg.eu/cell-line/UKBi013-A>). It was approved by the Ethics Committee of the Medical Faculty of the University of Bonn (approval no. 275/08), and informed consent was obtained from the patient. Differentiation of iPSC into sensory neurons was performed as previously reported²⁶ with slight modifications. Briefly, single-cell iPSCs were seeded at 3 \times 10⁵ cells cm⁻² in StemMAC iPSC-Brew (Miltenyi Biotec) in the presence of 10 μ M Rock-Inhibitor Y-27632 (Cell Guidance Systems) on Geltrex (Thermo Fisher Scientific)-coated T175 flasks at day -1. After 24 h the medium was changed to differentiation medium. Neural differentiation was initiated by dual-SMAD inhibition using 100 nM LDN 193189 (Axon Medchem BV) and 10 μ M SB 431542 (Biozol) from day 0 to day 6. To specify the differentiating cells into sensory neurons, 3 μ M CHIR 99021 (Miltenyi Biotec), 10 μ M SU5402 (Sigma-Aldrich) and 10 μ M DAPT (Axon Medchem BV) were added to the culture from day 3 to day 14. Two basal media were used during differentiation: medium 1 consists of knockout Dulbecco's modified Eagle's medium (Thermo Fisher Scientific) with 20% Knock Out Serum Replacement (Thermo Fisher Scientific), 2 mM (1 \times) GlutaMAX (Thermo Fisher Scientific), 100 μ M (1 \times) NEAA (Thermo Fisher Scientific) and 0.02 mM 2-mercaptoethanol (Thermo Fisher Scientific). Medium 2 consists of NBM (Thermo Fisher Scientific) supplemented with 1% N-2 supplement (Thermo Fisher Scientific), 2% B27 supplement (Thermo Fisher Scientific), 2 mM (1 \times) GlutaMAX (Thermo Fisher Scientific) and 0.02 mM 2-mercaptoethanol (Thermo Fisher Scientific). Between day 0 and day 3, cells were kept in medium 1, from day 4 to day 5 cells were kept in 75% medium 1 and 25% medium 2, from day 6 cells were kept in 50% medium 1 and 50% medium 2, from day 7 to day 9 cells were kept in 25% medium 1 and 75% medium 2, and from day 10 to day 14 differentiating cells were kept in 100% medium 2. At day 14, differentiated cells were dissociated with Accutase (Thermo Fisher Scientific) and frozen in cold CryoStor CS10 freezing medium (Sigma-Aldrich) at -80 °C. After 24 h frozen cells were transferred to a liquid nitrogen tank for long-term storage.

Cells were plated after thawing in Geltrex-coated 96-well imaging plates at a density of 40,000 cells per well in maturation medium. Maturation medium consisting of Neurobasal-A Medium (Thermo Fisher Scientific) supplemented with 1% N-2 supplement (Thermo Fisher Scientific), 2% B27 supplement (Thermo Fisher Scientific), 2 mM (1 \times) GlutaMAX (Thermo Fisher Scientific), 0.02 mM 2-mercaptoethanol (Thermo Fisher Scientific), 12 μ g ml⁻¹ of gentamicin (Thermo Fisher Scientific), 200 μ M ascorbic acid (Sigma-Aldrich), 0.1 μ g ml⁻¹ of human recombinant laminin LN521 (BioLamina), 10 ng ml⁻¹ of GDNF (Cell Guidance Systems), 10 ng ml⁻¹ of brain-derived neurotrophic factor (Cell Guidance Systems), 10 ng ml⁻¹ of NGF (Peprotech) and 10 ng ml⁻¹ of NT3 (Peprotech). Then, 4 d after plating cultures were treated with 1 μ g ml⁻¹ of mitomycin C (Sigma-Aldrich) for 2 h at 37 °C to inactivate proliferative cells. Medium was changed twice per week. Cells were matured for 3 weeks before stimulation.

Cell culture stimulation and fixation for HCS microscopy. DRG neurons and human iPSC-derived sensory neurons were stimulated in 96-well imaging plates. Compounds were dissolved in 12.5 μ l of PBS in 96-well V-bottomed plates, mixed with 50 μ l of medium from the culture wells, and added back to the same wells. Stimulations were performed with automated eight-channel pipettes (Eppendorf) at a low dispense speed on heated blocks, and stimulated cells were placed back

in the incubator. The cells were fixed for 10 min at RT by adding 100 μ l of 8% paraformaldehyde, resulting in a final concentration of 4%.

Quantitative HCS microscopy. Fixed DRG cells were treated with goat or donkey serum blocking (2% serum, 1% BSA, 0.1% Triton X-100, 0.05% Tween-20, 1 h, RT) and incubated with the respective primary antibodies diluted in 1% BSA in PBS at 4 °C overnight. After three washes with PBS (30 min, RT), cells were incubated with secondary Alexa dye-coupled antibodies (1:1,000, 1 h, RT). After three final washes (30 min, RT), wells of 96-well plates were filled with PBS, sealed and stored at 4 °C until scanning. For iPSC-derived cultures, the Nissl staining was performed after primary and secondary staining. Wells were rinse with 0.1% Triton X-100 (5 min, RT) in PBS, followed by a 20-min incubation with Nissl solution (1:500, RT). Three rinsing steps were performed as follows: 5 min PBS, 5 min 0.1% Triton X-100 and 30 min three final washes with PBS. Last, wells were filled with PBS, sealed and stored at 4 °C.

We used a Cellomics ArrayScan XTI microscope equipped with an X1 CCD camera and LED light source to scan stained cultures of DRG neurons in 96-well imaging plates. Binned images (2 \times 2; 1,104 \times 1,104 pixels) were acquired with \times 10 (numerical aperture = 0.3) EC Plan Neo-Fluor objective (Zeiss) for DRG and \times 20 objective for iPSC-derived nociceptors. Images were analyzed using the Cellomics software package. Briefly, images of UCHL1/Nissl staining were background corrected (low-pass filtration), converted to binary image masks (fixed threshold), segmented (geometric method) and the neurons identified by the object selection parameters: size of 80–7,500 μ m² (DRGs), 10–600 μ m² (iPSC sensory neurons (iPSC-SNs)), circularity (perimeter² per 4 π area) of 1–3; length:width ratio of 1–2 (DRGs), 1–3 (iPSC-SNs); average intensity of 800–1,200 (DRGs), 300–5,000 (iPSC-SNs); and total intensity of 2 \times 10⁵–5 \times 10⁷ (DRGs), 500–10⁹ (iPSC-SNs). The image masks were then used to quantify signal in other channels. To calculate spillover between fluorescence channels, three respective controls were prepared for each triple staining: (1) UCHL1/Nissl alone, (2) UCHL1/Nissl + antibody 1 and (3) UCHL1/Nissl + antibody 2. Raw fluorescence data of the controls were used to calculate the slope of best-fit straight lines by linear regression, which was then used to compensate spillover. Compensated data were scaled to a mean value of 1 for the unstimulated cells to adjust for variability between experimental days. One- and two-dimensional probability density plots were generated using R packages. Gating of subpopulations was performed by setting thresholds at local minima of probability density plots. Statistical analyses were performed with Student's *t*-tests, or one- or two-way analysis of variance (ANOVA) with respective post-hoc tests as indicated in the figure legends. *P* < 0.05 was considered to be statistically significant. Dose–response curves from HCS microscopy were generated using nonlinear regression curve fitting (three-parameter, standard Hill slope) using Prism software (GraphPad). The parameters of the model (top, bottom or pEC₅₀/pIC₅₀ values, where IC₅₀ is the half-maximal inhibitory concentration) were compared using the extra-sum-of-squares *F* test. High-content screening kinetic experiments were analyzed with R using ordinary two-way ANOVA. Bonferroni's post-hoc analysis was applied to determine *P* values of selected pairs defined in a contrast matrix using the R library multcomp. Error bars represent the s.e.m. of three independent replicate experiments using cells of different animals.

Analysis of DRG sections for PKA activation. Mice received intrathecal injection of PBS or ET (2 μ g of PA + 2 μ g of EF). At 2 h.p.i., L3–L6 DRGs or lumbar spinal cord were harvested and fixed with 4% paraformaldehyde (PFA) (Electron Microscopy Sciences) in PBS for 2 h on ice and dehydrated in 30% sucrose in PBS at 4 °C overnight. The DRGs were then embedded in OCT medium (Tissue-Tek) and snap-frozen in an isopentane/dry ice bath. Frozen blocks were cut into 12- μ m sections, mounted on slides, dried for 30 min at RT and stored at -80 °C. Thawed sections were post-fixed in 2% PFA for 10 min at 4 °C, rinsed in PBS for 30 min, incubated in goat serum blocking (2% serum, 1% BSA, 0.1% Triton X-100, 0.05% Tween-20, 1 h, RT) and incubated with respective primary antibodies diluted in 1% BSA in PBS at 4 °C overnight. After three washes with PBS (30 min, RT), sections were incubated with secondary Alexa dye-coupled antibodies (1:1,000, 1 h, RT). After three final washes (30 min, RT), the sections were mounted with Fluoromount-G (Southern Biotech) containing DAPI (0.5 μ g ml⁻¹).

Images of sections were acquired with a Leica DM6000B epifluorescence microscope controlled by Leica MetaMorph (v.1.4.0) using a \times 20 objective (Leica HC PLAN APO, 0.7). The images were analyzed using a customized Fiji ImageJ plugin. Briefly, UCHL1 images (8 bit) were background corrected (rolling ball radius of 500 pixels), blurred (Gaussian with 1 pixel) and contrast enhanced (enhanced contrast value of 0.7). Then a fixed threshold was applied (40–250) followed by watershed and particle analysis (size of 1,000–20,000, circularity of 0.3–1). The obtained image mask was transferred to the background-corrected pRII images.

Cell viability assay. To measure the induction of apoptosis, isolated DRG neurons were cultured for 2 d and stained live with Molecular Probes CellEvent Caspase-3/7 Green Detection Reagent (Thermo Fisher Scientific, catalog no. C10723, 4 μ M) for 1 h before PFA fixation. Fixed cells were stained for UCHL1 and cleaved caspase-3 followed by HCS microscopy analysis.

Transcriptional profiling analysis of the DRG. Mice were given an intrathecal injection of vehicle (PBS) or ET (2 µg of PA + 2 µg of EF). After 2 h, mice were given terminal injection of Avertin (500 mg kg⁻¹ intraperitoneally, MilliporeSigma) and perfused with 10 ml of cold PBS. Lumbar DRGs (L3–L6) were harvested, immediately homogenized in TRIzol (Thermo Fisher Scientific) and frozen on dry ice, then stored at –80 °C until further processing. Samples from two male and two female mice were collected each day over 3 d for *n* = 6 total per group. RNA isolation was performed using the RNeasy Micro kit (QIAGEN). The total RNA in each of the samples was quantified using an Agilent 4200 TapeStation instrument and normalized to 200 ng of input in 50 µl (4 ng µl⁻¹). The mRNA was captured using oligo(dt) beads as part of the KAPA mRNA HyperPrep workflow. Complementary DNA synthesis, adapter ligation and amplification were conducted subsequently as part of the same workflow. After amplification, residual primers were eluted away using KAPA Pure Beads in a 0.63× SPRI-based cleanup. The qPCR with the KAPA Library Quantification kit was run to confirm the functional concentration. Molarity values obtained from this assay were used to normalize all samples in equimolar ratio for one final pool. The pool was denatured and loaded on to an Illumina NextSeq 500 instrument, with a High-Output 75-cycle kit to obtain single-end 75-bp reads. The pool was loaded at 1.9 pM, with 5% PhiX spiked in as a sequencing control. The basecall files were demultiplexed through the Harvard BPF Genomics Core's pipeline (bc12fastq v.2.20.0.422), and the resulting fastq files were used in subsequent analysis. All fastq files passed the read quality checks performed using FastQC (v.0.11.5). The sequencing reads from each sample were aligned to the GRCh38 or mm10 genome builds from Ensembl (Genome Reference Consortium Mouse Build 38) and quantified using Salmon (v.1.5.2) and tximport (v.1.18.0) in RStudio (v.4.0). Differential gene expression analysis and variance-stabilizing transformation (to obtain normalized read counts) were performed using R/Bioconductor package DESeq2 (v.1.30.1). Gene ontology (GO) pathway enrichment analysis was performed using Bioconductor/R package ClusterProfiler (v.3.18.1). We used the enrichGO function in the ClusterProfiler package (with parameters key type = 'ENSEMBL', pAdjustMethod = 'BH', ont = 'BP' and qvalueCutoff = 0.05) to compare and plot the enriched Kyoto Encyclopedia of Genes and Genomes pathways. We visualized this pathway analysis using the dotplot function from ClusterProfiler (v.3.18.1).

Immunohistochemistry for pERK in the spinal cord. Mice (male C57BL/6) were pre-treated with vehicle or ET (2 µg per 5 µl, i.th) followed (2 h after) by vehicle or capsaicin (1 µg per 5 µl, i.th, Sigma-Aldrich, catalog no. M2028). Then, 20 min later, mice were deeply anesthetized with ketamine and xylazine and perfused through the ascending aorta with PBS, followed by 4% PFA (20 ml min⁻¹ for 3 min). L4–L5 spinal cord segments were dissected and post-fixed for 4 h. Transverse spinal cord sections (free floating, 40 µm) were cut and processed for immunofluorescence. In brief, sections were blocked with 1% BSA, 22.52 mg ml⁻¹ of glycine in PBS for 1 h at RT and incubated overnight at 4 °C with primary antibody against p-ERK (1:200; Cell Signaling, catalog no. 4370S). After incubation with the primary antibody, the sections were washed in PBS + Tween-20 (PBS-T) 3× for 5 min and incubated at room temperature for 2 h with Alexa Fluor-488 goat anti-rabbit (1:400 Invitrogen, catalog no. A11008). The sections were washed with PBS-T as described earlier, mounted on glass slides and covered with coverslips with Vectashield with DAPI (Vector, catalog no. H1200). Eight to twelve nonadjacent sections from the L4–L5 lumbar spinal cord of each mouse analyzed, and the numbers of immunoreactive neuronal profiles in the dorsal superficial laminae of the dorsal horn in each section, were counted (under a ×10 object field). The values from sections (per side of the dorsal horn of the spinal cord) were averaged for each animal.

Treatment with drugs and chemicals. Rimobant (Tocris) was dissolved in 4% DMSO and 1% Tween-80 in saline and administered intraperitoneally at 5 mg kg⁻¹ (10 ml kg⁻¹). Naltrexone (Tocris) was dissolved in saline and administered intraperitoneally at 10 mg kg⁻¹ (10 ml kg⁻¹). Naloxone (Sigma-Aldrich) was dissolved in saline and administered intraperitoneally at 2 mg kg⁻¹ (10 ml kg⁻¹). CGS15943 was dissolved in 5% DMSO and 0.3% Tween-80 in saline, and administered intraperitoneally at 10 mg kg⁻¹ (1 ml kg⁻¹). For induction of chemical sympathectomy, 6-hydroxydopamine free base (Tocris) was dissolved in 0.1% ascorbic acid in saline and administered intraperitoneally at 100 mg kg⁻¹ (10 ml kg⁻¹) 1 week before ET injection. BCI (EMD Millipore) was dissolved in 1% DMSO in saline and administered intrathecally (1.6 µg in 5 µl).

Behavioral tests. Brush test. Mice were placed in individual test compartments separated by an opaque divider on an elevated mesh-bottomed platform. The left hind paw was gently stroked in the direction of heel to toe with a soft paintbrush (Raphaël Kaerell fan brush, size 2). The number of fast paw withdrawals out of ten stimulations was recorded, with a 2-min interval between applications.

Measurement of mechanical and thermal sensitivity thresholds. Mechanical and thermal sensitivity thresholds were measured as previously described⁶¹ with minor modifications. Briefly, mice were habituated on the behavior apparatus for 2 d consecutively for 1 h each. After habituation, three baseline measurements were obtained on separate days before treatment. Mechanical sensitivity thresholds were measured using von Frey filaments and the up/down method⁷⁵. Thermal sensitivity

thresholds were measured using the Hargreaves' apparatus (Model 390G, IITC Life Science) with a 40-s cut-off.

Pinprick test. Mice were placed in individual test compartments separated by an opaque divider on an elevated mesh-bottomed platform. An Austerlitz insect pin (size 000) (FST) was applied gently to stimulate the plantar surface of the left paw without penetrating the skin. The number of fast paw withdrawals out of ten stimulations was recorded, with a 2-min interval between applications.

Randall–Selitto test. Mice were gently restrained with a cloth and allowed to acclimatize for 5 min. The base of the tail was stimulated using calibrated digital forceps (Rodent Pincher Algometer, BioSeb) and the pressure necessary to evoke a response was recorded. Clear signs of discomfort or attempts to escape were considered as responses. Three trials were performed with a 3-min rest period between each stimulation, and the results were averaged.

Cold and hot plate tests. For cold plate tests, mice were placed on a temperature-controlled metal plate (IITC Life Science) at 0 °C and the number of nocifensive responses (jumping or hind-paw licking, lifting or flinching) were recorded within a 5-min window. For hot plate tests, temperatures were set to 50 °C or 55 °C and the latency to response (jumping or hind paw licking) was recorded. A 90-s cut-off was imposed to avoid tissue injury.

Formalin model. Before formalin injection, mice were habituated for 45 min in individual chambers in an infrared Behavior Observation Box (iBOB; Harvard Apparatus), which allows recording of mice in the dark independent of an observer. Mice were then given an intraplantar injection of 10 µl of 5% NBF (Thermo Fisher Scientific) in 0.9% saline (MilliporeSigma). Injections were performed under light restraint without anesthesia. Mice were immediately placed in iBOB and recorded for 45 min. Videos were scored by a blinded observer to quantify the total time spent licking and shaking the injected paw in 5-min intervals. The first phase of the response was defined as 0–5 min and the second phase as 15–35 min post-formalin injection.

Carrageenan model. Carrageenan (MilliporeSigma) was dissolved in 0.9% saline (MilliporeSigma) to a 2% concentration and autoclaved. Mice were given an intraplantar injection of 20 µl of 2% carrageenan and mechanical sensitivity thresholds were monitored as described above.

Spared nerve injury model. Mice were anesthetized with 100 mg kg⁻¹ of ketamine (Patterson Veterinary) and 10 mg kg⁻¹ of xylazine (Patterson Veterinary) given via intraperitoneal injection. Then, 1 ml of sterile saline (Patterson Veterinary) was injected subcutaneously between the shoulder blades, and petrolatum ophthalmic ointment (Patterson Veterinary) was applied. The surgical area was shaved and disinfected with betadine (Patterson Veterinary) and ethanol (VWR). The skin and muscle layer were opened and separated using blunt dissection to reveal the sciatic nerve. Under a stereomicroscope, the tibial and peroneal nerves were ligated with suture (silk, 3/0, nonabsorbable) and a short segment below the ligation was cut and removed. The muscle layer was closed and skin was sutured (Ethilon, 4/0, absorbable). Mice were placed on a heating pad to recover. Sham surgery was performed identical to the regular procedure except that the sciatic nerve was exposed and the incision closed without carrying out the final lesion. Mechanical sensitivity thresholds were monitored as described above.

Wire hang test. Mice were placed on an elevated wire mesh and inverted for 5 min. The latency to fall was recorded. Each session consisted of three trials, of which the maximum value was used.

Rotarod. Motor function and coordination were measured using a rotarod apparatus (Med Associates). Mice were habituated on 3 d consecutively at a constant speed (5 r.p.m. for 60 s per trial, three trials per day). After the indicated treatment, mice were placed on an accelerating rotarod (4–40 r.p.m. in 5 min) and the time until the first passive rotation or fall was recorded. Each measurement consisted of three trials which were performed 15 min apart and averaged.

Biotelemetry. Under inhalatory anesthesia (isoflurane 2%) and sterile conditions, mice received the implant HDX-11 (ADInstruments) under the lateral abdomen skin, with electrodes positioned for ECG measures in the chest. After 5 d of recovery, animals were followed by 24 h for a baseline evaluation of heart rate (beats min⁻¹) and body temperature (°C). After 2 d (7 d after implant), animals received vehicle (aCSF) or ET (2 µg per 5 µl), intrathecally, and were followed by 24 h. Then 1 h after the end of measurements, mice were treated with adrenaline (0.2 mg kg⁻¹, intravenously) and target parameters evaluated for 60 min. Data were collected and analyzed by LabChart software (ADInstruments).

PNHD assay. The PNHD has been the gold standard for assessing the potency of BoNTs at the neuromuscular junction, but also the inhibitory effect of neutralizing antibodies^{66,77}. It mimics the blocking of respiratory function because it happens in nature when BoNTs penetrate the body. For the preparation of the hemidiaphragm,

after deep anesthesia, the left nerve-hemidiaphragm of male CD1 mice (Janvier Labs) was removed from the thoracic cage, after cutting the phrenic nerve above the heart atrium and the diaphragm all around the thoracic cavity, while carefully saving the lowest ribs of the ribcage. After cleaning of the tissue and installation on to the holder via the lowest rib, the phrenic nerve was inserted into the stimulation rings of the holder, while a hook was secured into the ligament of the diaphragm and connected to the transducer. The muscles were suspended (1 g passive tension) in organ baths containing 10 ml of Krebs–Henseleit buffer containing 118 mM NaCl, 4.7 mM KCl, 2.5 mM CaCl₂, 1.2 mM KH₂PO₄, 1.2 mM MgSO₄, 25 mM NaHCO₃, and 11 mM glucose, pH 7.4, at 37°C and gassed with carbogen. The phrenic nerve was stimulated with 20- μ s pulses delivered at 1 Hz. Toxins were added to the bath at a final concentration of 10–100 pM. Experimental data were recorded with software IOX v.2.9 from Emka Technologies. After application of the toxin into the bath, the contraction force of the organ was recorded every 30 s for 3 h. The half-paralysis time (t_{50} , min), that is, the time necessary to inhibit 50% of the initial contraction, was calculated as a measure for the potency of each toxin/concentration. Calculations were done by fitting a four-parameter dose–response logistic curve model ($Y = \text{bottom} + (\text{top} - \text{bottom}) / (1 + 10^{(\log(\text{IC}_{50}) - X) / \text{HillSlope}})$) on to the experimental data. Natural botulinum neurotoxins A from List Biologicals Laboratories was used as a positive control and LH_N/A as a negative control. PA was added when required at 10 nM working concentration. All toxins were tested to $n = 3$ independent experiments.

Statistics and reproducibility. Statistical analyses were performed using GraphPad Prism. For detailed statistical information, please see Supplementary Table 2. No statistical methods were used to predetermine sample sizes but our sample sizes are similar to those reported in previous publications^{61,78} and standard practices in the field. Data distribution was assumed to be normal, but this was not formally tested. Instead, graphs display individual data points and s.e.m. No animals or data points were excluded from the analyses. Behavioral tests were performed by observers blinded to the treatment groups or genotypes. Treatment groups were randomized and evenly distributed across cages and sex. Image analyses were repeated independently with similar results across three mice (Figs. 1c,e and 5a and Supplementary Fig. 3), three donors (Fig. 1j), four mice (Fig. 4c) or four experiments (Fig. 4f and Extended Data Fig. 6e). Image analysis for Extended Data Fig. 7a was replicated over four experiments from one culture of differentiated neurons. Images in Fig. 1h were obtained from online databases at the 2004 Allen Mouse Brain Atlas (<http://mouse.brain-map.org>) and the 2008 Allen Spinal Cord Atlas (<http://mousespinal.brain-map.org>). To the best of our knowledge, each was obtained from a single mouse using an ISH platform with validated reproducibility across ISH runs and independent riboprobe syntheses⁵⁵.

Reporting Summary. Further information on research design is available in the Nature Research Reporting Summary linked to this article.

Data availability

Transcriptional profiling data of the DRG after ET administration is available from the GEO database under no. GSE184619. Microarray data of sorted mouse DRG neuron populations³ is available from the GEO database under accession no. GSE55114. ScRNA-seq data of the mouse nervous system¹ are available from the SRA under the accession no. SRP135960 and at <http://mousebrain.org>. ScRNA-seq data of mouse DRG neurons across development⁴ are available from the GEO database under accession no. GSE139088. Microarray data from BioGPS.org⁵⁵ are available at <http://biogps.org>. ISH data of mouse brain and spinal cord are available from the 2004 Allen Mouse Brain Atlas⁵⁵ (<http://mouse.brain-map.org>) and the 2008 Allen Spinal Cord Atlas (<http://mousespinal.brain-map.org>). Source data are provided with this paper. Datasets generated during the present study are presented in the figures and available from the corresponding author upon reasonable request.

Materials availability

The LF_N-LC/A^{C699S} construct is available from Ipsen and requires a material transfer agreement.

Code availability

Customized code or algorithms were not used to generate results in the present study. HCS analysis of DRG neurons was performed using the Cellomics software package as described in Methods. Analysis of DRG sections was performed using Fiji ImageJ plugins as described in Methods. Transcriptional profiling data of the DRG were analyzed using RStudio as described in Methods.

References

- Abrahamsen, B. et al. The cell and molecular basis of mechanical, cold, and inflammatory pain. *Science* **321**, 702–705 (2008).
- Leysath, C. E. et al. Anthrax edema factor toxicity is strongly mediated by the N-end rule. *PLoS ONE* **8**, e74474 (2013).
- Park, S. & Leppla, S. H. Optimized production and purification of bacillus anthracis lethal factor. *Protein Expr. Purif.* **18**, 293–302 (2000).

- Pomerantsev, A. P. et al. A *Bacillus anthracis* strain deleted for six proteases serves as an effective host for production of recombinant proteins. *Protein Expr. Purif.* **80**, 80–90 (2011).
- Tao, L. et al. Engineered botulinum neurotoxin B with improved efficacy for targeting human receptors. *Nat. Commun.* **8**, 1–10 (2017).
- Pinho-Ribeiro, F. A. et al. Blocking neuronal signaling to immune cells treats streptococcal invasive infection. *Cell* <https://doi.org/10.1016/j.cell.2018.04.006> (2018).
- Neher, E. in *Methods in Enzymology* Vol. 207 123–131 (Academic, 1992).
- Lu, Y. et al. Presynaptic inhibition of primary nociceptive signals to dorsal horn lamina I neurons by dopamine. *J. Neurosci.* **38**, 8809–8821 (2018).
- Safronov, B. V., Pinto, V. & Derkach, V. A. High-resolution single-cell imaging for functional studies in the whole brain and spinal cord and thick tissue blocks using light-emitting diode illumination. *J. Neurosci. Methods* **164**, 292–298 (2007).
- Szucs, P., Pinto, V. & Safronov, B. V. Advanced technique of infrared LED imaging of unstained cells and intracellular structures in isolated spinal cord, brainstem, ganglia and cerebellum. *J. Neurosci. Methods* **177**, 369–380 (2009).
- Li, J., Kritzer, E., Ford, N. C., Arbabi, S. & Baccei, M. L. Connectivity of pacemaker neurons in the neonatal rat superficial dorsal horn. *J. Comp. Neurol.* **523**, 1038–1053 (2015).
- Ikeeda, H., Heinke, B., Ruscheweyh, R. & Sandkühler, J. Synaptic plasticity in spinal lamina I projection neurons that mediate hyperalgesia. *Science* **299**, 1237–1240 (2003).
- Al Ghamdi, K. S., Polgár, E. & Todd, A. J. Soma size distinguishes projection neurons from neurokinin 1 receptor-expressing interneurons in lamina I of the rat lumbar spinal dorsal horn. *Neuroscience* **164**, 1794–1804 (2009).
- Torsney, C. & MacDermott, A. B. Disinhibition opens the gate to pathological pain signaling in superficial neurokinin 1 receptor-expressing neurons in rat spinal cord. *J. Neurosci.* **26**, 1833–1843 (2006).
- Betelli, C., MacDermott, A. B. & Bardoni, R. Transient, activity dependent inhibition of transmitter release from low threshold afferents mediated by GABAA receptors in spinal cord lamina III/IV. *Mol. Pain* **11**, 64 (2015).
- Li, J., Kritzer, E., Craig, P. E. & Baccei, M. L. Aberrant synaptic integration in adult lamina I projection neurons following neonatal tissue damage. *J. Neurosci.* **35**, 2438–2451 (2015).
- Nakatsuka, T., Ataka, T., Kumamoto, E., Tamaki, T. & Yoshimura, M. Alteration in synaptic inputs through C-afferent fibers to substantia gelatinosa neurons of the rat spinal dorsal horn during postnatal development. *Neuroscience* **99**, 549–556 (2000).
- Clark, A. K. et al. Selective activation of microglia facilitates synaptic strength. *J. Neurosci.* **35**, 4552–4570 (2015).
- Dickie, A. C., McCormick, B., Lukito, V., Wilson, K. L. & Torsney, C. Inflammatory pain reduces C fiber activity-dependent slowing in a sex-dependent manner, amplifying nociceptive input to the spinal cord. *J. Neurosci.* **37**, 6488–6502 (2017).
- Chaplan, S. R., Bach, F. W., Pogrel, J. W., Chung, J. M. & Yaksh, T. L. Quantitative assessment of tactile allodynia in the rat paw. *J. Neurosci. Methods* **53**, 55–63 (1994).
- Simpson, L. L. Studies on the binding of botulinum toxin type A to the rat phrenic nerve-hemidiaphragm preparation. *Neuropharmacology* **13**, 683–691 (1974).
- Pellet, S. Progress in cell based assays for botulinum neurotoxin detection. *Curr. Top. Microbiol. Immunol.* **364**, 257–285 (2013).
- Chiu, I. M. et al. Bacteria activate sensory neurons that modulate pain and inflammation. *Nature* **501**, 52–57 (2013).

Acknowledgements

We thank K. Goldstein, S. Sannajust, M. Heyang, N. LoRocco and A. Albakri for excellent technical assistance, and T. Voisin for helpful discussions. We thank M. Dong and S. Tian for helpful discussions and related collaboration. Research was supported by the Burroughs Wellcome Fund, Chan-Zuckerberg Initiative and NIH (DP2AT009499, R01AI130019) to I.M.C.; NIH NIA 5T32AG000222 fellowship to N.J.Y.; NIH NIGMS T32GM007753 fellowship to D.V.N.; the Intramural Program of the NIAID, NIH to S.H.L.; Internal funds from Department of Anesthesiology, Stony Brook Medicine to M.P.; NIH R01NS036855 to B.P.B.; the European Regional Development Fund (NeuroWeg; nos. EFRE-0800407 and EFRE-0800408) and the Innovative Medicines Initiative 2 Joint Undertaking (116072-NGN-PET) to O.B.; NIH NINDS NS111929 to T.J.P.; and the São Paulo Research Foundation (FAPESP) (2013/08216-2 (Center for Research in Inflammatory Diseases) to T.M.C.; Deutsche Forschungsgemeinschaft (nos. 271522021 and 413120531), EFRE-0800384 and Leitmarktagentur.NRW LS-1-1-020d to T.H. The present study was supported in part by a sponsored research grant from Ipsen Pharmaceuticals to I.M.C.

Author contributions

N.J.Y., R.J.C. and I.M.C. conceived the project. N.J.Y., D.N., A.K.-C. and V.S.T. performed experiments and data analysis. J.L., A.B. and T.H. performed HCS microscopy analysis

on DRG neurons, DRG sections and human iPSC-derived sensory neurons. A.U.Q. and T.M.C. performed spinal cord immunostaining and biotelemetry analyses. H.X.B.Z. and B.P.B. performed electrophysiological analysis in DRG neurons. J.L. and M.P. performed spinal cord electrophysiology analysis. S.S. and T.P. performed ISH analysis of human DRG neurons. P.R., A.N. and O.B. provided human iPSC-derived sensory neurons. M.L. and B.L.P. provided recombinant anthrax toxin. M.M. and S.H.L. provided native and engineered anthrax toxins and Antxr2 CKO mice. S.M.L., S.P., V.T. and K.A.F. purified and characterized chimeric anthrax botulinum toxin. S.M. and J.M. performed the mPNHD assay. N.J.Y. and I.M.C. wrote the manuscript with input from all authors.

Competing interests

S.M.L., S.P., S.M., J.M., V.T. and K.A.F. are employees of Ipsen. I.M.C. has received sponsored research support from Ipsen, GSK and Allergan Pharmaceuticals, and is a member of scientific advisory boards for GSK and Kintai Pharmaceuticals. This work is related to patent applications PCT/US16/49099 and PCT/US16/49106, 'Compositions

and methods for treatment of pain', of which R.J.C., I.M.C., B.L.P., K.A.F., S.P. and S.M.L. are co-inventors. O.B. is a co-founder and shareholder of LIFE & BRAIN GmbH. The remaining authors declare no competing interests.

Additional information

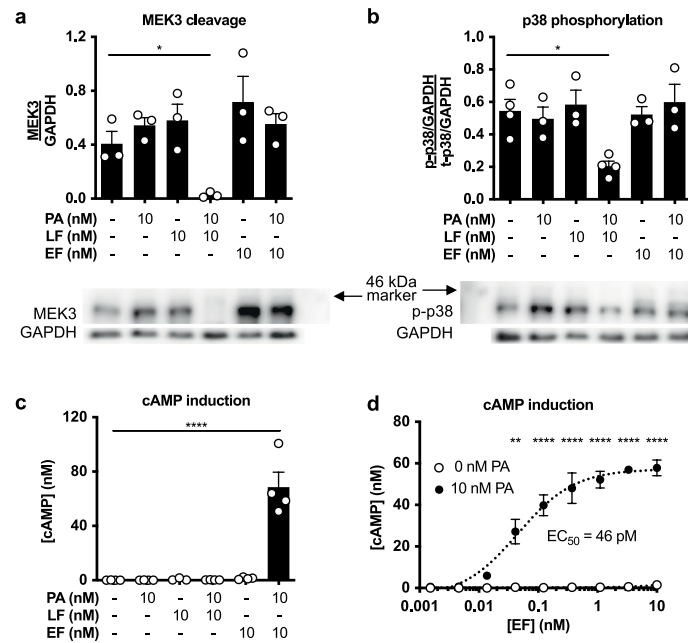
Extended data Extended data are available for this paper at <https://doi.org/10.1038/s41593-021-00973-8>.

Supplementary information The online version contains supplementary material available at <https://doi.org/10.1038/s41593-021-00973-8>.

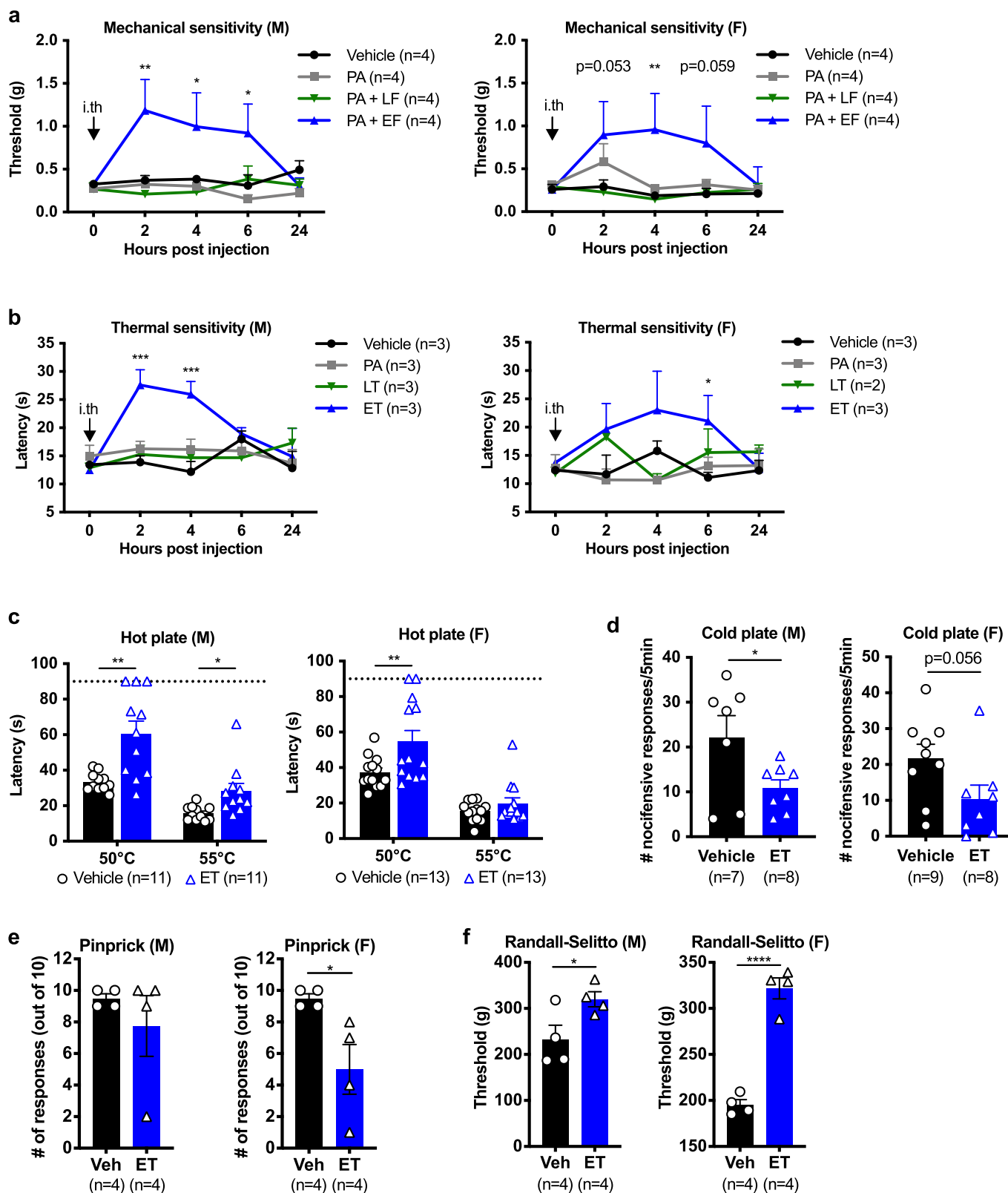
Correspondence and requests for materials should be addressed to Isaac M. Chiu.

Peer review information *Nature Neuroscience* thanks Stephen McMahon and the other, anonymous, reviewer(s) for their contribution to the peer review of this work.

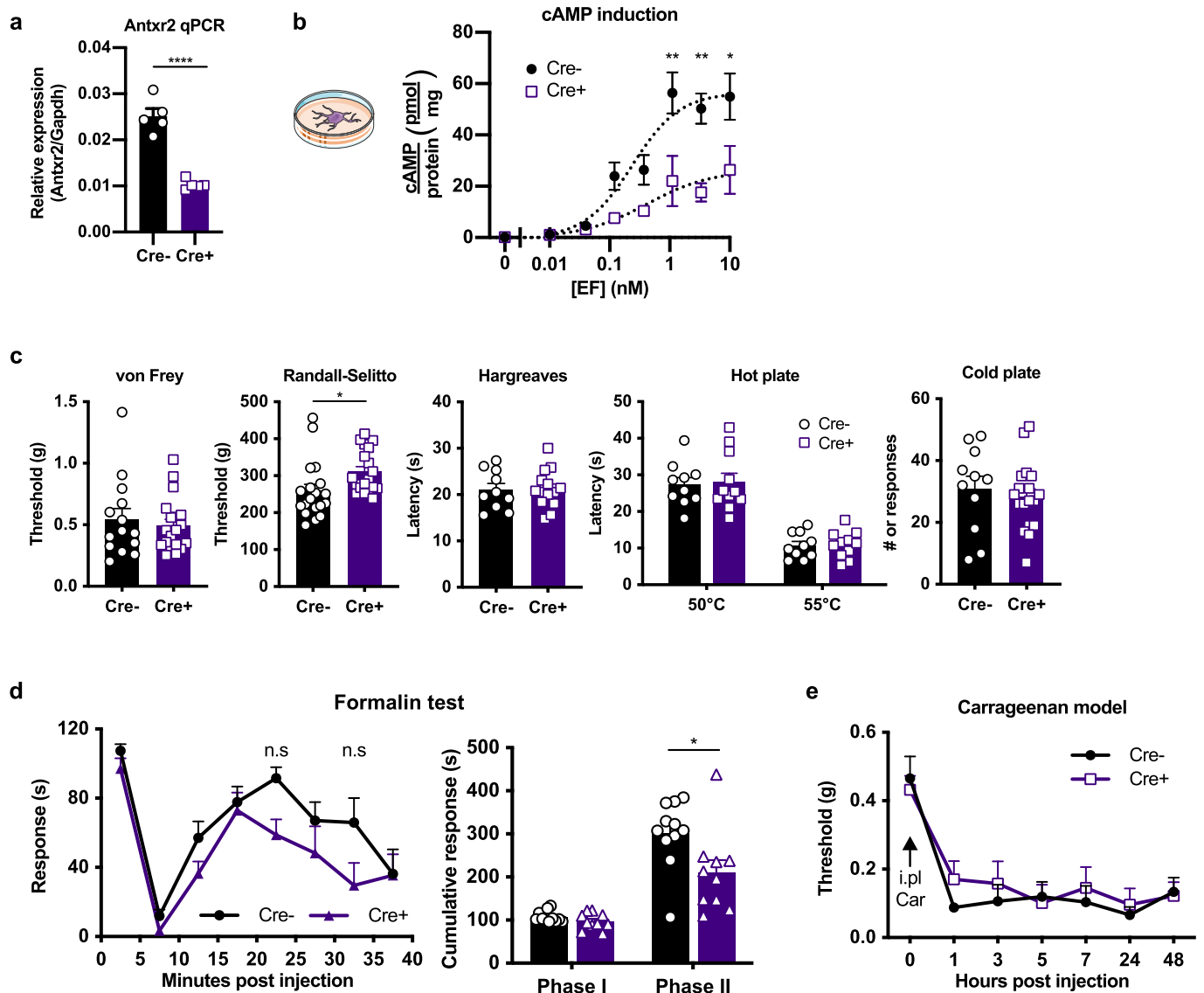
Reprints and permissions information is available at www.nature.com/reprints.



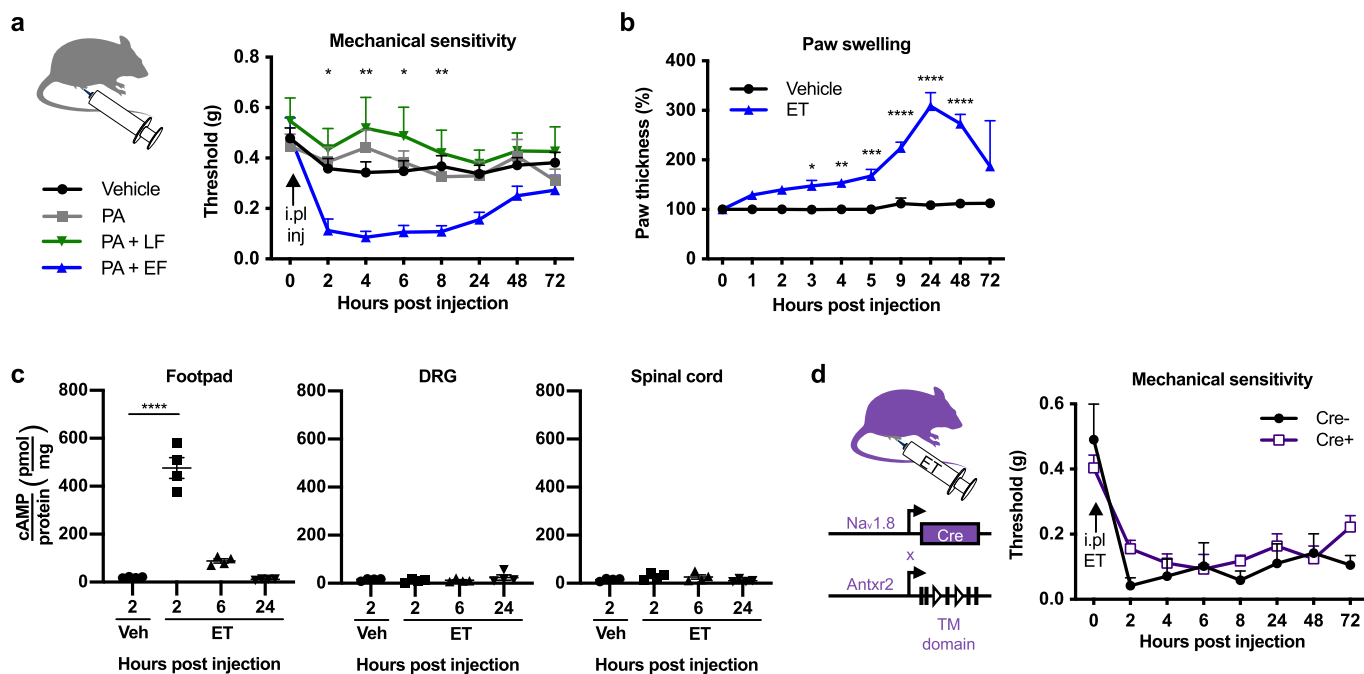
Extended Data Fig. 2 | Anthrax toxins modulate MAPK and cAMP signaling in DRG sensory neurons. (a, b) DRG cultures were treated with combinations of PA, LF and EF for 24 h. Levels of MEK3 expression and p38 phosphorylation were quantified by western blot. (n=3 experiments in (a); n=4 experiments for untreated and LT, n=3 experiments for PA, LF, EF and ET in (b).) (c) cAMP levels in DRG cultures treated with combinations of PA, LF and EF for 2 h. (n=4 experiments for untreated, PA, LT, EF and ET; n=3 experiments for LF.) (d) cAMP levels in DRG cultures treated for 2 h with varying concentrations of EF in the presence or absence of 10 nM PA (n=3 experiments). Statistical significance was assessed by one-way RM ANOVA with Dunnett's post hoc test (a), mixed-effect model with Dunnett's post hoc test (b), one-way ANOVA with Dunnett's post hoc test (c), or two-way ANOVA with Sidak's post hoc test (d). *p<0.05, **p<0.01, ****p<0.0001. Data represent the mean \pm s.e.m. For detailed statistical information, see Supplementary Table 2.



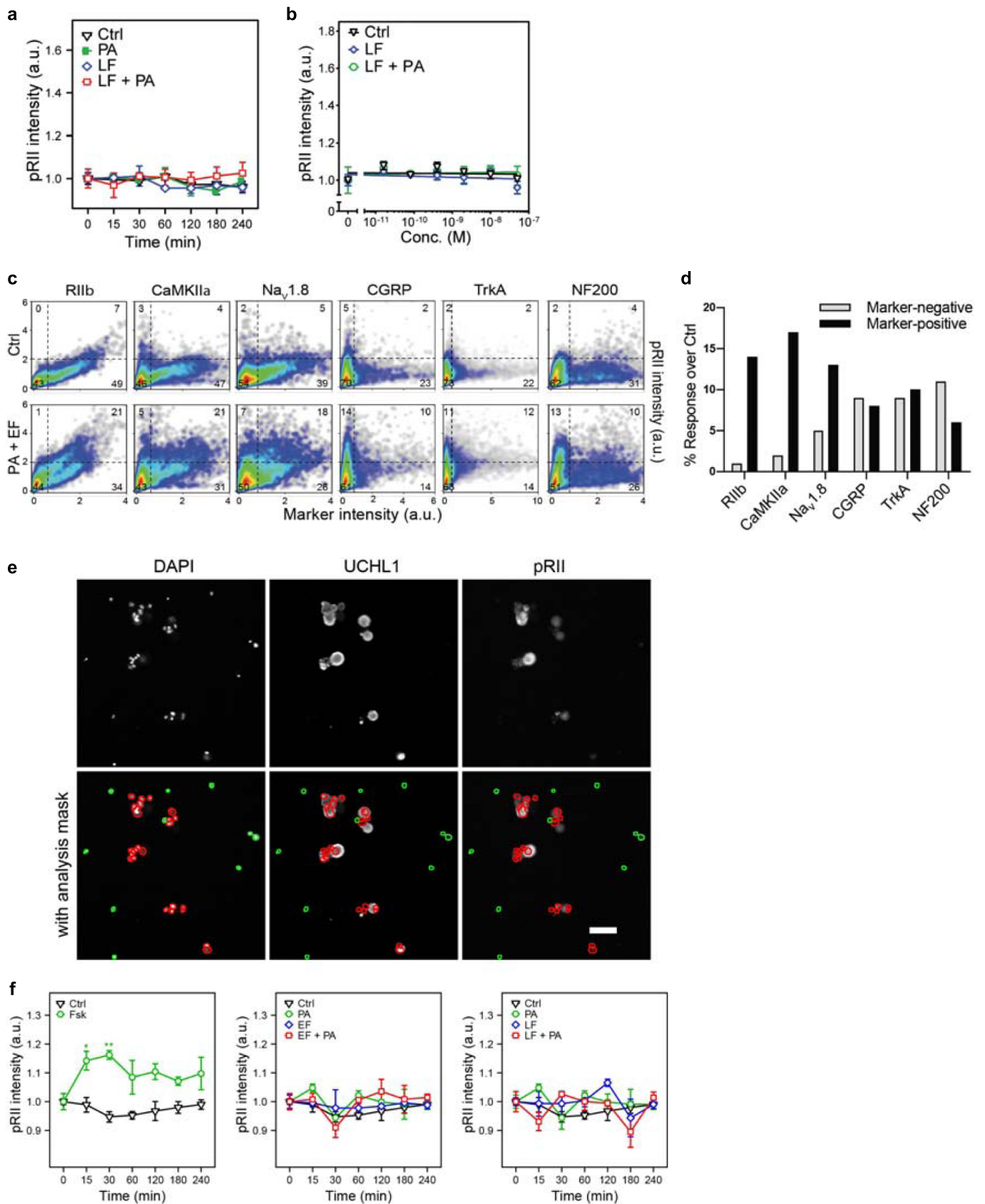
Extended Data Fig. 3 | ET-induced analgesia does not show significant sex-dependent effects. Breakdown of results in male and female mice from (a) Fig. 2b, (b) Fig. 2c, (c) Fig. 2f, (d) Fig. 2g, (e) Fig. 2h and (f) Fig. 2i. The sample sizes denoted in each panel represent the number of mice. The “*” symbol compares Vehicle versus ET in all panels. Statistical significance was assessed by two-way RM ANOVA with Dunnett’s post hoc test (a, b) or two-tailed unpaired t-test (c-f). *p<0.05, **p<0.01, ***p<0.001, ****p<0.0001. Data represent the mean ± s.e.m. For detailed statistical information, see Supplementary Table 2.



Extended Data Fig. 4 | ANT XR2 ablation from $Na_v1.8^{cre/+}$ neurons attenuates cAMP signaling in DRG culture but causes minimal effects on baseline sensory function. (a) qPCR analysis of *Antxr2* expression in DRGs harvested from $Na_v1.8^{cre/+}/Antxr2^{fl/fl}$ (Cre⁺) or $Na_v1.8^{+/+}/Antxr2^{fl/fl}$ (Cre⁻) mice (n=5 mice/group). (b) cAMP levels normalized to protein concentration in DRG neurons that were harvested from $Na_v1.8^{cre/+}/Antxr2^{fl/fl}$ (Cre⁺) or $Na_v1.8^{+/+}/Antxr2^{fl/fl}$ (Cre⁻) mice and treated with 10 nM PA and the indicated concentrations of EF for 2 h (n=3 wells). (c) Baseline pain behaviors of $Na_v1.8^{cre/+}/Antxr2^{fl/fl}$ mice (Cre⁺) and $Na_v1.8^{+/+}/Antxr2^{fl/fl}$ littermates (Cre⁻). (von Frey, n=14 mice for Cre⁻ and n=19 mice for Cre⁺; Randall-Selitto, n=19 mice/group; Hargreaves, n=10 mice for Cre⁻ and n=14 mice for Cre⁺; Hot plate, n=10 mice for Cre⁻ and n=11 mice for Cre⁺; Cold plate, n=11 mice for Cre⁻ and n=18 mice for Cre⁺.) (d) (Left) Acute pain-like behaviors measured in 5 min intervals in $Na_v1.8^{cre/+}/Antxr2^{fl/fl}$ (Cre⁺; n=10 mice) or $Na_v1.8^{+/+}/Antxr2^{fl/fl}$ (Cre⁻; n=11 mice) mice following intraplantar injection of 5% formalin. (Right) Cumulative responses during Phase I (0 - 5 min) or Phase II (15 - 35 min) of formalin-induced pain. (e) Mechanical sensitivity in $Na_v1.8^{cre/+}/Antxr2^{fl/fl}$ (Cre⁺; n=6 mice) or $Na_v1.8^{+/+}/Antxr2^{fl/fl}$ (Cre⁻; n=5 mice) mice following intraplantar injection of 20 μL of 2% carrageenan. Statistical significance was assessed by two-tailed unpaired t-test (a, c, 4d-right), two-way ANOVA with Sidak's post hoc test (b), or two-way RM ANOVA with Sidak's post hoc test (d-left, e). n.s., not significant, **p*<0.05, ***p*<0.01, *****p*<0.0001. Data represent the mean ± s.e.m. For detailed statistical information, see Supplementary Table 2.

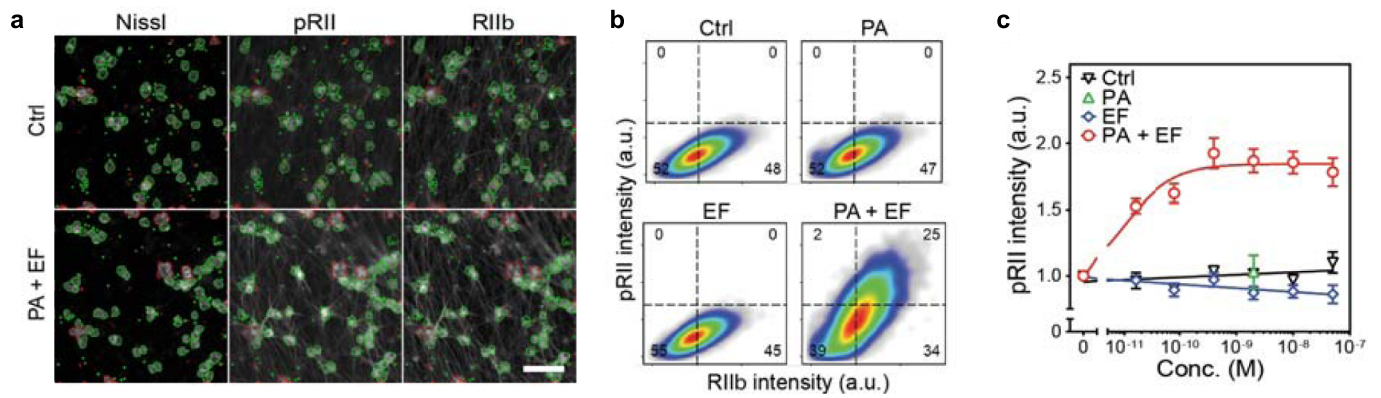


Extended Data Fig. 5 | Intraplantar administration of Edema Toxin induces mechanical allodynia and edema. (a) Mechanical sensitivity after intraplantar administration of vehicle (PBS; $n=27$ mice), PA ($2\ \mu\text{g}$; $n=17$ mice), LT ($2\ \mu\text{g}$ PA + $2\ \mu\text{g}$ LF; $n=10$ mice) or ET ($2\ \mu\text{g}$ PA + $2\ \mu\text{g}$ EF; $n=9$ mice). **(b)** Paw thickness after intraplantar administration of vehicle (PBS) or ET ($2\ \mu\text{g}$ PA + $2\ \mu\text{g}$ EF) ($n=6$ mice/group). **(c)** cAMP levels in the footpad, DRG or spinal cord after intraplantar administration of vehicle (PBS) or ET ($2\ \mu\text{g}$ PA + $2\ \mu\text{g}$ EF) ($n=4$ mice/group). **(d)** Mechanical sensitivity after intraplantar administration of ET ($2\ \mu\text{g}$ PA + $2\ \mu\text{g}$ EF) to $\text{Nav}_1.8^{\text{Cre+}}/\text{Antxr2}^{\text{fl/fl}}$ (Cre+; $n=7$ mice) or $\text{Nav}_1.8^{\text{Cre-}}/\text{Antxr2}^{\text{fl/fl}}$ (Cre-; $n=5$ mice) mice. Statistical significance was assessed by two-way RM ANOVA with Dunnett's post hoc test **(a)**, mixed-effects model with Sidak's post hoc test **(b)**, one-way ANOVA with Dunnett's post hoc test **(c)**, or two-way RM ANOVA with Sidak's post hoc test **(d)**. * $p<0.05$, ** $p<0.01$, **** $p<0.0001$. Data represent the mean \pm s.e.m. For detailed statistical information, see Supplementary Table 2.

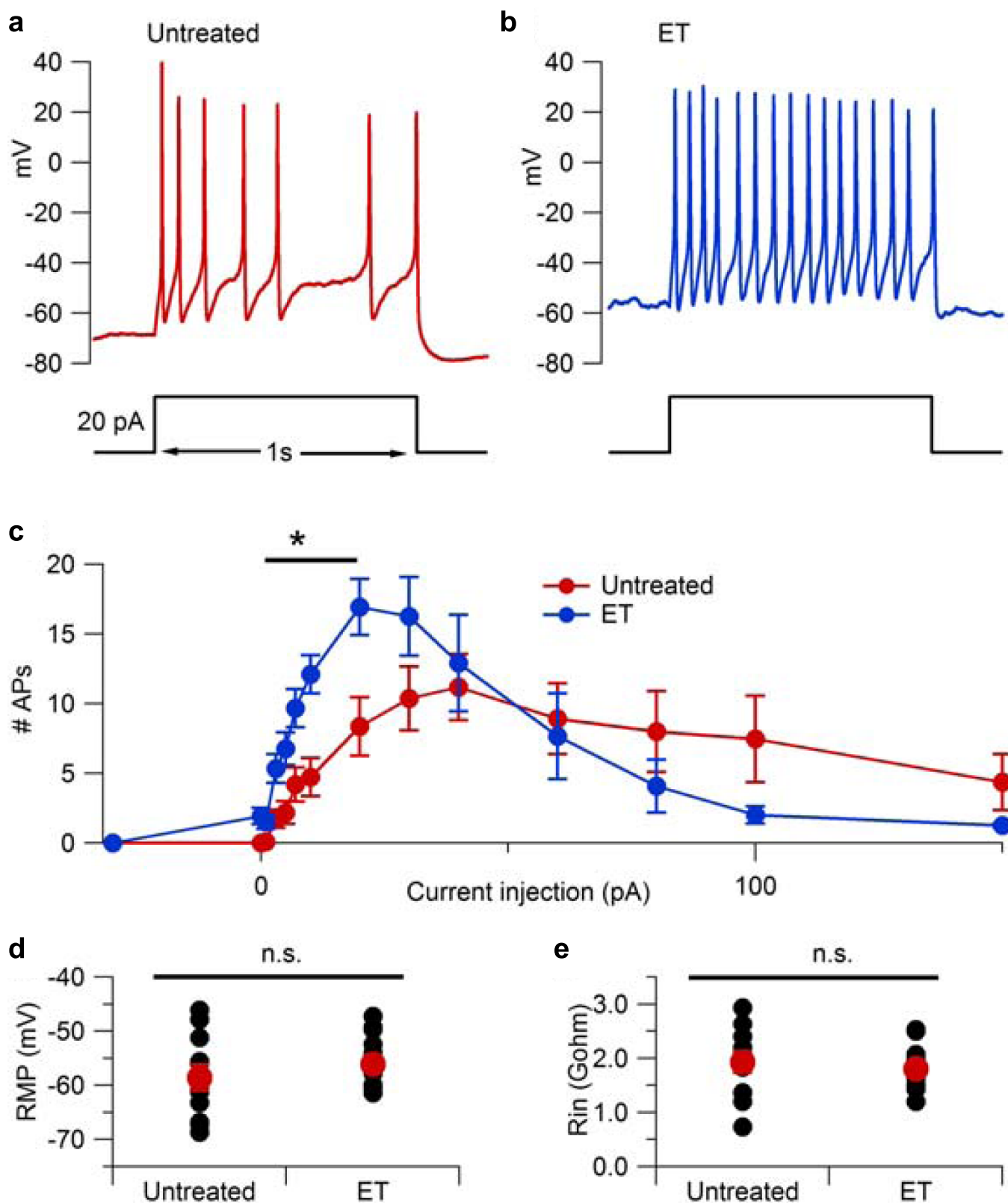


Extended Data Fig. 6 | See next page for caption.

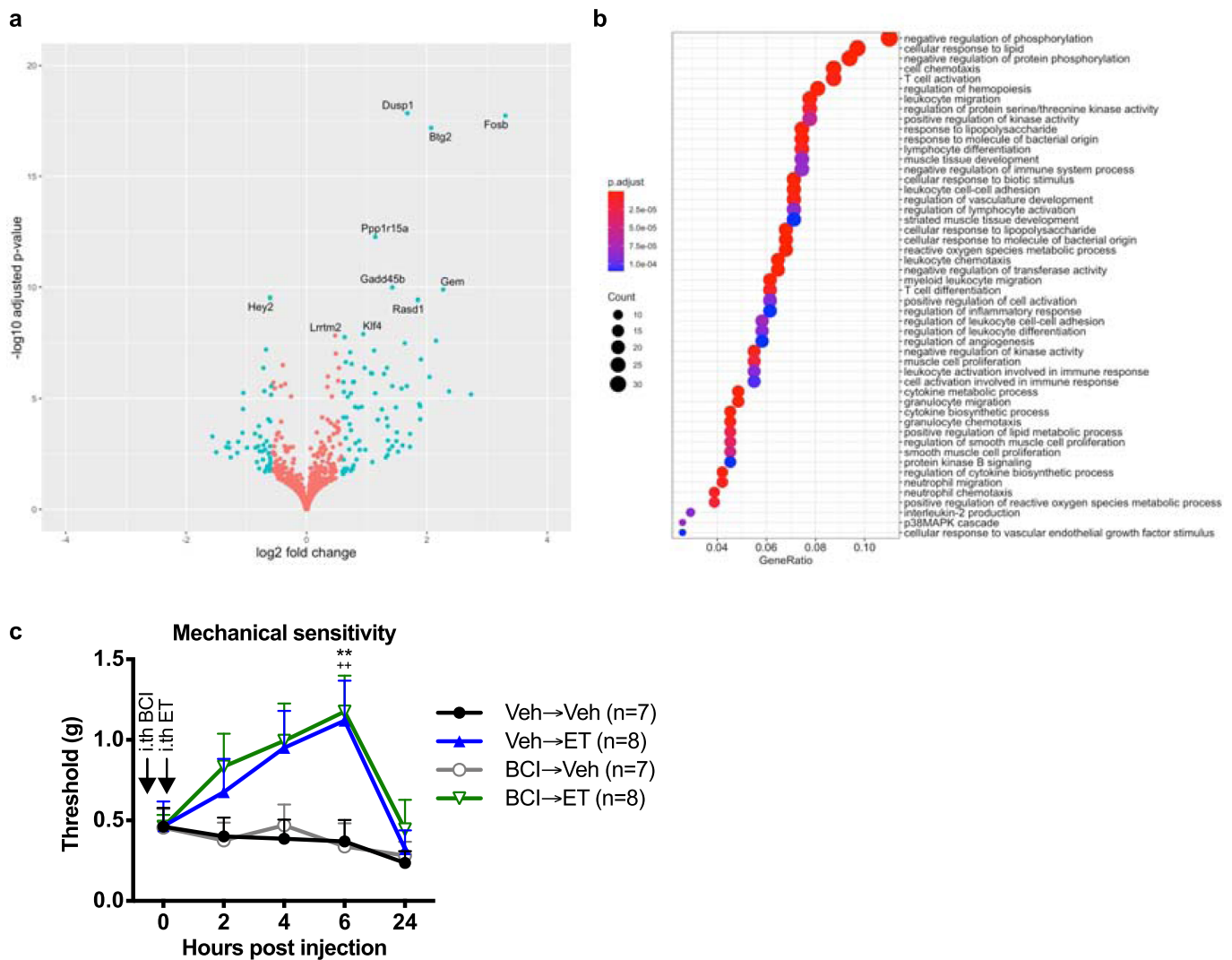
Extended Data Fig. 6 | Edema Toxin induces PKA signaling in DRG neurons but not non-neuronal cells. (a) Time-course of pRII intensity in DRG neurons stimulated with Ctrl (0.1% BSA), PA (10 nM), LF (10 nM) or the combination of both factors (n=3 experiments, >2500 neurons/condition). **(b)** Dose-response curve of pRII intensity in DRG neurons exposed to LF (0 - 50 nM, 2 h) in the presence of a constant concentration of PA (10 nM) (n=3 experiments, >2500 neurons/condition). **(c)** Single cell data of DRG neurons stimulated with control solvent (0.1% BSA) or EF and PA (10 nM each) for 2 h. The DRG neurons were stained for UCHL1, pRII, and the indicated subgroup markers (>5000 neurons per marker). **(d)** Changes in the percentage of pRII positive cells with ET treatment over Ctrl in each neuronal subgroup from **(c)**. The % response with Ctrl treatment was subtracted from the % response with ET treatment. **(e)** Representative images of mouse DRG neurons showing the modified cell identification to analyze PKA-II activation in non-neuronal cells (green), but not neurons or associated cells (red). Scale bar, 50 μ m. **(f)** Time-course of pRII intensity in the nuclei of UCHL1-negative non-neuronal cells stimulated with Ctrl (0.1% BSA), forskolin (10 μ M), PA (10 nM), EF (10 nM), and LF (10 nM) or the combination of these factors (n=4 experiments). Statistical significance was assessed by two-way ANOVA with Bonferroni's post hoc test **(d)**. * $p < 0.05$, ** $p < 0.01$, *** $p < 0.001$. Data represent the mean \pm s.e.m. For detailed statistical information, see Supplementary Table 2.



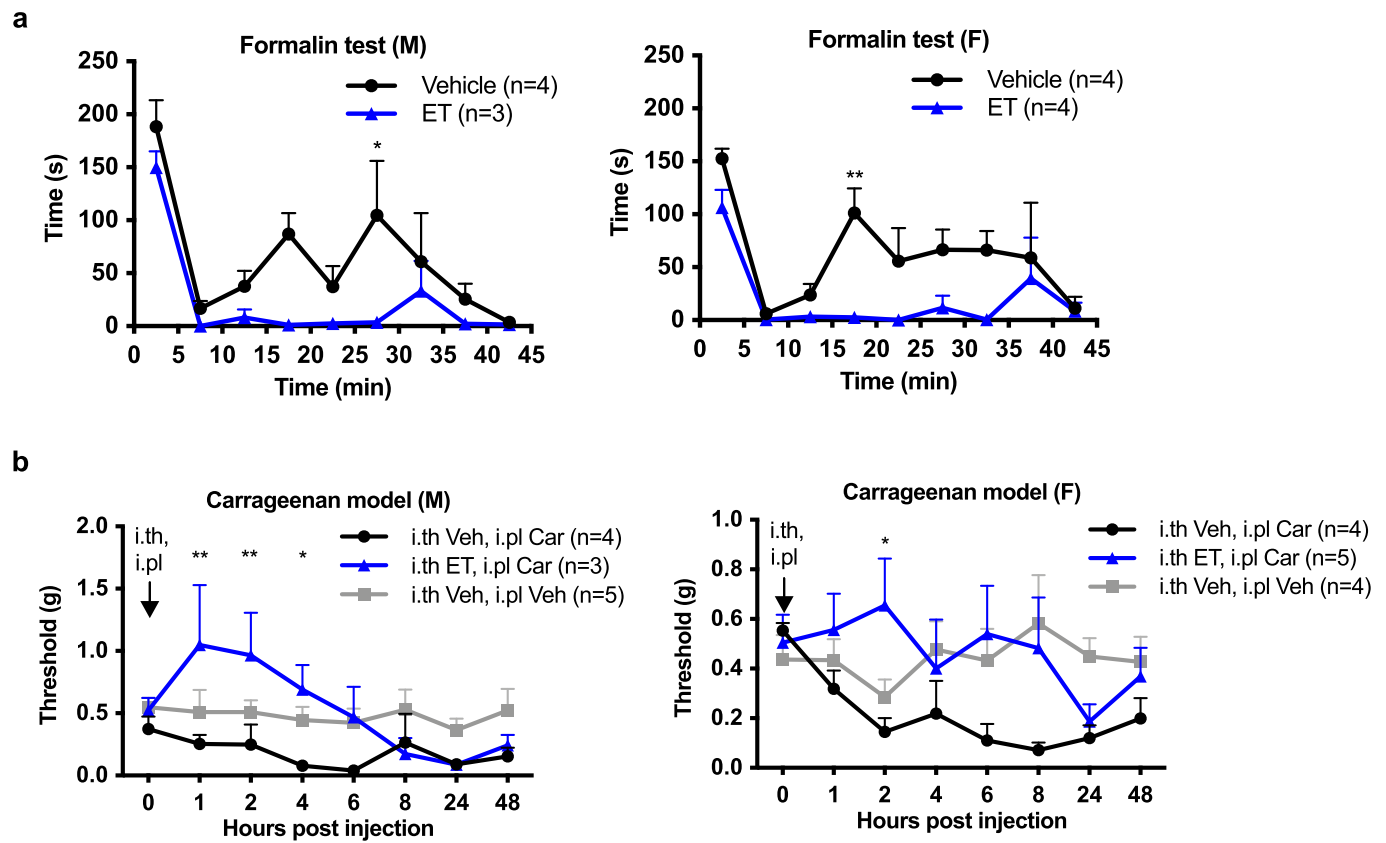
Extended Data Fig. 7 | Edema Toxin induces PKA signaling in human iPSC-derived sensory neurons. (a) Representative HCS microscopy images of human iPSC-derived nociceptors stimulated with vehicle control (Ctrl) or EF + PA (10 nM each) for 2 h. Cultures were labeled with fluorescent Nissl to identify the cells, and pRII and RIIB to quantify PKA-II signaling activity. Green or red encircled cells indicate automatically selected or rejected objects, respectively (see methods section). Scale bar, 100 μm . **(b)** Single cell data of human iPSC-derived nociceptors stimulated with control solvent (0.1% BSA) or EF (2 nM) and PA (10 nM) for 2 h. **(c)** Dose-response curve of pRII intensity in human iPSC-derived nociceptors exposed to EF (0 - 50 nM, 2 h) in the absence or presence of a constant concentration of PA (10 nM) ($n=8$ wells from one culture of differentiated neurons analyzed in four replicate experiments. >8000 neurons/condition). Data represent the mean \pm s.e.m.



Extended Data Fig. 8 | Edema Toxin treatment enhances excitability of small-diameter DRG neurons. Excitability of small diameter DRG neurons was examined after treatment with control media (Untreated) or ET (10 nM PA + 10 nM EF) for 2 – 10 h at 37°C. **(a)** Action potential firing elicited by a 1-s 20-pA current injection in a control small DRG neuron. **(b)** Action potential firing elicited by the same current injection in a representative ET-treated neuron. **(c)** Number of action potentials during 1-s current injections as a function of injected current (Untreated group: $n=11$ cells; ET group: $n=12$ cells). Data plotted as mean \pm s.e.m. **(d)** Resting potential of untreated ($n=11$ cells) and ET-treated ($n=12$ cells) neurons. **(e)** Input resistance of untreated ($n=11$ cells) and ET-treated ($n=12$ cells) neurons. Statistical significance was assessed by unpaired two-tailed Mann-Whitney test (**c-e**). n.s., not significant, $*p < 0.05$. For detailed statistical information, see Supplementary Table 2.



Extended Data Fig. 9 | Intrathecal administration of ET induces transcriptional changes in the DRG. (a) Mice received intrathecal injection of vehicle (PBS) or ET (2 μ g PA + 2 μ g EF) (n=6/group). Lumbar DRGs were harvested at 2 hours post-injection. Poly A-selected libraries were prepared from isolated RNA and sequenced on a NextSeq 500 sequencer. **(b)** Pathway analysis based on gene expression changes. **(c)** Pharmacological inhibition of DUSP1 does not affect ET-induced analgesia. The DUSP1/DUSP6 inhibitor BCI (1.6 μ g) or its vehicle (1% DMSO) was injected intrathecally 15 min prior to ET (2 μ g PA + 2 μ g EF) or its vehicle (PBS). (n=7 mice for Veh, Veh and BCI, Veh groups; n=8 mice for Veh, ET and BCI, ET groups.) Two-way repeated measures ANOVA with Tukey's post hoc test. **p<0.01, Veh, Veh vs. Veh, ET; +++p<0.01, BCI, Veh vs. BCI, ET. Data represent the mean \pm s.e.m. For detailed statistical information, see Supplementary Table 2.



Extended Data Fig. 10 | ET-induced pain blockade does not show sex-dependent effects in mouse models of pain. Breakdown of results in male and female mice from (a) Fig. 6d and (b) Fig. 6e. The sample sizes denoted in each panel represent the number of mice. The “*” symbol in (b) compares i.th Veh, i.pl Car vs. i.th ET, i.pl Car. Statistical significance was assessed by two-way RM ANOVA with Sidak’s (a) or Tukey’s (b) post hoc tests. * $p < 0.05$, ** $p < 0.01$. Data represent the mean \pm s.e.m. For detailed statistical information, see Supplementary Table 2.

Reporting Summary

Nature Research wishes to improve the reproducibility of the work that we publish. This form provides structure for consistency and transparency in reporting. For further information on Nature Research policies, see our [Editorial Policies](#) and the [Editorial Policy Checklist](#).

Statistics

For all statistical analyses, confirm that the following items are present in the figure legend, table legend, main text, or Methods section.

n/a Confirmed

- The exact sample size (n) for each experimental group/condition, given as a discrete number and unit of measurement
- A statement on whether measurements were taken from distinct samples or whether the same sample was measured repeatedly
- The statistical test(s) used AND whether they are one- or two-sided
Only common tests should be described solely by name; describe more complex techniques in the Methods section.
- A description of all covariates tested
- A description of any assumptions or corrections, such as tests of normality and adjustment for multiple comparisons
- A full description of the statistical parameters including central tendency (e.g. means) or other basic estimates (e.g. regression coefficient) AND variation (e.g. standard deviation) or associated estimates of uncertainty (e.g. confidence intervals)
- For null hypothesis testing, the test statistic (e.g. F , t , r) with confidence intervals, effect sizes, degrees of freedom and P value noted
Give P values as exact values whenever suitable.
- For Bayesian analysis, information on the choice of priors and Markov chain Monte Carlo settings
- For hierarchical and complex designs, identification of the appropriate level for tests and full reporting of outcomes
- Estimates of effect sizes (e.g. Cohen's d , Pearson's r), indicating how they were calculated

Our web collection on [statistics for biologists](#) contains articles on many of the points above.

Software and code

Policy information about [availability of computer code](#)

Data collection NIS-Elements (v4.30.02), Clampex (v10.3), pClamp (v9.2), LabChartPro (AdInstruments 2018, v8.1.13), Zen Black (Carl Zeiss, 2011 SP7, v14.0.0.201).

Data analysis GraphPad Prism (v6.07, v7.02, v8.0.1, v8.4.3, v9.2.0), Fiji ImageJ (v1.52h, v1.52p, v1.53.c), Cellomics software package, Olympus CellSens software (v1.18), Clampfit (v10.3), IgorPro (v6.2, v6.37), BruXton DataAccess (v9.4.0), IOX from Emka Technologies (v2.9), Thermo Scientific HCS Studio (v6.6.2, Build 8533), R (v3.6.0-4.0.0), R Studio (v1.4.1106), Salmon (v1.5.2), tximport (v1.18.0), DESeq2 (v1.30.1), ClusterProfiler (v3.18.1).

For manuscripts utilizing custom algorithms or software that are central to the research but not yet described in published literature, software must be made available to editors and reviewers. We strongly encourage code deposition in a community repository (e.g. GitHub). See the Nature Research [guidelines for submitting code & software](#) for further information.

Data

Policy information about [availability of data](#)

All manuscripts must include a [data availability statement](#). This statement should provide the following information, where applicable:

- Accession codes, unique identifiers, or web links for publicly available datasets
- A list of figures that have associated raw data
- A description of any restrictions on data availability

Transcriptional profiling RNAseq data of DRG samples after ET administration is available at the Gene Expression Omnibus (GEO) database under the accession code GSE184619. Microarray data of sorted mouse DRG neuron populations is available from the GEO database under the accession code GSE55114. Single-cell RNAseq data of the mouse nervous system is available from the Sequence Read Archive (SRA) under the accession code SRP135960 and at <http://mousebrain.org>. Single-cell RNAseq data of mouse DRG neurons across development is available from the GEO database under the

accession code GSE139088. Microarray data from BioGPS.org is available at <http://biogps.org>. ISH data of mouse brain and spinal cord are available from the Allen Mouse Brain Atlas (2004) (<http://mouse.brain-map.org>) and Allen Spinal Cord Atlas (2008) (<http://mousespinal.brain-map.org>). Datasets generated during this study are presented in the figures and available from the corresponding author upon reasonable request. Source data are provided with this paper for Fig. 7d and Extended Data Fig. 2a-b.

Field-specific reporting

Please select the one below that is the best fit for your research. If you are not sure, read the appropriate sections before making your selection.

Life sciences Behavioural & social sciences Ecological, evolutionary & environmental sciences

For a reference copy of the document with all sections, see [nature.com/documents/nr-reporting-summary-flat.pdf](https://www.nature.com/documents/nr-reporting-summary-flat.pdf)

Life sciences study design

All studies must disclose on these points even when the disclosure is negative.

Sample size	No statistical methods were used to pre-determine sample sizes but our sample sizes are similar to those reported in previous publications (Pinho-Ribeiro et al. Cell 2018, Chiu et al. Nature 2013) and standard practices in the field.
Data exclusions	No data were excluded from analysis.
Replication	The exact number of biological or technical replicates for each experimental group is listed in the corresponding figure legends. All imaging analyses were sampled across at least 3 animals or human donors. Cell culture experiments were repeated across 3-4 independent runs or performed with technical replicates. Electrophysiology experiments were repeated across multiple cultures or preps and the results combined. Animal experiments were performed with a minimum of 5 mice per group. Groups were either performed in parallel or combined over two independent experiments.
Randomization	Treatment groups were randomized and evenly distributed across cages and sex.
Blinding	Observers for behavior experiments were blinded to the treatment groups or genotypes.

Reporting for specific materials, systems and methods

We require information from authors about some types of materials, experimental systems and methods used in many studies. Here, indicate whether each material, system or method listed is relevant to your study. If you are not sure if a list item applies to your research, read the appropriate section before selecting a response.

Materials & experimental systems

n/a	Involved in the study
<input type="checkbox"/>	<input checked="" type="checkbox"/> Antibodies
<input checked="" type="checkbox"/>	<input type="checkbox"/> Eukaryotic cell lines
<input checked="" type="checkbox"/>	<input type="checkbox"/> Palaeontology and archaeology
<input type="checkbox"/>	<input checked="" type="checkbox"/> Animals and other organisms
<input type="checkbox"/>	<input checked="" type="checkbox"/> Human research participants
<input checked="" type="checkbox"/>	<input type="checkbox"/> Clinical data
<input checked="" type="checkbox"/>	<input type="checkbox"/> Dual use research of concern

Methods

n/a	Involved in the study
<input checked="" type="checkbox"/>	<input type="checkbox"/> ChIP-seq
<input checked="" type="checkbox"/>	<input type="checkbox"/> Flow cytometry
<input checked="" type="checkbox"/>	<input type="checkbox"/> MRI-based neuroimaging

Antibodies

Antibodies used	The following antibodies were used in this study: Rabbit polyclonal anti-MEK-3 (1:500, Santa Cruz Biotechnology, #sc-961), rabbit polyclonal anti-p38 (1:1000, Cell Signaling Technology, #9212), rabbit monoclonal anti-phospho-p38 (Thr180/Tyr182) (clone D3F9, Cell Signaling Technology, #4511, 1:1000), rabbit polyclonal anti-SNAP-25 (1:1000, Millipore Sigma #S9684), rabbit polyclonal anti-GAPDH (1:30,000, Millipore Sigma #G9545), goat anti-rabbit IgG (1:1000, Cell Signaling Technology, #7074), chicken polyclonal anti-UCHL1 (1:2000, Novus, Cambridge, UK, #NB110-58872), rabbit monoclonal anti-RIL α (phospho-Ser96) (1:1000, clone 151, Abcam, Cambridge, UK, #ab32390), mouse monoclonal anti-RIL β (1:2000, BD Transduction Laboratories, #610625), mouse monoclonal anti-NF200 (clone N52, Sigma, #N0142, 1:1000), mouse monoclonal anti-CaMKII alpha subunit (clone 6G9, Thermo Fisher Scientific, #MA1-048, 1:1000), mouse monoclonal anti-NaV1.8 (clone N134/12 Neuromab Facility, #75-166, 1:500), mouse monoclonal anti-CGRP (clone 4901, biorbyt, #orb319478, 1:500), goat polyclonal anti-TrkA, (R&D Systems, #AF1056, 1:500), goat polyclonal anti-TRPV1 (R&D Systems, #AF3066, 1:500), rabbit monoclonal anti-Cleaved Caspase 3 (Asp175, clone 5A1E, Cell Signaling Technology, #9664, 1:500), rabbit anti-p-ERK (Thr202/Tyr204) (D13.14.4E) (Cell Signaling Technology, #4370S, 1:200), highly cross-adsorbed Alexa 647, 555, and 488 conjugated secondary antibodies (Thermo Fisher Scientific).
Validation	rabbit polyclonal anti-MEK-3 (Santa Cruz Biotechnology, #sc-961) - Liu et al. JBC 2008, Liu et al. PNAS 2009, D'Agnillo et al. PlosOne 2013.

rabbit polyclonal anti-p38 (Cell Signaling Technology, #9212) and rabbit monoclonal anti-phospho-p38 (Thr180/Tyr182) (clone D3F9, Cell Signaling Technology, #4511)
- Validation by manufacturer with 2747 and 1752 citations each.

rabbit polyclonal anti-SNAP-25 (Millipore Sigma #S9684)
- Hackett et al. Toxins 2018, Elliott et al. Science Advances 2019, Duchesne De Lamotte et al. Front Pharmacol 2020.

rabbit polyclonal anti-GAPDH (1:30,000, Millipore Sigma #G9545)
- Validation by manufacturer with 1208 citations.

chicken polyclonal anti-UCHL1 (1:2000, Novus, Cambridge, UK, #NB110-58872)
- Isensee et al. PlosOne 2014, Cann et al. FEBS J. 2020, Isensee et al. JCB 2021.
- Cross validated in-house using PGP9.5 Monoclonal Antibody (31A3) (Invitrogen #MA1-83428).

rabbit monoclonal anti-RII α (phospho-Ser96) (clone 151, Abcam, #ab32390)
- Functional and cross validation in Isensee et al. J Cell Sci, 2014 & Isensee et al., J Cell Biol, 2018.

mouse monoclonal anti-RII β (1:2000, BD Transduction Laboratories, #610625)
- Knockout validated (Inan et al. (2006), J. Neurosci. 26, 4338-4349).

mouse monoclonal anti-NF200 (clone N52, Sigma, #N0142)
- Validation by manufacturer with 277 citations.

mouse monoclonal anti-CaMKII alpha (clone 6G9, Thermo, #MA1-048)
- Carbajal et al. J of Neurochemistry 2020.

mouse monoclonal anti-NaV1.8 (clone N134/12 Neuromab Facility, #75-166, 1:500)
- Knockout validated by Dr. Sulayman Dib-Hajj (see Neuromab data sheet)

mouse monoclonal anti-CGRP (clone 4901, biorbyt, #orb319478, 1:500)
- Validated in Nat Commun. 2018 Apr 24;9(1):1640. doi: 10.1038/s41467-018-04049-3.

goat polyclonal anti-TrkA (R&D Systems, #AF1056)
- Functional correlation with response to ligand NGF (Loos et al., Cell Syst. 2018 May 23;6(5):593-603.e13. doi: 10.1016/j.cels.2018.04.008)

goat polyclonal anti-TRPV1 (R&D Systems, #AF3066)
- Cross-validated with another knockout validated TRPV1 antibody (rabbit polyclonal anti-TRPV1 from Alomone labs, # ACC-030) (Isensee et al., PLoS One, 2014, DOI: 10.1371/journal.pone.0115731)

rabbit monoclonal anti-Cleaved Caspase 3 (Asp175, clone 5A1E, Cell Signaling Technology, #9664, 1:500),
- Validation by manufacturer with 3075 citations.

rabbit anti-p-ERK (Thr202/Tyr204) (D13.14.4E) (Cell Signaling Technology, #4370S, 1:200)
- Berta T et al. Neuroscience. 2013 (PMID: 23707980), Liu CC et al. Sci Rep. 2016 (PMID: 27670299), Zhang Y et al. Neuron. 2018 (PMID: 30122375), Bertacchi M et al. EMBO Mol Med. 2019 (PMID: 31318166).

Animals and other organisms

Policy information about [studies involving animals](#); [ARRIVE guidelines](#) recommended for reporting animal research

Laboratory animals

C57BL/6J mice were purchased from Jackson Laboratory (Bar Harbor, ME) and bred at Harvard Medical School. For high content screening (HCS) microscopy experiments, male C57BL/6N mice were obtained from Charles River. For the mPNHD assay, male CD1 mice were purchased from Janvier Labs. For histological analysis of pERK and biotelemetry experiments, C57BL/6 mice were obtained from the Central Animal Care Facility of Ribeirao Preto Medical School, University of Sao Paulo (USP). For spinal cord electrophysiology experiments, Sprague-Dawley rats were purchased from Envigo. Nav1.8-Cre mice were provided by John Wood (University College London)56 on the C57BL/6 background. Antxr2fl/fl mice in which the transmembrane domain of Antxr2 is flanked by loxP sites were obtained from Jackson Laboratory (#027703) on the C57BL/6 background. Mice lacking functional ANTXR2 in Nav1.8-lineage neurons were generated at Harvard Medical School by crossing Nav1.8-Cre mice with Antxr2fl/fl mice to obtain Nav1.8cre+/+/Antxr2fl/fl mice and control Nav1.8+/+/Antxr2fl/fl littermates. Genotyping of this strain was performed as previously described20. Advillin-CreERT2 mice on a mixed C57Bl6J and CD1 background were provided by David Ginty (Harvard Medical School). Mice lacking functional ANTXR2 in somatosensory neurons were generated at Harvard Medical School by crossing Advillin-CreERT2 mice with Antxr2fl/fl mice to obtain AdvillincreERT2+/+/Antxr2fl/fl mice and control Advillin+/+/Antxr2fl/fl littermates. Endothelial cell-specific Cdh5cre+/+/Antxr2fl/fl conditional ANTXR2 KO mice and their Cdh5+/+/Antxr2fl/fl control littermates; myeloid cell-specific LysMcre+/+/Antxr2fl/fl or LysMcre/cre/Antxr2fl/fl conditional ANTXR2 KO mice and their control littermates (LysMcre/cre/Antxr2+/+, LysMcre+/+/Antxr2+/+ or LysMcre+/+/Antxr2fl/+) were generated and bred by Stephen Leppla (NIH) and transported to Harvard Medical School for testing. Both endothelial- and myeloid-specific ANTXR2 KO mouse strains were on the C57BL/6 background.

Expression analyses of Antxr2 (Figures 1c, 1e-f, 1i and Extended Data Fig. 4a), analyses involving primary cells or tissue (Figures 6c, 7b and 7d-f; Extended Data Figures 2a-d, 4b, 5c and 9c; Supplementary Figures 1a, 5 and 10a-b), transcriptional profiling analysis of the DRG (Extended Data Fig. 9c) and all behavior experiments were performed with age-matched mice between 6-14 weeks of age. Male and female mice were used at equivalent ratios for behavior experiments, except for the following which were performed with male mice only: Fig. 2j, 6a and 6b. For high content screening (HCS) microscopy experiments, male C57BL/6N mice were used between 8-10 weeks of age and >24 g in weight. For the mPNHD assay, male CD1 mice were used between 18-28 g in weight at the time of

experiment. For histological analysis of pERK and biotelemetry experiments, male C57BL/6 mice were used between 6-10 weeks of age. For spinal cord electrophysiology experiments, Sprague-Dawley rats were used between P18 - P27 of age at equivalent ratios of males and females.

Animals were housed in temperature ($22 \pm 2^\circ\text{C}$) and humidity ($55 \pm 5\%$) controlled care facilities at the respective institutions on a 12 h light/dark cycle and provided with food and water ad libitum.

Wild animals

This study did not involve wild animals.

Field-collected samples

This study did not involve samples collected from the field.

Ethics oversight

Animal experiments were approved by the Harvard Medical School Institutional Animal Care and Use Committee, Stony Brook University Institutional Animal Care and Use Committee, the Committee for Ethics in Animal Research of the Ribeirao Preto Medical School (Process no 16/2021), or the State Office for Nature, Environment and Consumer Protection North Rhine-Westphalia (LANUV) in Germany in compliance with German animal welfare law. The mPNHD assay was performed in accordance with Council Directive No. 2010/63/UE of September 22nd, 2010, on the protection of animals used for scientific purpose in France.

Note that full information on the approval of the study protocol must also be provided in the manuscript.

Human research participants

Policy information about [studies involving human research participants](#)

Population characteristics

For post mortem donors of DRG tissues, the sex, age and cause of death are listed in Supplementary Table 1. For generation of human iPSC-derived sensory neurons, the iPSC line UKBi013-A was derived from a healthy 50-54 year old male, caucasian donor (<https://hpscereg.eu/cell-line/UKBi013-A>).

Recruitment

Post mortem DRG tissues were provided by the Southwest Transplant Alliance from medically cleared donors and no biases were present in the selection process. The iPSC line UKBi013-A was derived from a self-selected, healthy donor.

Ethics oversight

For post mortem DRG tissues, human tissue procurement procedures were approved by the Institutional Review Boards at the University of Texas at Dallas. Generation of human iPSC-derived sensory neurons was approved by the Ethics Committee of the Medical Faculty of the University of Bonn (approval number 275/08), and informed consent was obtained from the patient. All samples were de-identified prior to use.

Note that full information on the approval of the study protocol must also be provided in the manuscript.